

CR 171958

CSDL-T-939

**REDUCING SHUTTLE-PAYLOAD
DYNAMIC INTERACTION
WITH NOTCH FILTERS**

by

Brent D. Appleby

February 1987

(NASA-CR-171958) REDUCING SHUTTLE-PAYLOAD
DYNAMIC INTERACTION WITH NOTCH FILTERS M.S.
Thesis (Draper (Charles Stark) Lab., Inc.)
122 p

CSDL 22B

N87-16862

Unclass

G3/16 43810



The Charles Stark Draper Laboratory, Inc.

555 Technology Square
Cambridge, Massachusetts 02139

REDUCING SHUTTLE-PAYLOAD
DYNAMIC INTERACTION
WITH NOTCH FILTERS

by

BRENT D. APPLEBY

S.B., Mechanical Engineering, MIT
(1984)

SUBMITTED IN PARTIAL FULFILLMENT
OF THE REQUIREMENTS FOR THE
DEGREE OF MASTER OF SCIENCE

at the

MASSACHUSETTS INSTITUTE OF TECHNOLOGY

February 1987

© Charles Stark Draper Laboratory Inc., 1987

Signature of Author

Brent Appleby

Department of Aeronautics & Astronautics
January 8, 1987

Approved by

Philip D. Hattis

Dr. Philip D. Hattis
Technical Supervisor, CSDL

Certified by

Wallace E. VanderVelde

Professor Wallace E. VanderVelde
Thesis Supervisor

Accepted by

Professor Harold Y. Wachman
Chairman, Departmental Graduate Committee

REDUCING SHUTTLE-PAYLOAD
DYNAMIC INTERACTION
WITH NOTCH FILTERS

by

BRENT D. APPLEBY

Submitted to the Department of Aeronautics
and Astronautics on January 8, 1987,
in partial fulfillment of the requirements
for the Degree of Master of Science

This thesis investigates using notch filters to reduce the spill-over of low-frequency bending modes into the measurement signal. The notch filters were designed using a simplified frequency domain model of the Shuttle-payload dynamics and of the Shuttle's attitude control system along with a sinusoidal input describing function representation of the nonlinear phase plane controller. A simulation of the Space Shuttle with large payloads attached to its robot arm was used to test the notch filter design. The simulation results show that notch filtering the measurement signal to remove the low-frequency Shuttle-payload dynamics can greatly increase the range of stable operation. Since the bending modes are not known exactly before flight and will generally be time-varying, on-line frequency identification was also added to place the notch filters at the bending mode frequencies.

Thesis Supervisor: Dr. Wallace E. VanderVelde
Professor of Aeronautical and Astronautical Engineering

Technical Supervisor: Dr. Philip D. Hattis
Section Chief, Charles Stark Draper Laboratory

ACKNOWLEDGEMENTS

I would like to thank Phil Hattis for giving me the freedom to explore various thesis ideas and for his assistance in the writing of this document. I would also like to thank Prof. Wallace VanderVelde for his careful reading of the manuscript and his valuable comments.

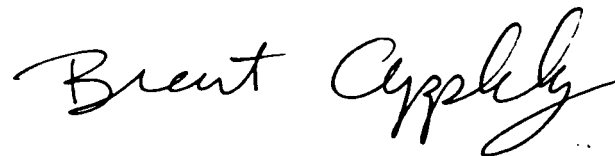
My fellow students, Heidi, Dennis, Naz, and Greg also deserve my appreciation for listening to my ideas and providing valuable advice. I would also like to acknowledge the support and assistance of the Dept. 10C staff.

I would like to thank my parents for allowing me to pursue my education at MIT. A special thanks goes to my wife Stacy who has put up with me and has supported me in my pursuit of graduate degrees.

This report was prepared at The Charles Stark Draper Laboratory, Inc. under contract number NAS9-17560 with the National Aeronautics and Space Administration. The work was supported by NASA Johnson Space Center (JSC).

Publication of this report does not constitute approval by the Draper Laboratory or NASA of the findings or conclusions contained herein. It is published solely for the exchange and stimulation of ideas.

I hereby assign my copyright of this thesis to The Charles Stark Draper Laboratory, Inc., Cambridge, Massachusetts.

A handwritten signature in cursive script that reads "Brent Appleby". The signature is written in black ink and is centered on the page.

Brent Appleby

Permission is hereby granted by The Charles Stark Draper Laboratory, Inc. to the Massachusetts Institute of Technology to reproduce any or all of this thesis.

TABLE OF CONTENTS

1	INTRODUCTION	9
2	FLEXIBILITY IN SPACECRAFT	12
2.1	Introduction	12
2.2	Modelling Flexible Structures	12
2.2.1	Model Reduction.....	14
2.2.2	Controlled and Residual States	15
2.3	State Estimator.....	15
2.4	Controller	16
2.5	Effect of Residual Modes	18
2.5.1	Observation and Control Spillover	19
2.6	Stabilization by Reducing Spillover	20
2.6.1	Placing Sensors at Nodes	21
2.6.2	Annihilation of Control and Observation Spillover	21
2.6.3	Notch Filters	23
3	IDENTIFICATION OF BENDING MODE FREQUENCIES	25
3.1	Introduction	25
3.2	Design Considerations and Constraints	26
3.3	Power Spectral Density	26
3.4	Phase_Lock Loops	28
3.4.1	Phase Detector	29
3.4.2	Variable Frequency Oscillator	29
3.4.3	Filter.....	30
3.4.4	Advantages and Disadvantages of PLL's	31
3.5	Bandpass Filters and Zero-Crossing Measurement	32
3.6	Bandpass Filter Design	33
3.6.1	Choice of Analog Lowpass Design	34
3.6.2	Filter Order and Implementation	35
3.7	Frequency Estimation	40
3.8	Estimating Modal Amplitude	42
3.9	Timing Considerations	44

4	NOTCH FILTERS	47
4.1	Introduction	47
4.2	Notch Filter Design	47
4.3	Effect of Notch Filters	51
5	REVIEW OF SPACE SHUTTLE ATTITUDE CONTROL SYSTEM	58
5.1	Introduction	58
5.2	Overview of the On-Orbit Attitude Control System	58
5.3	Control Jets	60
5.4	Inertial Measurement Unit	62
5.5	State Estimator	63
5.6	Phase Plane Controller	66
5.7	Sources of Bending Mode Dynamics	66
5.8	Problems Caused by Flexibility	70
6	ANALYTIC ANALYSIS OF CLOSED-LOOP SYSTEM	73
6.1	Introduction	73
6.2	Sinusoidal Input Describing Function	73
6.2.1	Using Describing Functions to Predict Limit Cycles	76
6.2.2	Accuracy of Describing Function Approximation	83
6.3	Describing Function Representation of Phase Plane	83
6.4	Simplified Representation of Shuttle	85
6.4.1	Shuttle Dynamics	85
6.4.2	Inertial Measurement Unit	87
6.4.3	State Estimator	89
6.4.4	Combined System	91
6.5	Stability Analysis	92
6.6	Design Considerations	99
7	SIMULATION RESULTS	100
7.1	Introduction	100
7.2	Computer Simulation	100
7.3	Simulation Results	101
8	CONCLUSIONS AND RECOMMENDATIONS.....	110
	BIBLIOGRAPHY	112
	APPENDIX: HAL CODE	114

LIST OF FIGURES

3.1	Phase-Lock Loop.....	28
3.2	Phase Detector.....	29
3.3	Linearized PLL.....	30
3.4	Zero-Crossing Measurement.....	32
3.5	Lowpass Filter Prototypes.....	34
3.6	Butterworth Pole Pattern.....	36
3.7	Chebyshev Pole Pattern.....	36
3.8	Bandpass Filter Comparison.....	37
3.9	Effect of Cascading on Filter Poles.....	38
3.10	Wordlength Effect on Filter Poles.....	39
3.11	Linear Approximation for Zero-Crossing Measurement.....	40
3.12	Beat Response.....	43
3.13	Example of Aliasing.....	45
4.1	Butterworth Lowpass Prototype Pole Locations.....	48
4.2	Notch Filter Frequency Response.....	50
4.3	Rigid Body Plus Bending Mode.....	52
4.4	Frequency Response of Plant.....	53
4.5	Notch Filter Centered on Bending Mode.....	54
4.6	Notch Filter Centered 5% Low.....	55
4.7	Notch Filter Centered 5% High.....	56
5.1	Attitude Control System.....	59
5.2	Jet Locations and Directions.....	61
5.3	State Estimator.....	64
5.4	Disturbance Acceleration Estimator Step Response.....	64
5.5	Angular Rate Estimator Frequency Response.....	65
5.6	Typical Phase Plane Trajectories.....	67
5.7	Phase Plane Controller.....	68
5.8	Typical Trajectory for Stable Limit Cycle.....	69
5.9	Payload Pivoted out of Shuttle Bay.....	71
5.10	Payload Attached to RMS.....	71
5.11	Typical Fundamental Frequencies for Payload Attached to RMS.....	72

6.1	Describing Function Approximation.....	74
6.2	Describing Function in Closed-Loop System.....	76
6.3	Linear Closed-Loop System.....	77
6.4	Finding Gain That Places Poles on Imaginary Axis.....	79
6.5	Limit Cycle Prediction.....	80
6.6	Limit Cycle Amplitude and Frequency Determination.....	81
6.7	Limit Cycle Stability Determination.....	82
6.8	Nonlinearity for Rate Limit Firing.....	84
6.9	Describing Function for Rate Limit Firing.....	86
6.10	Simplified Model of Shuttle Dynamics.....	87
6.11	Delay Approximation.....	88
6.12	Simplified State Estimator.....	89
6.13	Simplified Estimator Frequency Response.....	90
6.14	Combined Simplified System.....	91
6.15	Effect of Control Spillover.....	93
6.16	Effect of Adding Notch Filter.....	94
6.17	How 2nd Order Filter Can Be Better at Preventing Limit Cycles.....	95
6.18	Stability Boundary without Notch Filters.....	96
6.19	Stability Boundary with Notch Filters.....	97
6.20	Effect of Errors in Notch Center Frequency.....	98
7.1	LSAD Stability Simulation with Space Telescope.....	102
7.2	Structural Frame of Reference.....	103
7.3	Stability Range for the Space Telescope.....	104
7.4	Stability Range for the 65k Payload.....	105
7.5	Limits of Stable Operation for Space Telescope (x=700) ..	106
7.6	Limits of Stable Operation for Space Telescope (x=900) ..	107
7.7	Typical Simulation Run with Space Telescope.....	109

CHAPTER 1

INTRODUCTION

The design of many spacecraft control systems is based upon a rigid body model but actual spacecraft will have some flexible dynamics. When the flexible modes are outside the bandwidth of the control system, they will not affect control system stability. For some spacecraft, the bending modes may spillover into the control system bandwidth. This spillover can lead to unwanted jet firings and may destabilize the system.

The Space Shuttle is an example of a spacecraft in which flexibility is of concern. The Shuttle's control system assumes rigid body dynamics. The bending modes of the orbiter are well outside the control bandwidth and so are not a problem. When the Shuttle is manipulating large payloads on-orbit, however, flexible modes can be low enough in frequency to spillover into the control system bandwidth.

The Shuttle is capable of handling payloads that weigh as much as 65,000 lbs. which is over a quarter of a typical Shuttle on-orbit mass of 226,000 lbs. Such large payloads attached to the Shuttle by its long, flexible robot arm can lead to low-frequency, large-amplitude dynamic interaction. These bending modes are picked up by the Shuttle's sensors and can lead to undesirable and sometimes destabilizing jet firings.

Before each flight, a range of possible payload-arm-autopilot configurations are simulated on a computer to determine the stable operating points. For large payloads, the stable operating range can be very restricted. It is therefore highly desirable to come up with a way of reducing the effect of low-frequency dynamics and thus expanding the

range of stable payload operation. It is also desirable that the solution be a change in the control system software rather than a hardware change as this is much cheaper and easier to implement.

This thesis investigates the use of notch filters centered on the estimated bending frequencies to reduce the effect of low-frequency Shuttle-payload dynamic interaction. The Shuttle-payload dynamics that are studied are with payloads attached to the Shuttle's Remote Manipulator System (RMS). Other payload-orbiter connections such as payloads pivoted out of the cargo bay on a tilt table can lead to low-frequency bending modes. Payloads attached to the RMS will, however, present greater problems in that the bending modes will be hard to predict and will tend to vary with time as the RMS changes in orientation.

The thesis is organized into the following chapters:

Chapter 2 looks at the problems caused by flexibility in the spacecraft and briefly reviews a few techniques for reducing bending mode spillover.

Chapter 3 presents a technique for the identification of bending mode frequencies.

Chapter 4 presents the design of the notch filters.

Chapter 5 is a review of the Space Shuttle and its on-orbit control system.

Chapter 6 uses a simplified model of the Shuttle and its control system along with a describing function representation of the nonlinear phase plane controller to analyze the effect of the notch filters on the closed-loop system performance.

Chapter 7 presents simulation results for two large payloads attached to the Shuttle's RMS with and without the notch filters.

Chapter 8 gives conclusions and a few recommendations for further work.

CHAPTER 2

FLEXIBILITY IN SPACECRAFT

2.1 Introduction

This chapter investigates the effect flexibility has on the closed-loop attitude control of spacecraft. The way uncontrolled bending modes can alter the performance of a simple control system made up of a linear state estimator and linear state feedback is shown in detail. Control and observation spillover of residual flexible modes is shown to be destabilizing. Reducing the spillover of residual flexible motion should therefore improve attitude control of spacecraft.

2.2 Modelling Flexible Structures

In theory, flexible structures require an infinite number of modes to completely describe their motion. Flexible structures are distributed parameter systems whose dynamics can be represented by partial differential equations. In practice, however, the structure is modelled with its mass lumped at a finite number of node points. Using finite element methods, the structure can be represented by a second-order matrix differential equation,

$$M \ddot{q} + D \dot{q} + S q = f \quad (2.1)$$

where

q = generalized displacement vector

M = mass matrix

D = damping matrix

S = stiffness matrix

f = input force vector

The system can now be described by,

$$\dot{x} = \begin{bmatrix} \dot{\eta} \\ \ddot{\eta} \end{bmatrix} = \begin{bmatrix} 0 & I \\ -\Omega^2 & -2\zeta\Omega \end{bmatrix} \begin{bmatrix} \eta \\ \dot{\eta} \end{bmatrix} + \begin{bmatrix} 0 \\ \Phi^T \end{bmatrix} f \quad (2.8)$$

or

$$\dot{x} = A x + B u \quad (2.9)$$

The sensors are assumed to measure various linear and angular positions and rates. The measurements can be represented as,

$$y = H_1 q + H_2 \dot{q} \quad (2.10)$$

$$y = H_1 \Phi \eta + H_2 \Phi \dot{\eta} \quad (2.11)$$

$$y = \begin{bmatrix} H_1 \Phi & H_2 \Phi \end{bmatrix} \begin{bmatrix} \eta \\ \dot{\eta} \end{bmatrix} \quad (2.12)$$

$$y = C x \quad (2.13)$$

2.2.1 Model Reduction

The state space representation of a flexible structure given by Equations 2.9 and 2.13 is a convenient form to work with. However, including all the modes from the finite element model can lead to very large matrices. This model may often be too large to be practical in the evaluation and design of the control system.

A smaller, evaluation model is often constructed as a truncated version of the finite element model. This truncation can be as simple as

The finite element model can be transformed into modal coordinates by,

$$q = \Phi \eta \quad (2.2)$$

where

η = modal displacement vector

Φ = mode shape matrix

The matrix of mode shapes satisfies the equation,

$$\Phi^T M \Phi = I \quad (2.3)$$

where I is the identity matrix. The system written in modal coordinates becomes,

$$M \Phi \ddot{\eta} + D \Phi \dot{\eta} + S \Phi \eta = f \quad (2.4)$$

Multiplying by Φ^T gives,

$$(\Phi^T M \Phi) \ddot{\eta} + (\Phi^T D \Phi) \dot{\eta} + (\Phi^T S \Phi) \eta = \Phi^T f \quad (2.5)$$

With proportional or light damping, this is often rewritten as,

$$\ddot{\eta} + 2\zeta\Omega \dot{\eta} + \Omega^2 \eta = \Phi^T f \quad (2.6)$$

where

Ω = diagonal matrix of natural frequencies

ζ = diagonal matrix of damping ratios

To put the system into state space form let,

$$x = \begin{bmatrix} \eta \\ \dot{\eta} \end{bmatrix} \quad (2.7)$$

including only the low frequency modes. More sophisticated techniques involve the use of quadratic cost functions to rank the importance of each mode to various constraints. The evaluation model is made large enough to retain an accurate representation of the structure but not so large as to be unwieldy to use.

2.2.2 Controlled and Residual States

The number of controlled states in most spacecraft is quite small. Flight computer limitations allow only the rigid-body and perhaps a few of the dominant bending modes to be tracked and controlled. The system model can be divided into controlled and residual states. The states used in a feedback control system will be called the controlled states, and the remaining states called residual states. Using this division, the states in Eq. 2.9 can be rearranged as,

$$\begin{bmatrix} \dot{x}_c \\ \dot{x}_r \end{bmatrix} = \begin{bmatrix} A_c & 0 \\ 0 & A_r \end{bmatrix} \begin{bmatrix} x_c \\ x_r \end{bmatrix} + \begin{bmatrix} B_c \\ B_r \end{bmatrix} u \quad (2.14)$$

and Eq 2.13 becomes,

$$y = \begin{bmatrix} C_c & C_r \end{bmatrix} \begin{bmatrix} x_c \\ x_r \end{bmatrix} \quad (2.15)$$

2.3 State Estimator

The state estimator provides estimates of the system's states to the feedback controller given the set of measurements. The estimated state, x_e , follows the differential equation,

$$\dot{x}_e = A_c x_e + B_c u + K(y - C_c x_e) \quad (2.16)$$

$$\dot{x}_e = (A_c - K C_c) x_e + B_c u + K y \quad (2.17)$$

Let the estimation error, e , be defined as,

$$e = x_c - x_e \quad (2.18)$$

The governing differential equation for the estimation error is,

$$\dot{e} = \dot{x}_c - \dot{x}_e = A_c x_c + B_c u - (A_c - K C_c) x_e - B_c u - K(C_c x_c + C_r x_r) \quad (2.19)$$

$$\dot{e} = (A_c - K C_c) (x_c - x_e) - K C_r x_r \quad (2.20)$$

$$\dot{e} = (A_c - K C_c) e - K C_r x_r \quad (2.21)$$

If the real part of the eigenvalues of $(A_c - K C_c)$ are all negative, then the estimator will be stable. Without residual mode dynamics and other noise, the estimation error will decay to zero. The residual states act as a driving term to the error equation.

2.4 Controller

The full-state feedback controller takes the measured states, if available, or the estimated states and produces the command vector u . If all the states are available, the input u is,

$$u = -G x_c \quad (2.22)$$

making the closed-loop system,

$$\dot{x}_c = (A_c - B_c G) x_c = A_{c1} x_c \quad (2.23)$$

The performance of the closed-loop system depends upon the eigenvalues of A_{c1} . With full-state feedback, the eigenvalues can be placed arbitrarily.

When the states are not directly available the estimated states, x_e , are used to determine the input,

$$u = -G x_e \quad (2.24)$$

making the system,

$$\dot{x}_c = A_c x_c - B_c G x_e \quad (2.25)$$

which can be rewritten as,

$$\dot{x}_c = (A_c - B_c G) x_c + B_c G e \quad (2.26)$$

The residual state dynamics can be represented by,

$$\dot{x}_r = A_r x_r - B_r G (x_c - e) \quad (2.27)$$

Combining Equations 2.21, 2.26, and 2.27 gives the entire closed-loop system,

$$\begin{bmatrix} \dot{x}_c \\ \dot{e} \\ \dot{x}_r \end{bmatrix} = \begin{bmatrix} A_c - B_c G & B_c G & 0 \\ 0 & A_c - K C_c & -K C_r \\ -B_r G & B_r G & A_r \end{bmatrix} \begin{bmatrix} x_c \\ e \\ x_r \end{bmatrix} \quad (2.28)$$

2.5 Effect of Residual Modes

If no residual modes were present, the system would be,

$$\dot{z} = \begin{bmatrix} \dot{x} \\ \dot{e} \end{bmatrix} = \begin{bmatrix} A_c - B_c G & B_c G \\ 0 & A_c - K C_c \end{bmatrix} \begin{bmatrix} x \\ e \end{bmatrix} = A_{11} z \quad (2.29)$$

The eigenvalues of a matrix of the form,

$$\text{eig} \begin{bmatrix} A & | & B \\ \hline 0 & | & C \end{bmatrix} = \text{eig}(A) \text{eig}(C) \quad (2.30)$$

so the eigenvalues of the matrix A_{11} in Eq. 2.29 are,

$$\text{eig}(A_{11}) = \text{eig}(A_c - B_c G) \text{eig}(A_c - K C_c) \quad (2.31)$$

which are just the poles of the controller and the poles of the state estimator. If the controller and estimator designs are stable then the closed-loop system will be stable.

With residual modes the system is,

$$\begin{bmatrix} \dot{z} \\ \dot{x}_r \end{bmatrix} = \begin{bmatrix} A_{11} & | & 0 \\ \hline -B_r G & B_r G & | & A_r - K C_r \end{bmatrix} \begin{bmatrix} z \\ x_r \end{bmatrix} \quad (2.32)$$

or

$$\begin{bmatrix} \dot{z} \\ \dot{x}_r \end{bmatrix} = \begin{bmatrix} A_{11} & A_{12} \\ A_{21} & A_{22} \end{bmatrix} \begin{bmatrix} z \\ x_r \end{bmatrix} \quad (2.33)$$

If either A_{12} or A_{21} equal zero, then the eigenvalues of the entire system would be the poles of the closed-loop system without the residual modes, $\text{eig}(A_{11})$, plus the poles of the residual modes, $\text{eig}(A_{22})$. In other words, the residual modes would add its poles to the closed-loop system without changing the control system poles.

If A_{12} and A_{21} are non-zero, then the poles of the control system and of the residual modes will be changed. This means that the control system will not perform as it was designed, possibly going unstable.

2.5.1 Observation and Control Spillover^{1,2}

The submatrix A_{12} in Eq. 2.33 represents residual mode dynamics picked up by the sensors. This spillover of residual mode dynamics into the measurements is called **observation spillover**. Similarly, the submatrix A_{21} in Eq. 2.33 represents the excitation of the residual modes by the control input and is called **control spillover**.

With no observation spillover, the residual mode dynamics can be represented as,

$$\dot{x}_r = A_r x_r - B_r G x_e \quad (2.34)$$

The control spillover does not change the poles of the residual mode system, but acts as a driving term. The residual modes will be excited, but will not be driven unstable. The controlled states and estimation error will act as if no residual modes exist if there is no observation

spillover. Exciting the residual modes can often be undesirable, but without residual mode dynamics spilling over into the measurements, the system will remain stable.

If there is observation spillover but no control spillover, the estimation error will be,

$$\dot{e} = (A_c - K C_c) e - K C_r x_r \quad (2.35)$$

The residual modes will act as a driving noise in the estimation error equation. This in turn will affect the performance of the control system with

$$\dot{x}_c = (A_c - B_c G) x_c + B_c G e \quad (2.36)$$

the controlled state dynamics being driven by the estimation error which is driven by the residual mode dynamics. The poles of the estimator and controller, however, will not change.

Control and observation spillover can degrade the performance of the entire closed-loop system. Control spillover leads to excitation of the residual modes. Observation spillover will tend to increase the estimation error which in turn will affect the system states. Both control and observation spillover must be present, however, to drive the closed-loop system unstable.

2.6 Stabilization by Reducing Spillover

For a simple linear system, spillover of residual mode dynamics moves the poles of the closed-loop system which can destabilize the system. In nonlinear systems, it is harder to mathematically show the effect of spillover. Many spacecraft use on-off thrusters, making their control systems highly nonlinear. For such spacecraft, unmodelled bend-

ing dynamics picked up by the sensors can lead to jet firings which further excite the residual modes. As in linear systems, this combination of observation and control spillover can destabilize the system.

By reducing spillover, the real system should behave more like the designed model of the system and potential instabilities from unmodelled dynamics should be reduced.

2.6.1 Placing Sensors at Nodes

One way of reducing observation spillover is to prevent residual mode dynamics from being measured by sensors. If the residual dynamics were known very well, the sensors could be placed at or near the nodes of the residual modes. There would be little or no observation spillover of a residual mode that has a node near to or at a sensor location.

This is impractical for many spacecraft. It assumes that residual mode shapes will be accurately known, that these modes will not change with time, and that the control system designer has control over the placement of sensors. These assumptions will not be true for many spacecraft. In particular, for the Space Shuttle only one sensor, the Inertial Measurement Unit (IMU), is used and its position is fixed in the Shuttle. This method therefore would not be useful.

2.6.2 Annihilation of Control and Observation Spillover⁴

A technique has been developed that can remove observation or control spillover for certain systems. For control spillover annihilation, the desired control, \bar{u} , will differ from the actual control, u , by

$$\bar{u} = D u \quad (2.37)$$

This makes the controlled and residual state system, Eq. 2.14,

$$\dot{x}_c = A_c x_c + B_c Du \quad (2.38)$$

$$\dot{x}_r = A_r x_r + B_r Du \quad (2.39)$$

Control spillover will be eliminated if $B_r D = 0$. The actual control is chosen to

$$\min_u ||u - \bar{u}|| = \min_D ||u - Du|| \quad (2.40)$$

subject to $B_r D = 0$

Elimination of observation spillover is accomplished in a similar manner by changing the measurement signal as

$$\bar{y} = T y \quad (2.41)$$

The estimation error equation, Eq. 2.21, will now become

$$\dot{e} = (A_c - K T C_c) e - (K T C_r) x_r \quad (2.42)$$

Observation spillover will be eliminated if $T C_r = 0$. As before, the measurement used will be chosen to

$$\min_y ||y - \bar{y}|| = \min_T ||y - Ty|| \quad (2.43)$$

subject to $T C_r = 0$

For this technique to work the system $(A_c, B_c D)$ must be controllable or $(A_c, T C_c)$ must be observable. This method will only work for systems with a large number of overlapping control inputs or many overlapping sensors and when the spillover from only a few residual modes is to be

removed. For every residual mode eliminated, the dimension of the control or measurement space will be reduced by two. Eliminating only a few residual modes will therefore seriously restrict the control or estimation of the system states.

For the Space Shuttle, only one sensor that measures attitude is used, making observation spillover annihilation impossible. While there are many available control jets, they are all located on the effectively rigid orbiter itself. The controls on the robot arm and attached payload are not available to the attitude control system so the available control can be modelled as acting at one point. Control spillover annihilation therefore is also impossible. By disallowing all control action that excites the residual bending modes, there will be no way to control the orbiter itself.

2.6.3 Notch Filters

Notch filtering the measurement signal is another way of reducing observation spillover. Notch filters are bandstop filters that reject a narrow band of frequency. Running the measurement signal through a series of notch filters that are centered on the residual bending mode frequencies will drastically reduce the observation spillover and help to stabilize the system. The narrower the notch, the less effect the filters will have on the rest of the measurement signal. Notch filtering is a good way of reducing observation spillover without hurting the estimation of the controlled states.

Notch filtering will work well when the residual bending mode frequencies are well known. Observation spillover will increase sharply with error between the residual mode frequencies and the notch filter center frequencies. In conjunction with notch filters, on-board frequency estimation should be used which can lock onto and track the bending frequencies. This thesis looks at using notch filters combined with

real-time frequency identification to reduce observation spillover and stabilize flexible spacecraft. Specifically, this technique is designed and evaluated for the Space Shuttle with flexibly attached payloads.

CHAPTER 3

IDENTIFICATION OF BENDING MODE FREQUENCIES

3.1 Introduction

In dealing with the problems caused by flexibility, it is important to know the frequencies of the bending modes. The design approach of this thesis uses notch filters where accurate knowledge of the bending frequencies is crucial.

Accurate a priori knowledge of the bending frequencies is, however, unrealistic. Computer models of spacecraft dynamics are valuable analysis tools but should not be depended upon to accurately predict bending frequencies. The models will have simplifications and perhaps more importantly, the spacecraft itself will be constantly changing. A spacecraft's configuration changes in a flight; solar panels will rotate, fuel burns will alter mass properties, etc., having a complicated effect upon the bending modes.

It is therefore highly desirable to be able to identify bending frequencies in flight using the spacecraft's various sensors. In particular, this thesis looks at identifying bending frequencies for the Space Shuttle using its Inertial Measurement Unit (IMU). The identification scheme used in this design was therefore chosen with digital computer implementation in mind. Two alternative frequency identification methods are also briefly reviewed.

3.2 Design Considerations and Constraints

The first design constraint is that the method chosen must be able to identify frequencies to a relatively high accuracy. The identified frequencies will be sent to narrow notch filters, so small errors in the estimated frequencies can lead to dramatically reduced performance. In addition to locking on to the bending frequencies, the frequency estimator must be able to track frequencies as they vary with time.

It is reasonable to assume that rough predictions of the bending frequencies will be available for most spacecraft. Therefore the identification scheme should be able to use this a priori knowledge, when available, to improve its performance.

Finally the frequency identification scheme in this thesis is designed with the Space Shuttle in mind. Therefore only methods that can be implemented on a digital computer are considered.

3.3 Power Spectral Density

One of the most common methods of identifying the frequencies of a signal is by computing its power spectral density (PSD). The power spectral density breaks the signal up into its frequency components. Spikes in the PSD will represent the bending modes.

The power spectral density is defined as the Fourier Transform of the autocorrelation function,

$$\text{PSD} = \mathcal{F}\{R_{xx}(\tau)\} = \int_{-\infty}^{\infty} R_{xx}(\tau) e^{j\omega\tau} d\tau \quad (3.1)$$

where

$$R_{xx}(\tau) = E[x(t)x(t+\tau)] \quad (3.2)$$

with $E[]$ representing the expected value. The PSD is commonly calculated by averaging periodograms of a signal where a periodogram is defined as

$$\frac{1}{T} |\mathcal{F}\{x(t)\}|^2 \quad (3.3)$$

where T is the time span of the sample. As T becomes large and as the number of periodograms averaged becomes large, then the averaged periodogram approaches the power spectral density.

On a digital computer, the PSD is calculated by taking a large time sequence and dividing it up into smaller sequences. Each of these time records is put through a Fast Fourier Transform (FFT) to calculate its periodogram. These periodograms are then averaged to approximate the power spectral density of the signal.

Computing the power spectral density of the measurement signal was rejected as the frequency identification scheme because it has serious drawbacks for our application. First, it is mainly used in off-line processing. It is not a recursive algorithm; it requires large sequences to be manipulated (transformed, averaged, filtered, etc.). A spacecraft's digital flight computer is usually not well equipped for such applications.

A second drawback is the difficulty of resolving frequencies with a PSD. With a Discrete Fourier Transform, the frequency resolution is equal to $1/T$ where T is the total time span of the sample.

As an example, the Space Shuttle may get bending frequencies down to about 0.04 Hz with large payloads attached to its Remote Manipulator System (RMS). The frequency resolution required for notch filtering would be around 0.002 Hz. For a decent PSD let 10 periodograms be averaged. This means each periodogram must be at

least 500 seconds long and the total sample length would be over an hour.

Obtaining good frequency resolution complicates the problems of limited computer capacity and leads to long identification times making the tracking of time varying frequencies nearly impossible. The power spectral density as a frequency identification method was therefore rejected.

3.4 Phase-Lock Loops

Phase-lock loops (PLL) can be used to lock onto and track oscillating signals. A PLL takes the output of a variable frequency oscillator and compares it to the input signal. The difference is used to adjust the variable oscillator until it locks onto the signal. The signal's frequency and phase can thus be identified and tracked. The block diagram of a PLL is shown in Figure 3.1.

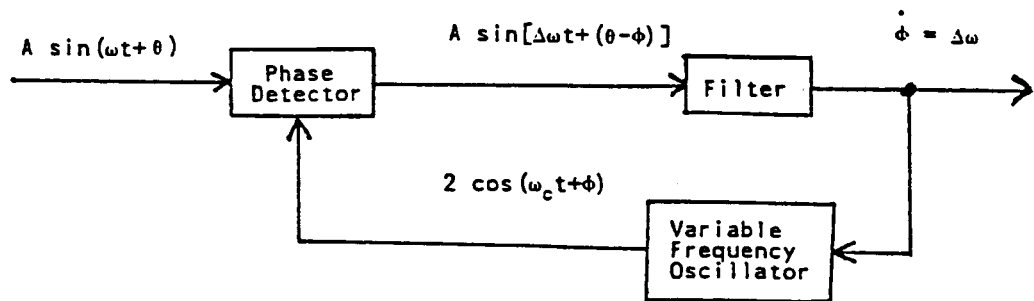


Figure 3.1 Phase-Lock Loop

3.4.1 Phase Detector

The phase detector takes the input signal and output of the variable frequency oscillator and produces a signal related to the error in frequency and phase. A diagram of the phase detector is shown in Figure 3.2. The input signal is multiplied with the variable frequency oscillator output. This results in two terms, the sine of the frequency and phase difference and the sine of the frequency and phase sum. The second of these terms is eliminated by a lowpass filter. When error in frequency and phase is small, the sine of the error will be approximately the error itself and the PLL will act almost linearly.

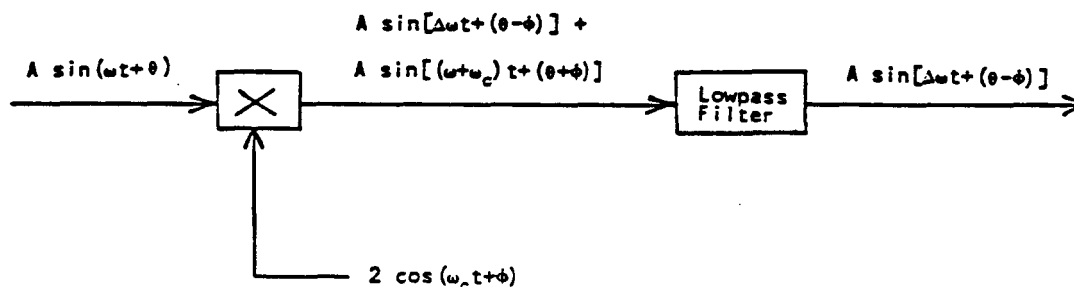


Figure 3.2 Phase Detector

3.4.2 Variable Frequency Oscillator

In many diagrams of a PLL the variable frequency oscillator is labeled a voltage controlled oscillator (VCO). A VCO produces an oscillating signal at a center frequency plus small frequency and phase corrections controlled by an input voltage. On a digital computer, the variable frequency oscillator would be designed to act as a VCO. A center frequency, ω_c , is chosen as the best guess of the frequency of the input signal. The closer ω_c is to the actual frequency, the better the PLL will perform.

3.4.3 Filter

The filter section can be a simple gain or a proportional plus integral gain, or even chosen to make the PLL act as an extended Kalman filter. The filter section can best be understood by looking at a linearized PLL block diagram, Figure 3.3.

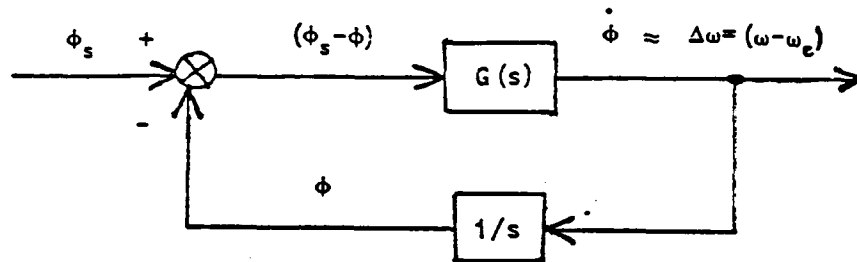


Figure 3.3 Linearized PLL

If $G(s)$ is chosen to be a simple gain, K , then the closed-loop linearized system will be

$$\frac{\phi}{\phi_s} = \frac{K}{s + K} \quad (3.4)$$

If K is positive, then the phase will exponentially approach the signal's phase with time constant $1/K$.

If an integral gain is added to the filter, $G(s) = K_1 + K_2/s$ then the closed-loop system would be

$$\frac{\phi}{\phi_s} = \frac{K_1 s + K_2}{s^2 + K_1 s + K_2} \quad (3.5)$$

where K_1 and K_2 are chosen for desired performance. More complicated filters can be designed for more refined performance. These linearized filter designs are then analyzed with the nonlinear PLL.

3.4.4 Advantages and Disadvantages of PLL's

Phase-lock loops are very effective at identifying and tracking frequencies in real-time. They have been used in a wide variety of applications. PLL's are particularly good if implemented in hardware rather than software as they are available as integrated circuits making them cheap and easy to use.

Phase-lock loops use a priori knowledge of bending mode frequencies. The closer the center frequency of the variable oscillator is to the actual bending frequency, the faster the PLL will lock onto the right frequency. Better a priori information will therefore lead to better performance.

In the phase-lock loop described above, it was assumed that the amplitude of the input signal was known. This will not be true in practice. Imprecise knowledge of the amplitude will have a direct impact on the performance of the PLL. Macala⁵ suggests using bandpass filters to isolate each bending mode and then using a limiter on each mode to give a constant, known amplitude.

Using phase-lock loops is often recommended for real-time frequency identification. A series of PLL's can be used with center frequencies set near the expected bending frequencies and they will lock onto and track the bending modes in flight. For hardware implementation, PLL's seem to be the best choice for real-time frequency identification. For this thesis, however, a software identification scheme is desired. While PLL's could be designed and implemented in software, a simpler method was chosen and is described in the next section.

3.5 Bandpass Filters and Zero-Crossing Measurement

The frequency identification method chosen for this thesis is very straightforward. A series of bandpass filters are used to isolate each bending mode. The time between zero-crossings for each of these modes is measured and is equal to half the signal's period. Every time the signal crosses zero, there will be a new measurement of the signal frequency. This is shown in Figure 3.4 for one bending mode.

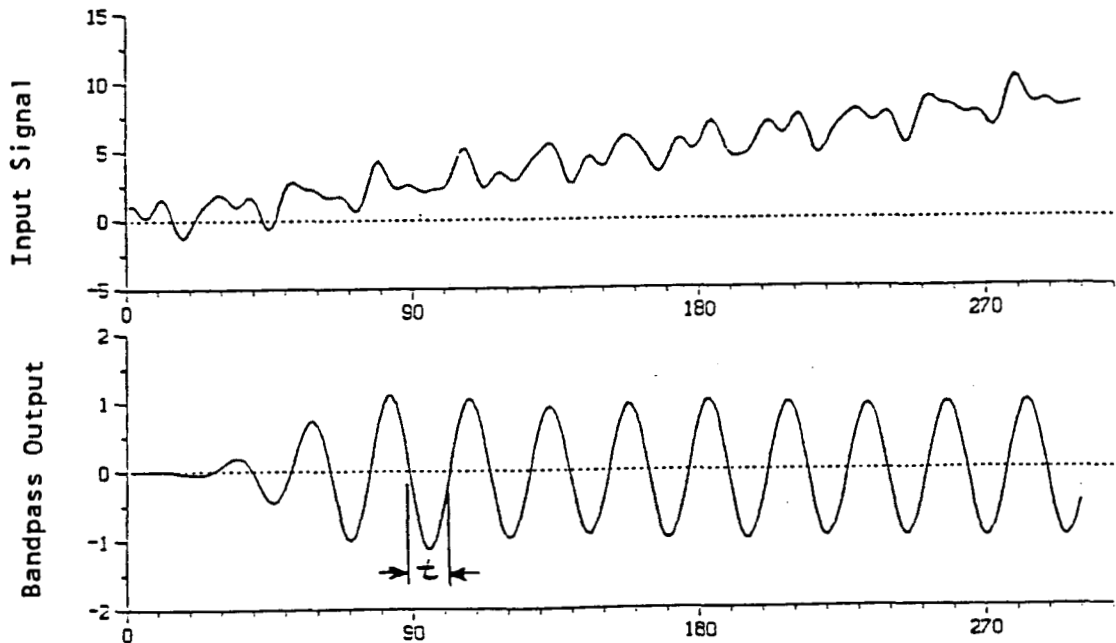


Figure 3.4 Zero-Crossing Measurement

3.6 Bandpass Filter Design

The bandpass filters are designed as in Stearns⁶ by taking an analog lowpass filter, and then converting to a digital formulation.

Given an analog lowpass filter with transfer function $H_{LP}(s)$ having a cutoff frequency of ω_c , an analog bandpass filter can be constructed with the frequency transformation,

$$H_{BP}(s) = H_{LP}\left(\frac{s^2 + \omega_1\omega_2}{s}\right) \quad (3.6)$$

with

$$\omega_c = \omega_2 - \omega_1 \quad (3.7)$$

where ω_1 and ω_2 are the passband frequencies.

A bilinear transform can be used to convert from the analog bandpass filter to a digital bandpass filter. The bilinear transform will distort the frequencies, so the passband frequencies in the analog filter are prewarped to obtain the desired digital passband frequencies. This prewarping is accomplished by

$$\begin{aligned} \omega_1' &= \tan(\omega_1 T/2) \\ \omega_2' &= \tan(\omega_2 T/2) \end{aligned} \quad (3.8)$$

where T is the time-step of the digital filter. The digital transfer function, H_{DBP} , can now be obtained from the transformation

$$H_{DBP}(z) = H_{BP}\left(\frac{z-1}{z+1}\right) \quad (3.9)$$

where z is the z -transform variable which is defined as

$$z = e^{sT} \quad (3.10)$$

This discrete transfer function can now be directly used to obtain the filter's difference equation.

3.6.1 Choice of Analog Lowpass Filter Design

Three common types of lowpass filters are Butterworth, Chebyshev, and Elliptic. Figure 3.5 shows the frequency response of these filters. The Butterworth design has a smooth frequency response. The Chebyshev design allows ripples in the passband but has a sharper cutoff than the Butterworth. The Elliptic filter allows ripples in both the passband and stopband but has a still sharper cutoff. These characteristics will be retained when the lowpass filter is transformed into a bandpass filter. Ripples in the passband of the lowpass filter will lead to ripples in the passband of the bandpass filter, etc.

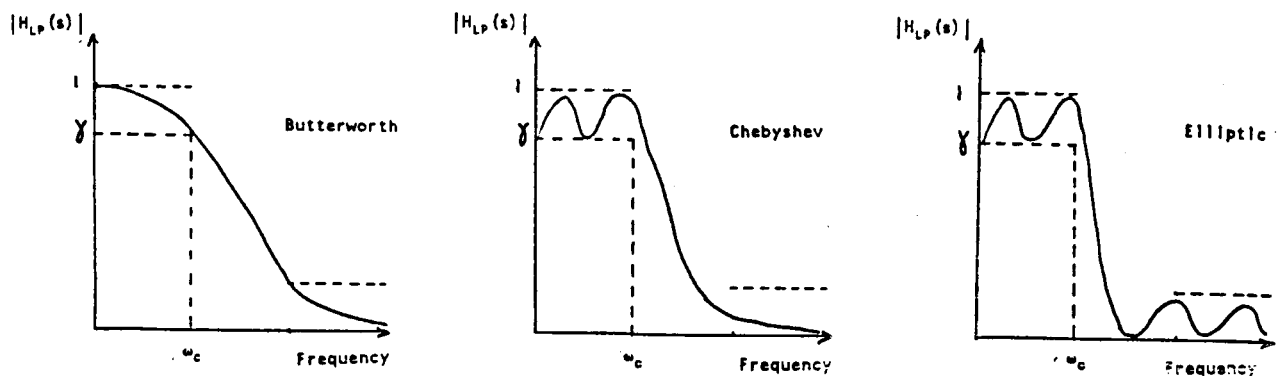


Figure 3.5 Lowpass Filter Prototypes

For frequency identification, the bandpass filters will be centered on the a priori guesses of the bending mode frequencies. The bandpass filters should be designed to provide more attenuation for frequencies further away from the passband. This means ripples in the stopbands are undesirable and the Elliptic filter will be ruled out. Another reason for rejecting the Elliptic filter is that it is by far the hardest of the three to design.

Deciding between the Butterworth and Chebyshev designs will depend upon whether ripples in the passband are tolerable. The Chebyshev design will be better at rejecting frequencies outside the passband and so for many applications it would be the better choice. To minimize the distortion of the measurement signal, the number of notch filters may be limited to bending modes with significant amplitude. The output of the bandpass filters may therefore be needed to estimate the amplitude of the bending modes. Ripples in the passband will distort this amplitude, so if amplitude estimation will be used, the Butterworth design would be better. In this thesis the Butterworth design was chosen for this reason.

Figures 3.6 and 3.7 show the pole pattern in the s-plane for the Butterworth and Chebyshev lowpass filters. There is no real difference in the difficulty of designing or implementing either filter.

3.6.2 Filter Order and Implementation

Choosing the filter order is a tradeoff between speed and noise rejection. A larger filter will be better at rejecting frequencies outside the passband but will use more computer code and have greater problems with numerical stability.

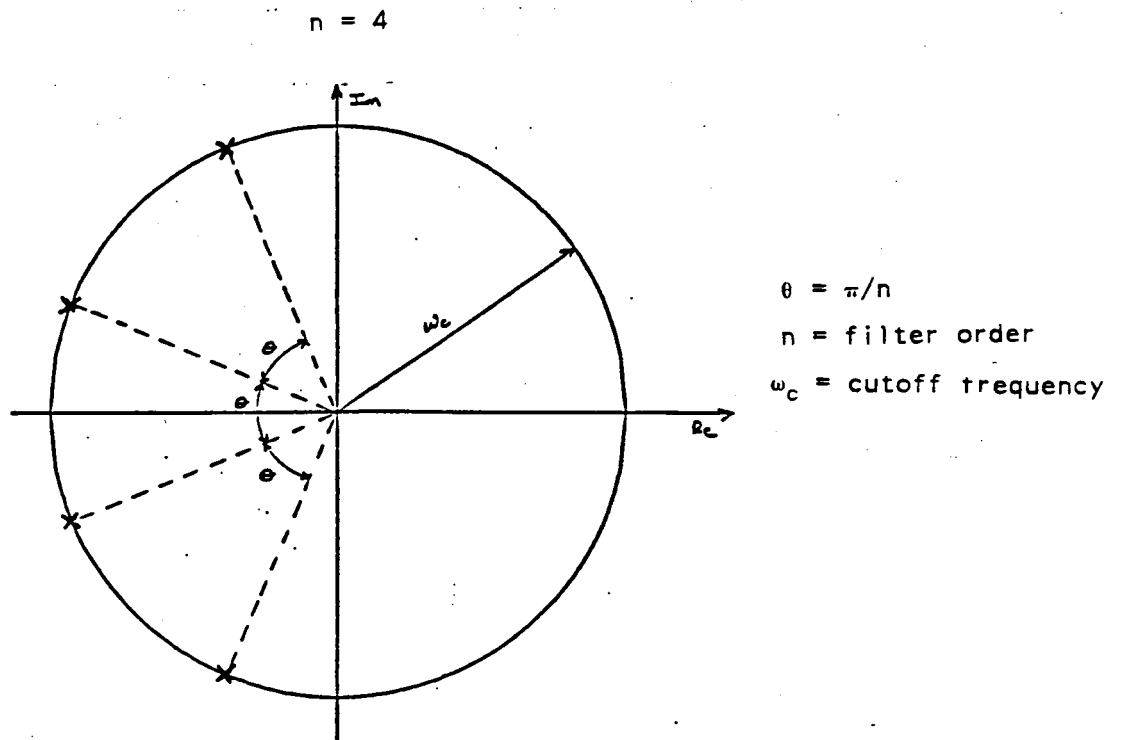


Figure 3.6 Butterworth Pole Pattern

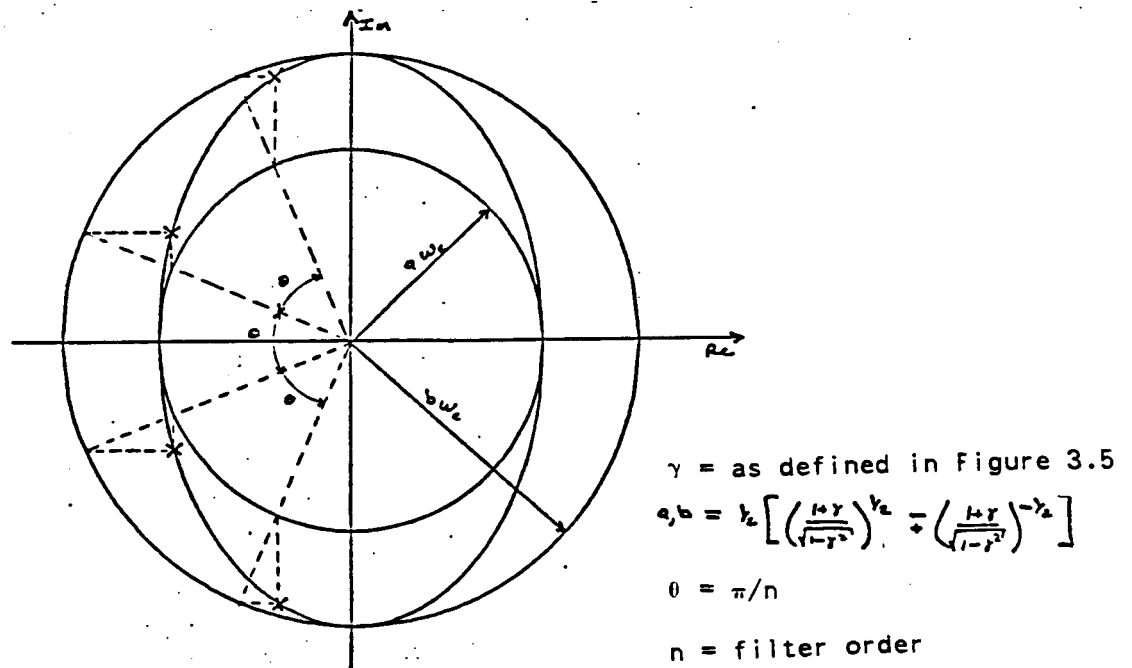


Figure 3.7 Chebyshev Pole Pattern

The bandpass filter will be twice the order of the lowpass filter prototype. An 8th order bandpass filter will have sides that drop away like 4th order lowpass filters. Figure 3.8 shows the magnitude response for Butterworth and Chebyshev 4th and 8th order bandpass filters. For this thesis the 8th order Butterworth bandpass filter was selected because the 4th order did not seem to adequately reject frequencies outside the passband.

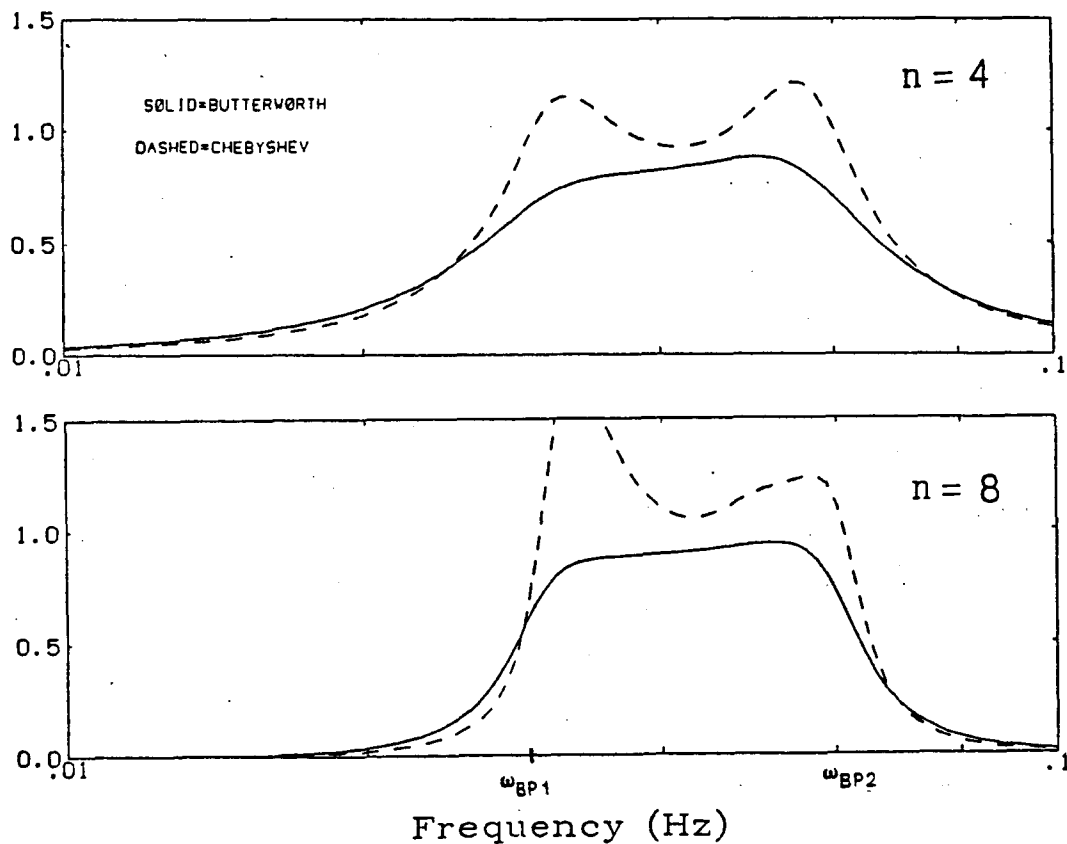


Figure 3.8 Bandpass Filter Comparison

In implementing a digital filter, finite wordlengths become important. Rounding off the filter coefficients will change the performance of the filter. Larger filters will, in general, require higher precision coefficients. Large filters should therefore be designed by cascading smaller filters. The 8th order digital bandpass filter can be broken up into two 4th order bandpass filters which come from each pair of complex conjugate lowpass poles. Figure 3.9 shows the effect cascading has on an 8th order bandpass filter with double precision coefficients. Some of the poles of the uncascaded filter fall outside the unit circle actually making the filter slightly unstable.

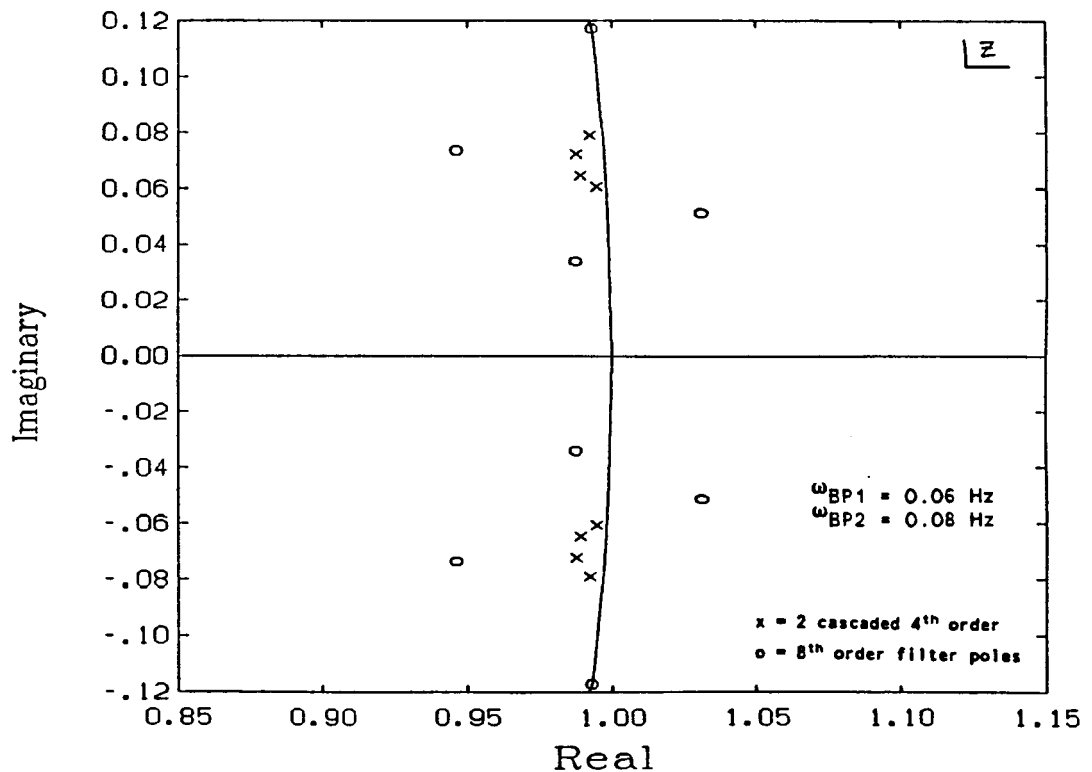


Figure 3.9 Effect of Cascading on Filter Poles

In addition to cascading, it is also important to use a large enough coefficient wordlength. Figure 3.10 shows half of the complex conjugate poles for a cascaded 8th order bandpass filter with different wordlengths. Straight single precision is inadequate, but calculating the coefficients in double precision and truncating to single precision for implementation shows little variation from full double precision implementation. Since single precision will mean less computer load, calculating in double precision and truncating to single precision for implementation is the method picked for this thesis.

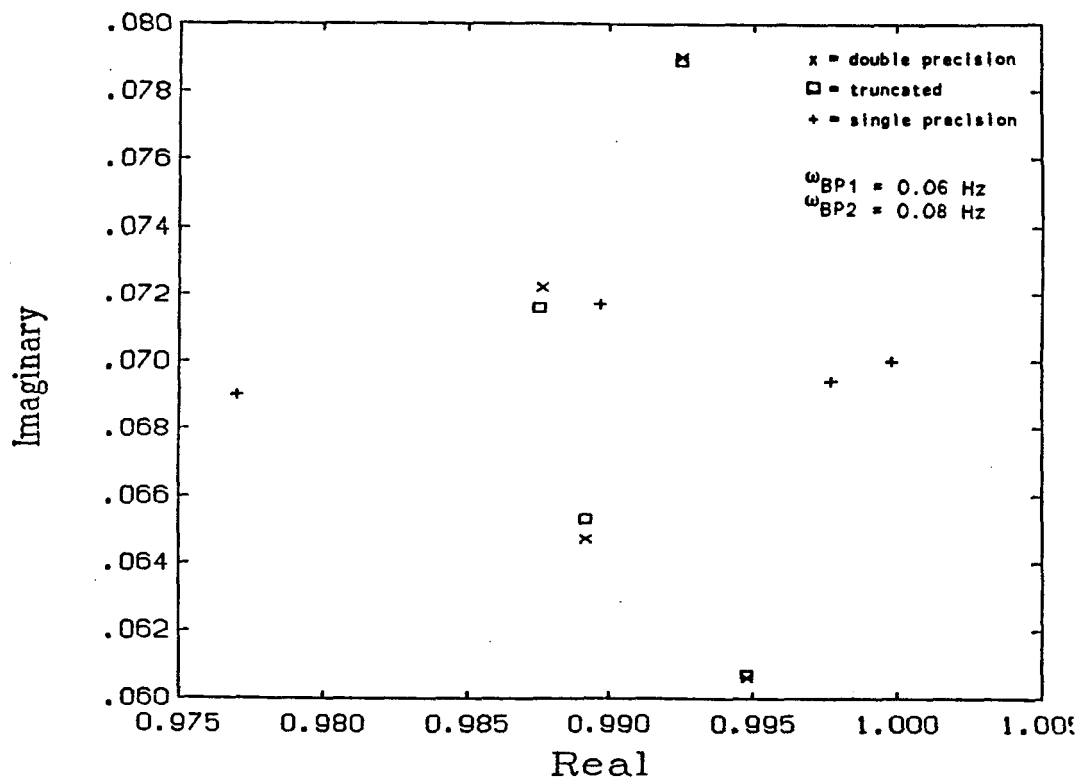


Figure 3.10 Wordlength Effect on Filter Poles

3.7 Frequency Estimation

For each mode isolated by the bandpass filters, the frequency can be estimated by measuring the time between the signals zero-crossings. This will give a measurement of half the period of the bending mode. After each bandpass cycle, the sign of the output is compared to the sign of previous output. A change of sign will indicate that the signal has crossed zero.

To determine when during the time-step the crossing occurred, the signal is assumed to be linear throughout a time-step. This linear assumption will be good if the time-step, ΔT , is much smaller than the period, T . Figure 3.11 shows the linear approximation for the zero-crossing.

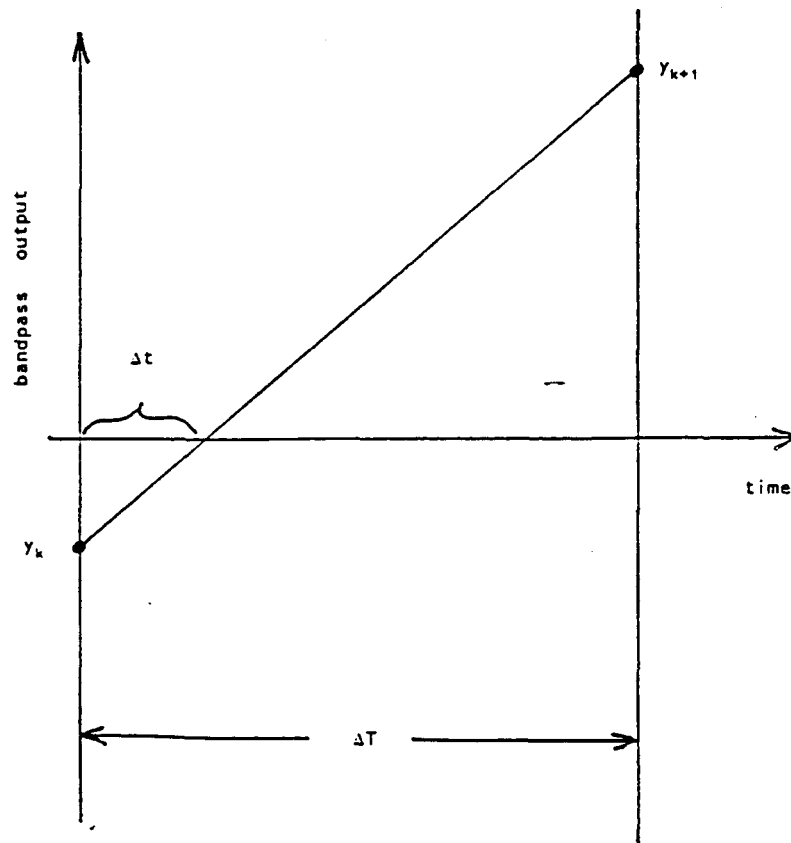


Figure 3.11 Linear Approximation for Zero-Crossing Measurement

From Figure 3.11, the fraction of the time-step where the crossing occurs, Δt , will be

$$\Delta t = \frac{y_k \Delta T}{y_k - y_{k+1}} \quad (3.11)$$

The total time between crossings is calculated as

$$T_m = (\Delta T - \Delta t_{\text{previous crossing}}) + K \Delta T + \Delta t \quad (3.12)$$

where K is the number of time-steps in the half-period where no crossings occurred and T_m will be the measured half-period. Each crossing will yield a new measurement of the frequency, ω_m , which will be

$$\omega_m = \frac{\pi}{T_m} \quad (3.13)$$

Nearby bending modes will only be partially attenuated by the band-pass filter. These external modes leaking into the bandpass filter's output will act as a driving noise in the frequency estimation. This noise will cause the measured frequency to oscillate about the true frequency. Smoothing of the frequency measurement was therefore added to filter out these perturbations while tracking the mean of the signal, which should correspond to the actual bending frequency.

To smooth the signal, the frequency measurement is passed through a second-order system. The natural frequency and damping ratio can be varied to achieve a good tradeoff between noise rejection and tracking speed. For the Shuttle with large payloads attached to its RMS, bending frequencies of interest usually fall between 0.03-0.2 Hz. A second-order system with a natural frequency of 0.015 Hz and a damping ratio of 0.707 was found to give good performance.

When the bending mode frequencies are closely spaced together or when the bending modes cannot be predicted very well, many bandpass filters with narrow passbands should be used to prevent multiple bending modes from getting through a single bandpass filter. A beat response will occur when two bending modes of similar frequency and amplitude get through the same bandpass filter. This beat response is shown in Figure 3.12 along with its effect on the measured and smoothed frequency. Periodically, the time between zero-crossings will be quite short, leading to spikes in the measured frequency. The smoother will try to follow these spikes causing large errors in the estimated frequency.

A test was inserted to check whether the measured frequency is more than 10% different than the estimated frequency. If it is, then the measurement is changed to be limited to the 10% difference. This will eliminate large spikes and yet allow actual step changes in the frequency to be tracked.

3.8 Estimating Modal Amplitude

A notch filter can be assigned to each estimated bending mode. This will distort the measurement signal more than is necessary since many bending modes may be too small to be of concern. Limiting the notch filtering to only those modes with significant amplitudes will reduce observation spillover while minimizing the distortion of the notched signal. Estimating the modal amplitudes was therefore included with the frequency estimation.

The amplitude of each bending mode is estimated using the output of each bandpass filter. This output is oscillatory and will have the form $A \sin \omega t$. Squaring this output will give

$$(A \sin \omega t)^2 = A^2 \sin^2 \omega t = \frac{A^2}{2} - \frac{A^2}{2} \cos 2\omega t \quad (3.14)$$

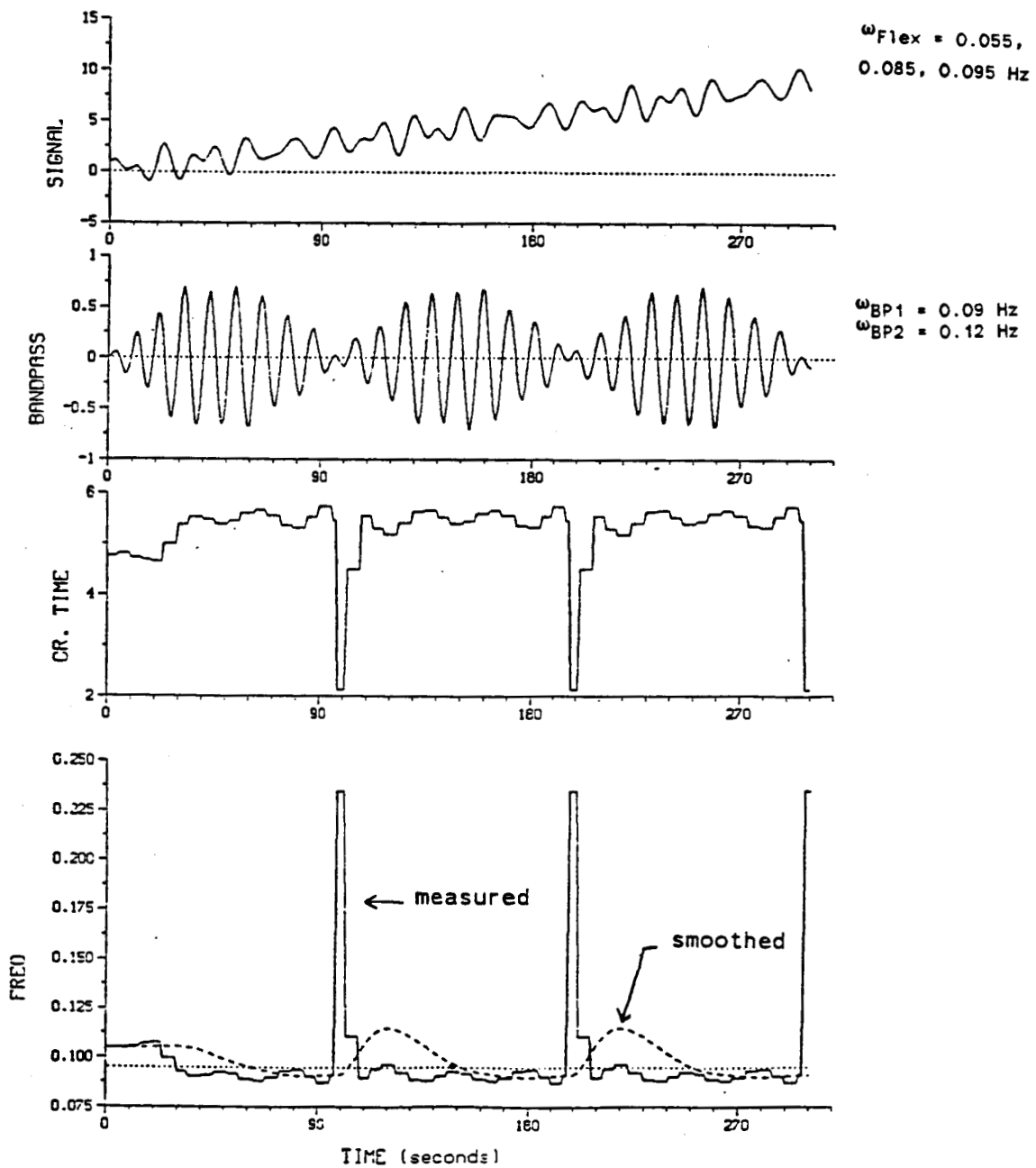


Figure 3.12 Beat Response

Passing this through a lowpass filter will eliminate the second term leaving $A^2/2$. The amplitude can then be found by multiplying by 2 and taking the square root. For the Shuttle, the measurement will be an attitude but the angular rates will be of greater concern. The amplitude of the angular rate can be estimated from the attitude as

$$A_{\text{rate}} \approx A \omega_e \quad (3.15)$$

where ω_e is the estimated frequency. In summary, the angular rate of a bending mode is estimated from the attitude measurement as

$$\begin{aligned} \text{Measured Attitude} &\rightarrow \text{Bandpass} \rightarrow ()^2 \rightarrow \text{Lowpass} \\ &\rightarrow \times 2 \rightarrow ()^{1/2} \rightarrow \times \omega_e = \text{Angular Rate Estimate} \end{aligned}$$

3.9 Timing Considerations

The digital bandpass filters don't necessarily need to run at the same rate that the measurements used for attitude control are taken. A longer time-step will lessen the computer load. The bandpass time-step should, however, be short enough to prevent aliasing, and to keep the linear assumption used in determining the zero-crossing time valid.

When an oscillating signal is represented by a discrete set of points, the sinusoidal signal that passes through the points will not be unique. This is called aliasing; an example is presented in Figure 3.13. Aliasing will occur when there are bending modes of significant amplitude with frequencies above the Nyquist frequency, F_N , which is defined as

$$F_N = \frac{1}{2 \Delta T} \quad (3.16)$$

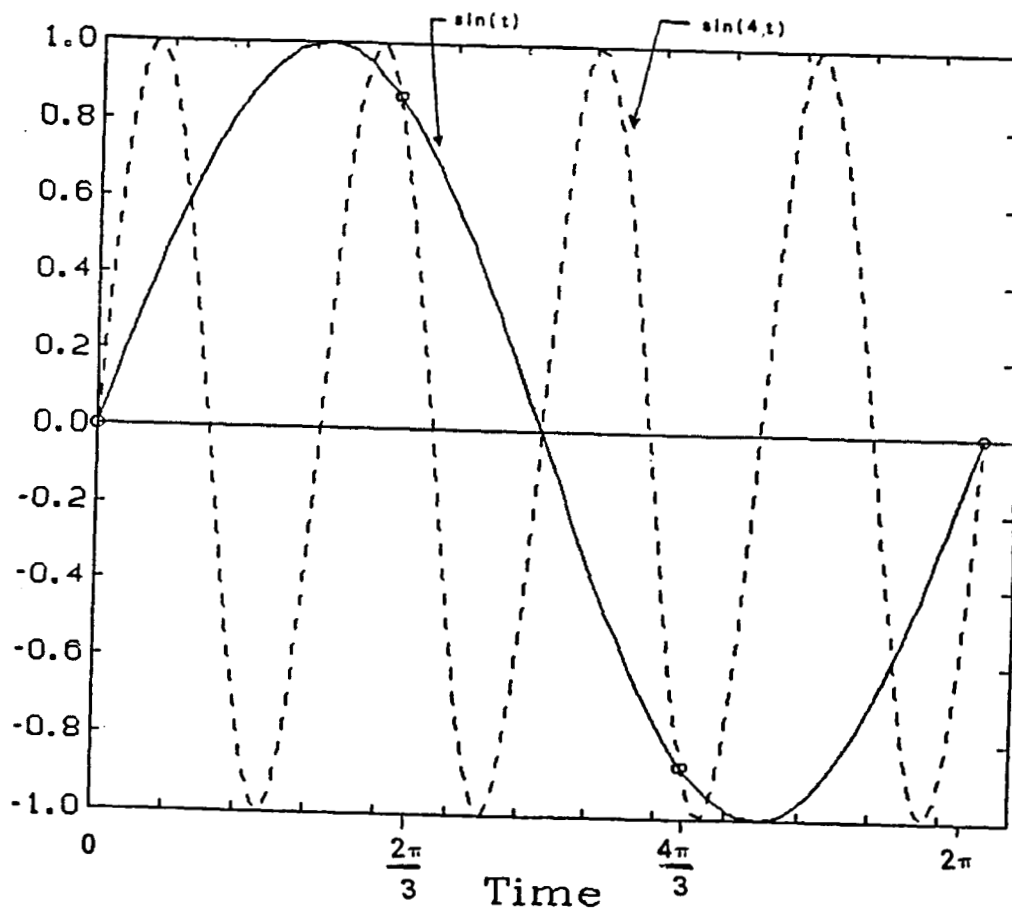


Figure 3.13 Example of Aliasing

For the shuttle, the significant bending modes are usually below around 0.2 Hz. Choosing the time-step of the bandpass filters to give a Nyquist frequency well above 0.2 Hz will prevent any aliasing problems.

In determining the zero-crossing time, the signal was assumed to be linear over a sampling period. This assumption will be good if the bending mode's period is much longer than the bandpass time-step. Again taking 0.2 Hz as the worst case, the smallest expected period will be 5 seconds. A bandpass time-step much less than this will justify the linear assumption used.

The attitude of the Shuttle is measured every 0.16 seconds. The bandpass filters are chosen to run for only one axis at each measurement. This will make the bandpass time-step three times the measurement interval, as there are three axes, so $\Delta T_{BP} = 0.48$ seconds. This gives a Nyquist frequency of 1.04 Hz which is well above 0.2 Hz. The shortest expected important modal period is around 5 seconds which is over 10 times the bandpass time-step. Running the bandpass filters one axis at a time will give a short enough time-step and the computer load of the frequency identification will be cut by a factor of three.

CHAPTER 4

NOTCH FILTERS

4.1 Introduction

This chapter presents the design of the notch filters, particularly 2nd and 4th order filters. A simple model consisting of a rigid body plus one bending mode is used to represent a flexible spacecraft. The combined frequency response of this model and the notch filters is used to compare the different order filters and to study how errors in the bending frequency estimates can affect the system. Added phase lag due to the notch filters is seen to be of potential concern suggesting that the 2nd order filter may be a better choice than higher order designs.

4.2 Notch Filter Design⁶

The notch filters are designed very much like the bandpass filters in Section 3.6. An analog lowpass filter prototype is selected. The lowpass prototype is then transformed into a bandstop filter which is converted into digital form by the use of a bilinear transform.

The Butterworth design was chosen as the lowpass prototype because its smooth frequency response will minimize distortion of the signal outside the stopband. The pole patterns of the Butterworth lowpass prototypes for 2nd and 4th order notch filters are shown in Figure 4.1.

Given the lowpass filter with transfer function $H_{LP}(s)$ having a cut-off frequency ω_c , an analog bandstop filter can be constructed with the frequency transformation,

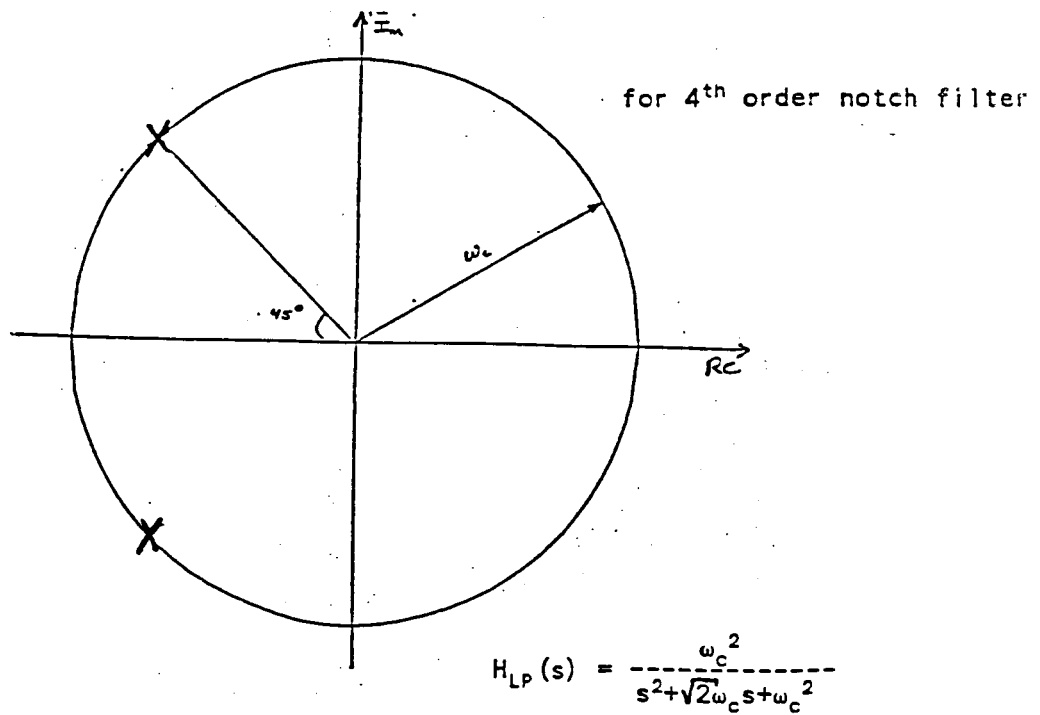
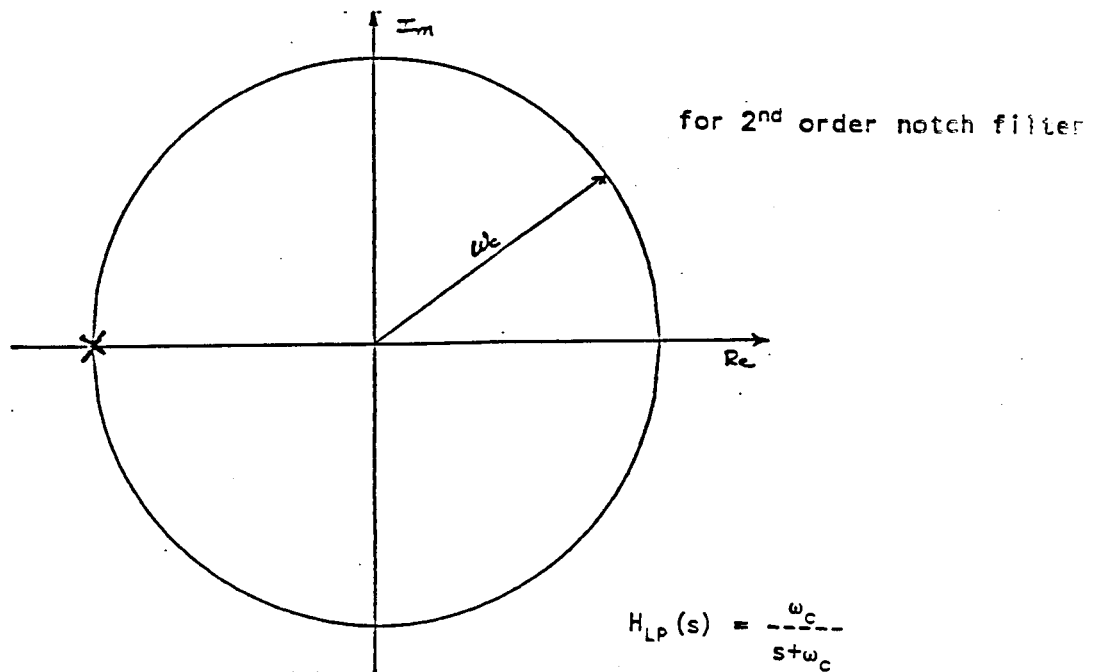


Figure 4.1 Butterworth Lowpass Prototype Pole Locations

$$H_{BS}(s) = H_{LP}\left(-\frac{\omega_c^2 s}{s^2 + \omega_1 \omega_2}\right) \quad (4.1)$$

with

$$\omega_c = \omega_2 - \omega_1 \quad (4.2)$$

where ω_1 and ω_2 are the stopband frequencies. When ω_1 and ω_2 are close together, the stopband will be in the shape of a narrow notch. The center frequency of this bandstop, or notch filter, will be

$$\omega_N = \frac{\omega_1 + \omega_2}{2} \quad (4.3)$$

Ideally, the center frequencies of the notch filter will be equal to the bending mode frequencies. The notch filter should have a stopband wide enough to allow for small errors in the estimated frequency but not too wide as to overly distort the signal. For the rest of this chapter and in the final design, the passband frequencies are chosen as $\omega_1 = 0.9 \omega_N$ and $\omega_2 = 1.1 \omega_N$.

A bilinear transform is used to convert the analog notch filter to a digital form. As with the bandpass filter, the stopband frequencies are prewarped by

$$\begin{aligned} \omega_1' &= \tan(\omega_1 T/2) \\ \omega_2' &= \tan(\omega_2 T/2) \end{aligned} \quad (4.4)$$

where T is the time-step of the digital notch filter. The digital transfer function, H_N , can now be obtained by the transformation

$$H_N(z) = H_{BS}\left(\frac{z-1}{z+1}\right) \quad (4.5)$$

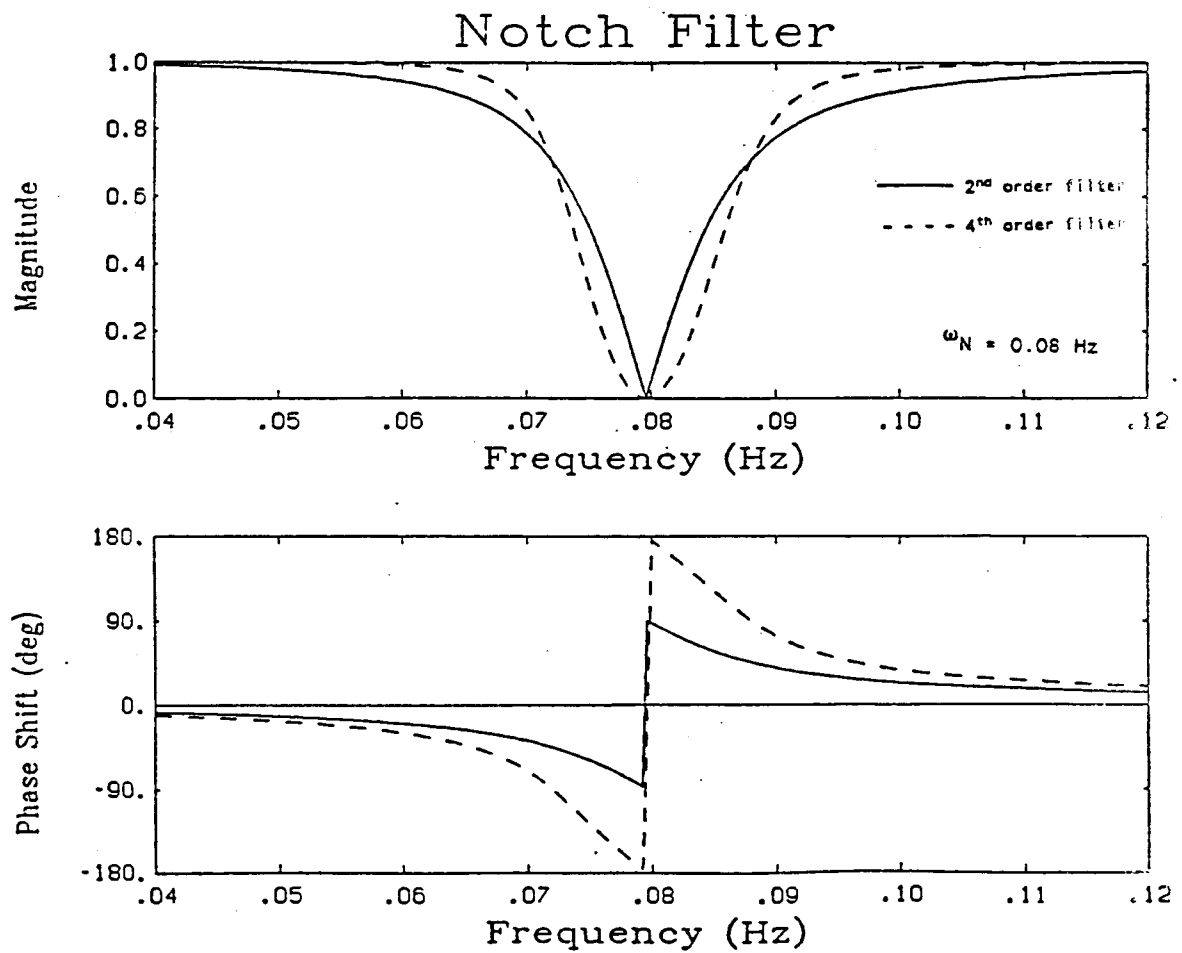


Figure 4.2 Notch Filter Frequency Response

The frequency response of a 2nd and 4th order notch filter is shown in Figure 4.2. The 4th order notch filter has sharper cutoffs in the magnitude response but has twice the phase shift of the 2nd order filter. If added phase lag is of concern, a higher order filter is not necessarily better than a low order filter.

4.3 Effect of Notch Filters

To study the effect of the notch filters, a simple plant consisting of a rigid body plus one bending mode is used to represent a flexible spacecraft. This simple model is used to compare different order notch filters and to study how errors in estimating the bending frequencies may alter the performance of the system.

A block diagram of the simple spacecraft model is shown in Figure 4.3. Part of the rigid body control acceleration goes into exciting the bending mode; this fraction is represented by β . For this analysis, $\beta=0.1$ and the structural damping, $\zeta_b=0.005$. Figure 4.4 shows the frequency response of this system. The spike in the magnitude response is due to the bending mode and can lead to closed-loop instabilities.

Figure 4.5 shows the combined frequency response of the plant and notch filter. Both 2nd and 4th order notch filters eliminate the spike in the magnitude response. The 4th order filter, however, adds a larger phase shift. Figures 4.6 and 4.7 show the combined frequency response with the notch filter center frequency in error by 5% low and high respectively.

The 2nd and 4th order filters can easily remove the flexible motion from the signal when the bending frequency is known. When there is an error in the frequency estimate, the effect of the notch filters can substantially change. A high estimate is of particular concern because the notch filters will add phase lag at the bending frequency with only

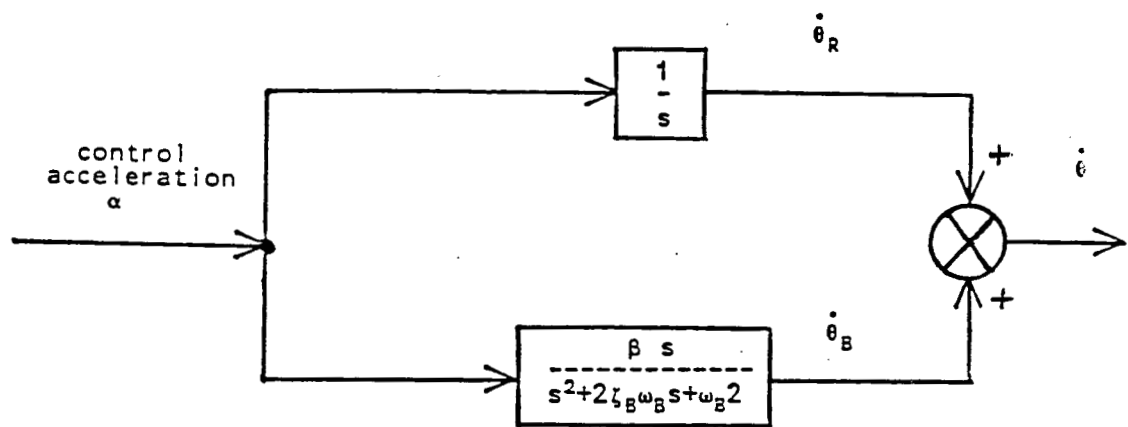


Figure 4.3 Rigid Body Plus Bending Mode

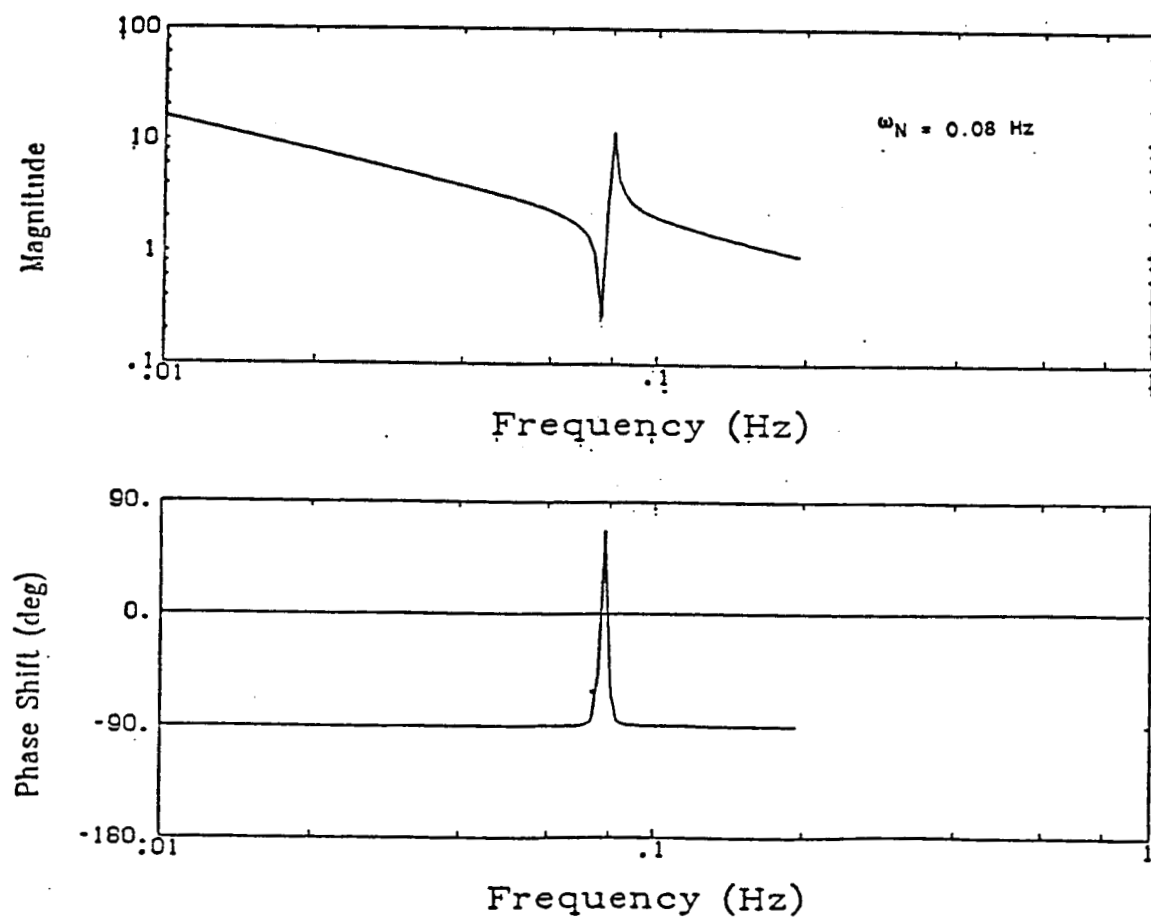


Figure 4.4 Frequency Response of Plant

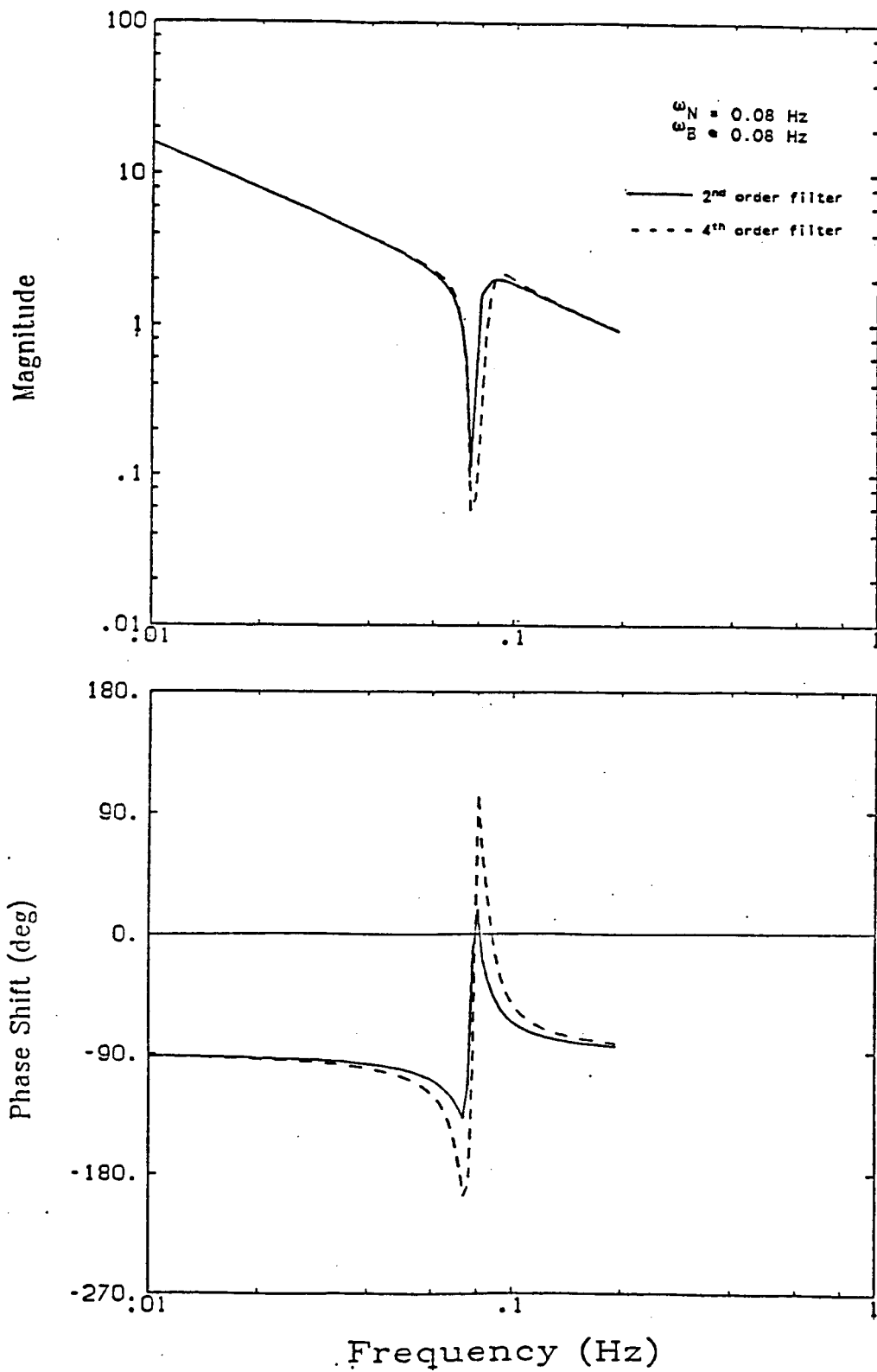


Figure 4.5 Notch Filter Centered on Bending Mode

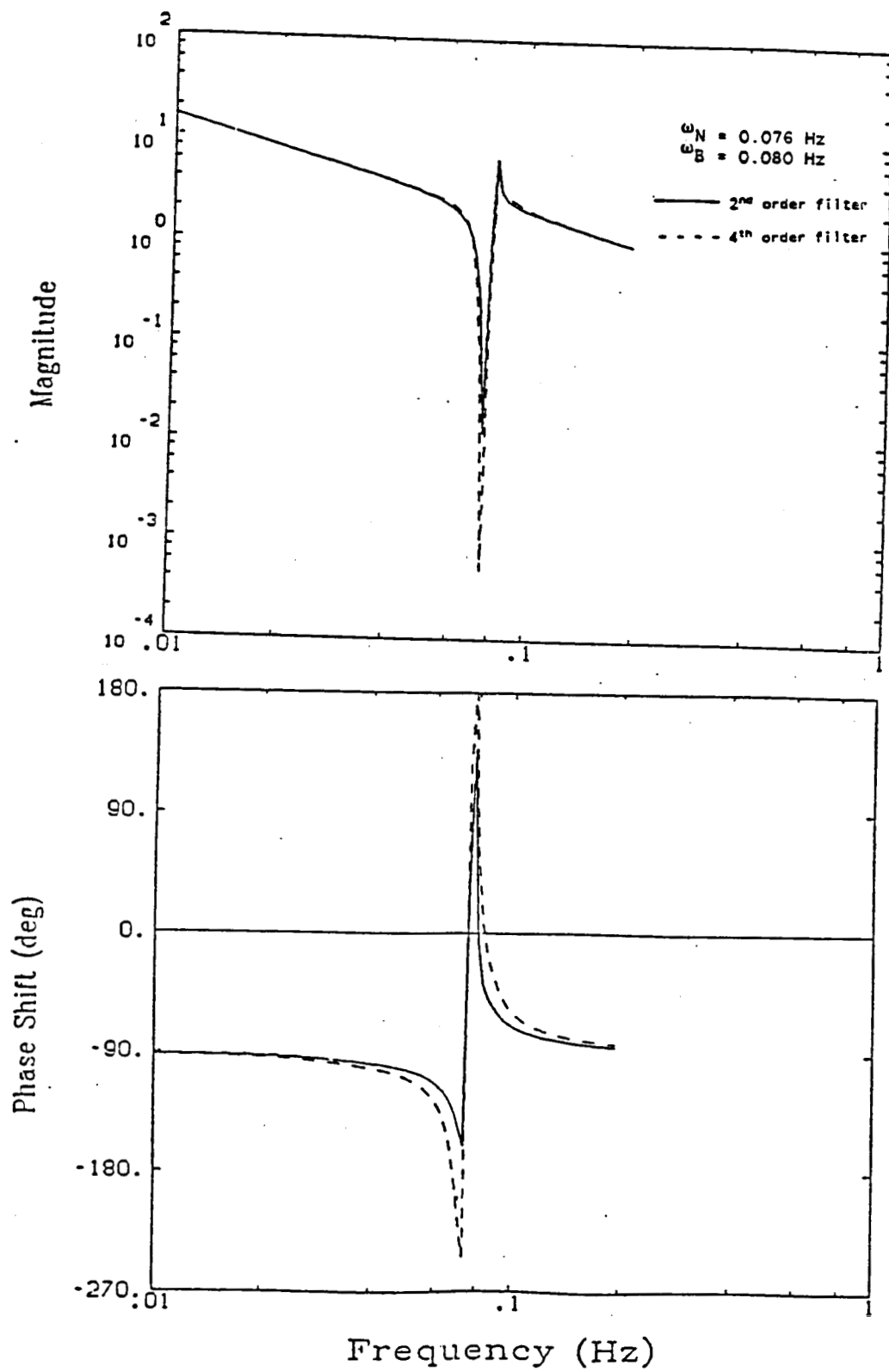


Figure 4.6 Notch Filter Centered 5% Low

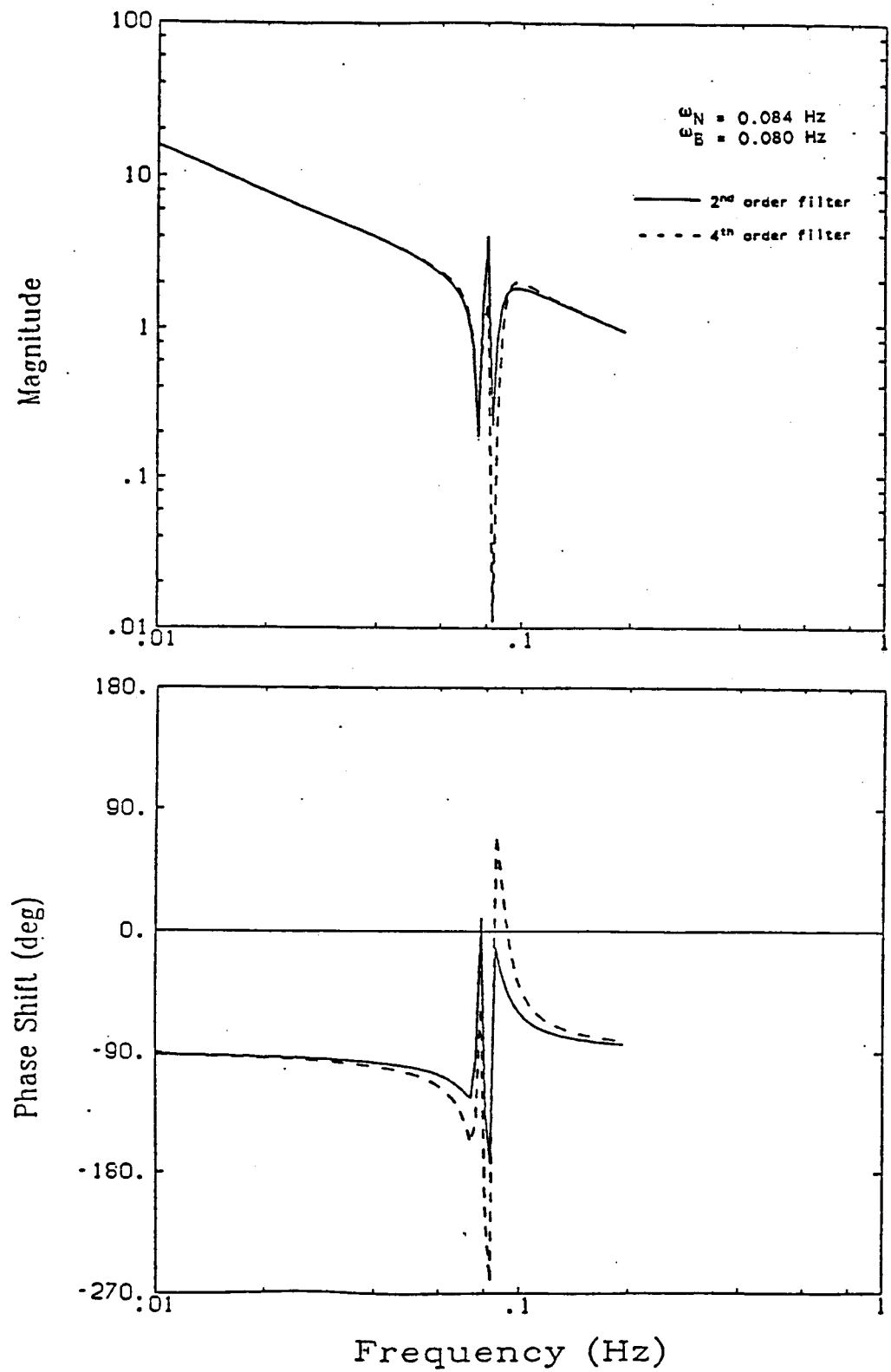


Figure 4.7 Notch Filter Centered 5% High

partial attenuation of the magnitude. This added phase lag will tend to destabilize the system. From the frequency plots, the 2nd order filter would seem to be the better choice. The slightly better magnitude response of the 4th order filter does not make up for the added phase lag introduced.

CHAPTER 5

REVIEW OF SPACE SHUTTLE ATTITUDE CONTROL SYSTEM

5.1 Introduction

The spillover reduction technique described in the last two chapters was designed with the Space Shuttle in mind. This chapter reviews the Shuttle's attitude control system to allow more detailed design and analysis of the notch filters and their effect on the closed-loop system. The sources of flexible dynamics are also reviewed. There are many problems created when this flexibility interacts with the attitude control system. It is hoped that notch filtering of the measurement signal would help alleviate some of these problems.

5.2 Overview of the On-Orbit Attitude Control System⁷

A block diagram of the space shuttle on-orbit attitude control system is shown in Figure 5.1. Attitude and rate errors, θ_e and ω_e , are sent to the phase plane control system which produces a commanded acceleration, a_c . The control jets are fired to produce an acceleration, a , as close as possible to a_c . The resulting attitude of the Shuttle is measured by the Inertial Measurement Unit (IMU). This measured attitude, θ_m , along with the feedforward prediction of the rate change due to the jet firing, $\Delta\omega_{\text{PRED}}$, are used to produce an estimate of the angular rate, ω . The estimated rate and measured attitude are fed back to form the error signal. The control system cycles every 80 ms, with IMU measurements every 160 ms.

The control system operates for each axis separately. Euler coupling between axes is usually not of concern because the angular rates are usually quite small. Euler coupling will appear as a small acceleration

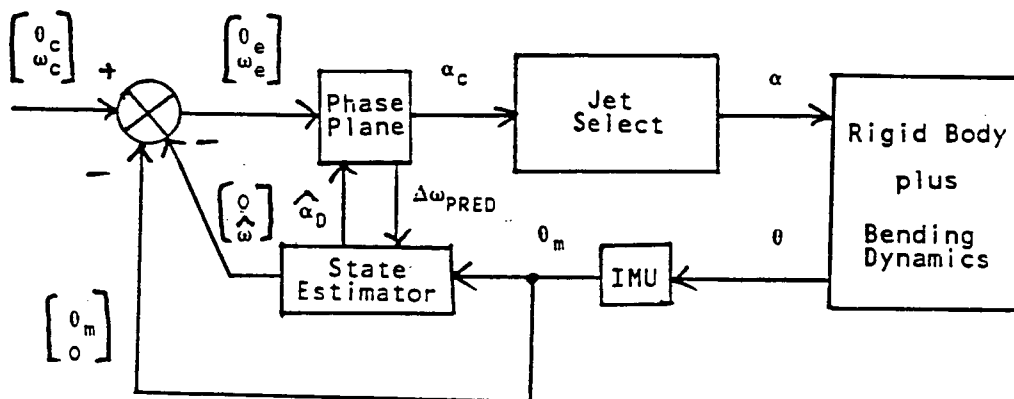


Figure 5.1 Attitude Control System

disturbance which can be estimated along with external disturbances such as those due to gravity gradient torques.

The control system has two levels of operation. For larger control action, the Primary Reaction Control System (PRCS) is used. The PRCS uses the primary jets to control the spacecraft. For tighter control about an operating point, the Vernier Reaction Control System (VRCS) is used. The VRCS uses the much less powerful vernier jets. The deadbands and rate limits of the phase plane, the state estimator gains, and the jet selection method are different for PRCS and VRCS modes of operation.

5.3 Control Jets

The control jets are selected to fire to produce an acceleration which matches as closely as possible the commanded acceleration. The control jets used for attitude control are a number of on-off thrusters that are placed around the Shuttle. There are 38 primary jets which produce a force of 870 lbs., and 6 vernier jets which produce 24 lbs. of force. The jet locations and the directions in which they fire are shown in Figure 5.2.

The primary and vernier jets are selected by two different methods. The primary jets are selected by a table look-up scheme of preselected jet combinations. The vernier jets are selected by a dot product algorithm. The predicted acceleration vector for each vernier jet is dotted with the commanded acceleration vector. The jet with the largest dot product will come closest to producing the commanded acceleration and so is selected to be fired. If a second jet has a dot product of greater than 0.5 times the first jet's dot product, then this second jet will also fire. Similarly, if a third jet has a dot product of greater than 0.4 times the first jet's dot product, then it will fire too.

ORIGINAL PAGE IS
OF POOR QUALITY

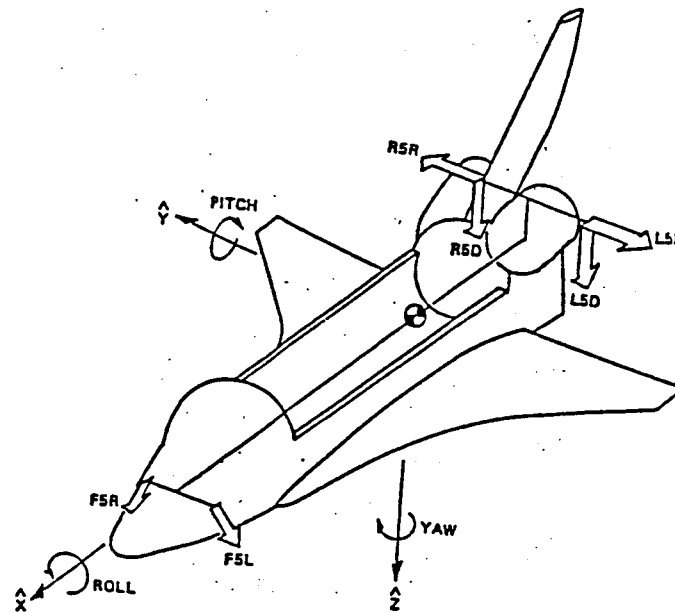
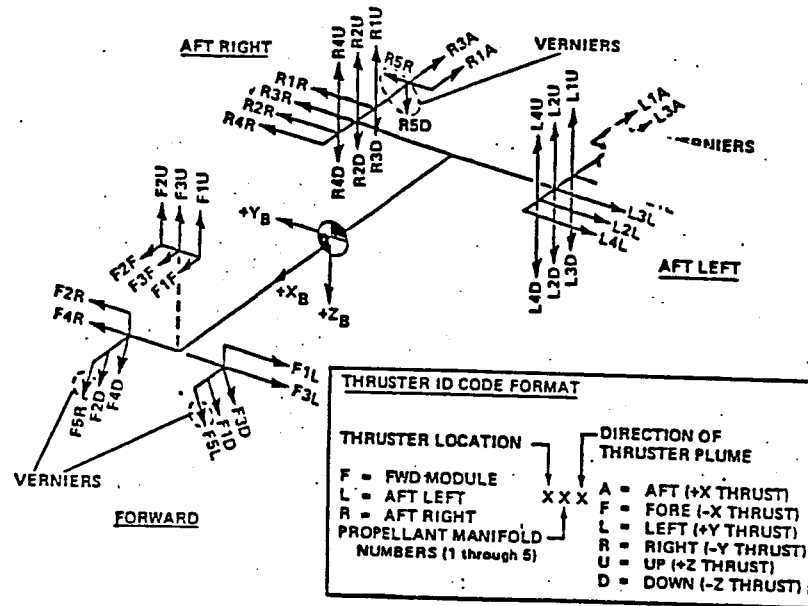


Figure 5.2 Jet Locations and Directions

The change in the Shuttle's angular rate that each jet will produce over one 80 ms cycle is predicted before each flight and loaded into the computer. Up to six sets of these predicted rate changes can be loaded for various expected inertia configurations. When a jet fires, the predicted angular rate change is fed forward to the state estimator. This feedforward information improves the performance of the estimator.

5.4 Inertial Measurement Unit

The Inertial Measurement Unit (IMU) has a stable platform that is kept fixed in inertial space by a set of gyroscopes. The outside of the IMU is fixed to the body of the Shuttle. The stable platform is isolated from the body frame by a series of gimbals. Reading the gimbal angles gives the orientation of the Shuttle with respect to an inertial frame of reference.

The measured gimbal angles are used to form a quaternion that specifies the relationship between the Shuttle's body axes and the inertial frame. For each measurement cycle, this quaternion is constructed and compared to the previous quaternion to produce an attitude increment. The measured attitude used for the state estimator is the previous measured attitude plus the latest attitude increment.

The measurement cycle time is 160 ms, so the measurements are incorporated on every other control cycle. There is a delay in the processing of the attitude measurement of 232 ms. The measured attitude will therefore be approximately three control cycles old when it is used. This delay acts as an additive, frequency dependent phase lag of around 90 deg/Hz.

5.5 State Estimator

The state estimator takes the measured attitude plus the predicted angular rate change due to the jet firings and produces an estimate of the disturbance acceleration and the vehicle angular rate. Sources of the disturbance acceleration will include bending motion, ignored Euler coupling, and external torques such as gravity gradient and aerodynamic torques. The disturbance acceleration estimate is fed to the rate estimator and is also used to adjust a bias switch line in the phase plane. The estimated angular rate is fed back to produce the rate error which drives the control system.

A simple block diagram of the state estimator is shown in Figure 5.3. The state estimator is broken up into two components, a disturbance acceleration estimator and an angular rate estimator. The two were separated to allow independent design so as to achieve different desired response characteristics. The acceleration estimator is designed to track slowly varying disturbances such as those due to gravity gradient torques. The step response of the disturbance acceleration estimator is shown in Figure 5.4.

The rate estimator is designed to correct errors in the jet feedforward information. Different sets of gains are therefore used when primary and vernier jets are in operation. The primary jets produce much larger rate changes, so the estimator gains for primary operation were chosen to give a faster response. When the vernier jets are used, the estimator does not need to be as fast, so the gains were chosen to give a smaller bandwidth which will be better at rejecting noise. The frequency response of the rate estimator for both primary and vernier jets is shown in Figure 5.5.

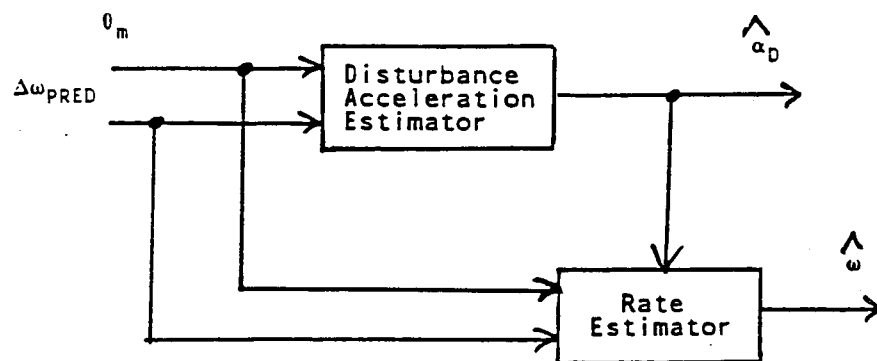


Figure 5.3 State Estimator

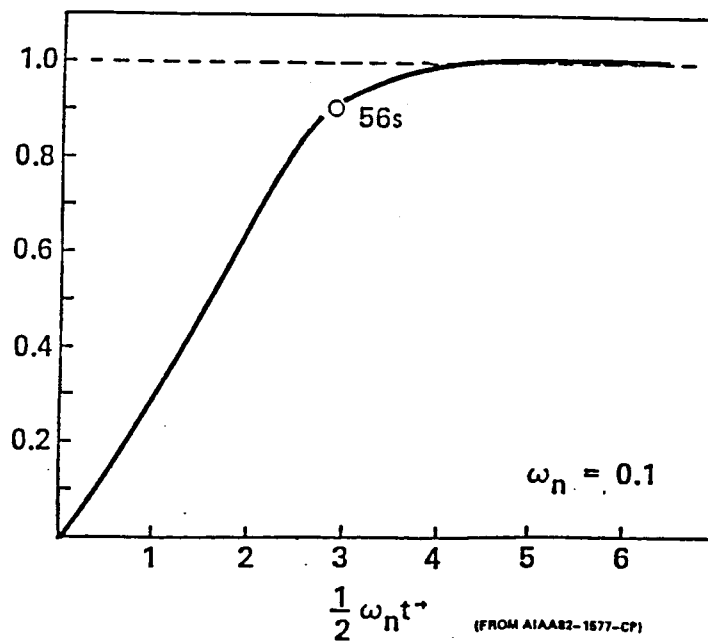


Figure 5.4 Disturbance Acceleration Estimator Step Response

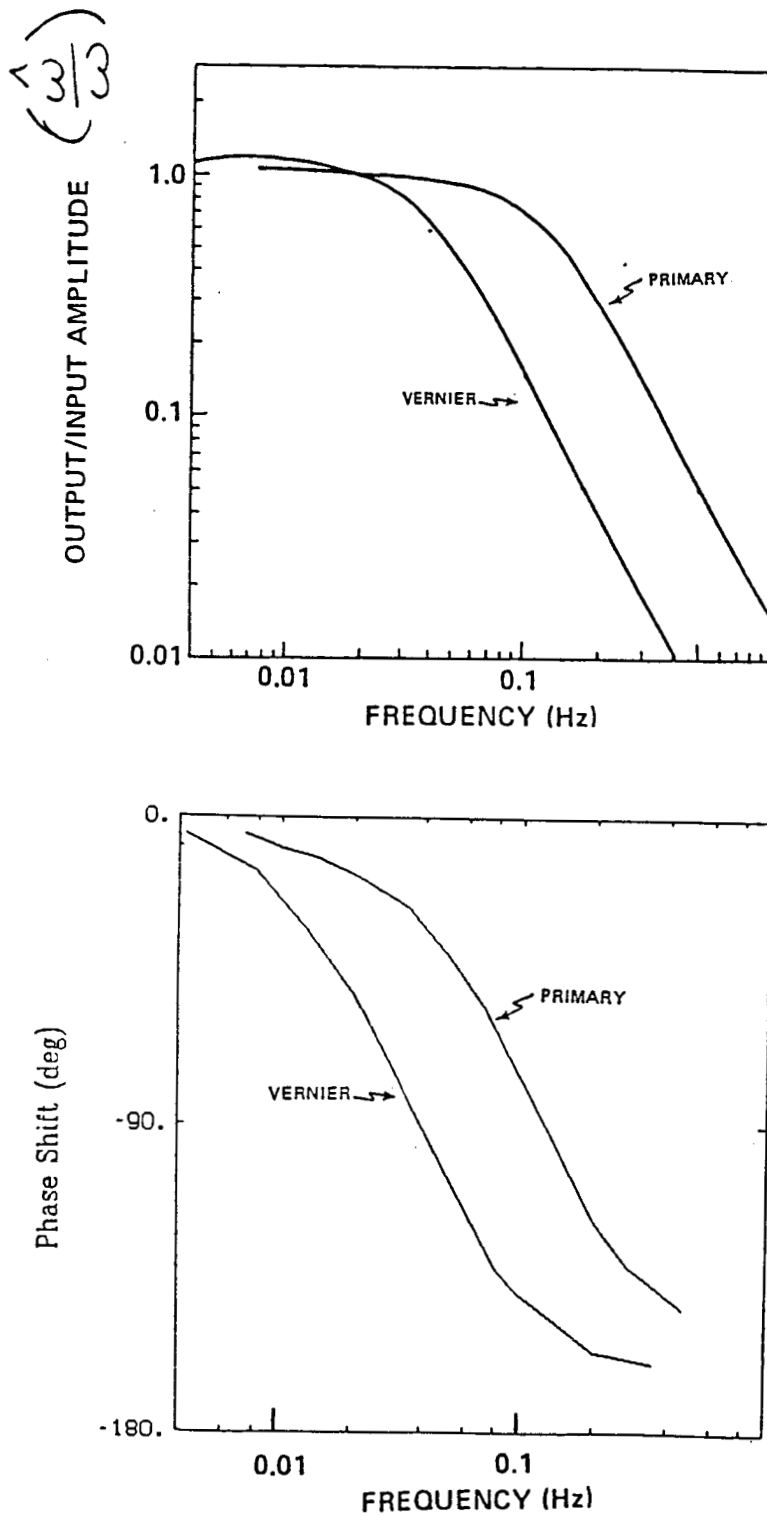


Figure 5.5 Angular Rate Estimator Frequency Response

5.6 Phase Plane Controller

The phase plane controller takes the attitude and rate error for each axis separately and produces a jet firing command for each axis. The jet selection logic takes these commands and determines which jets to turn on or off. Figure 5.6 shows typical phase plane trajectories for the different jet firing commands. The phase plane controller is shown in Figure 5.7. The phase plane deadband and rate limit have a big effect on the performance of the system. Tight deadbands and rate limits will give better tracking about the operating point but will lead to increased jet firings and may also destabilize the system. A typical trajectory is shown in Figure 5.8 where a large initial error is brought into a stable limit cycle about the operating point.

5.7 Sources of Bending Mode Dynamics

The flexibility of concern are those bending modes that are sensed by the IMU but are only partially attenuated by the state estimator. These bending modes will have frequencies below around 0.2 Hz. The flexibility of the orbiter itself will have bending frequencies well above this. Payloads attached to the Shuttle by flexible connections can, however, often lead to low frequency vibrations.

Payloads pivoted out of the Shuttle bay on a tilt table can produce this type of low frequency motion. Examples of such payloads include the Inertial Upper Stage and Centaur with spacecraft. These pivoted payloads can be characterized as having one dominant bending mode. Such payloads can be as heavy as 65,000 lbs. which is over a quarter of the orbiter's 226,000 lbs. A great deal of analytic and simulation analysis^{8,9} has been done for pivoted payloads. This analysis has shown that unwanted jet firings, undesirable excitation of the payload, and even closed-loop instability can result from the low frequency payload-orbiter dynamic interaction.

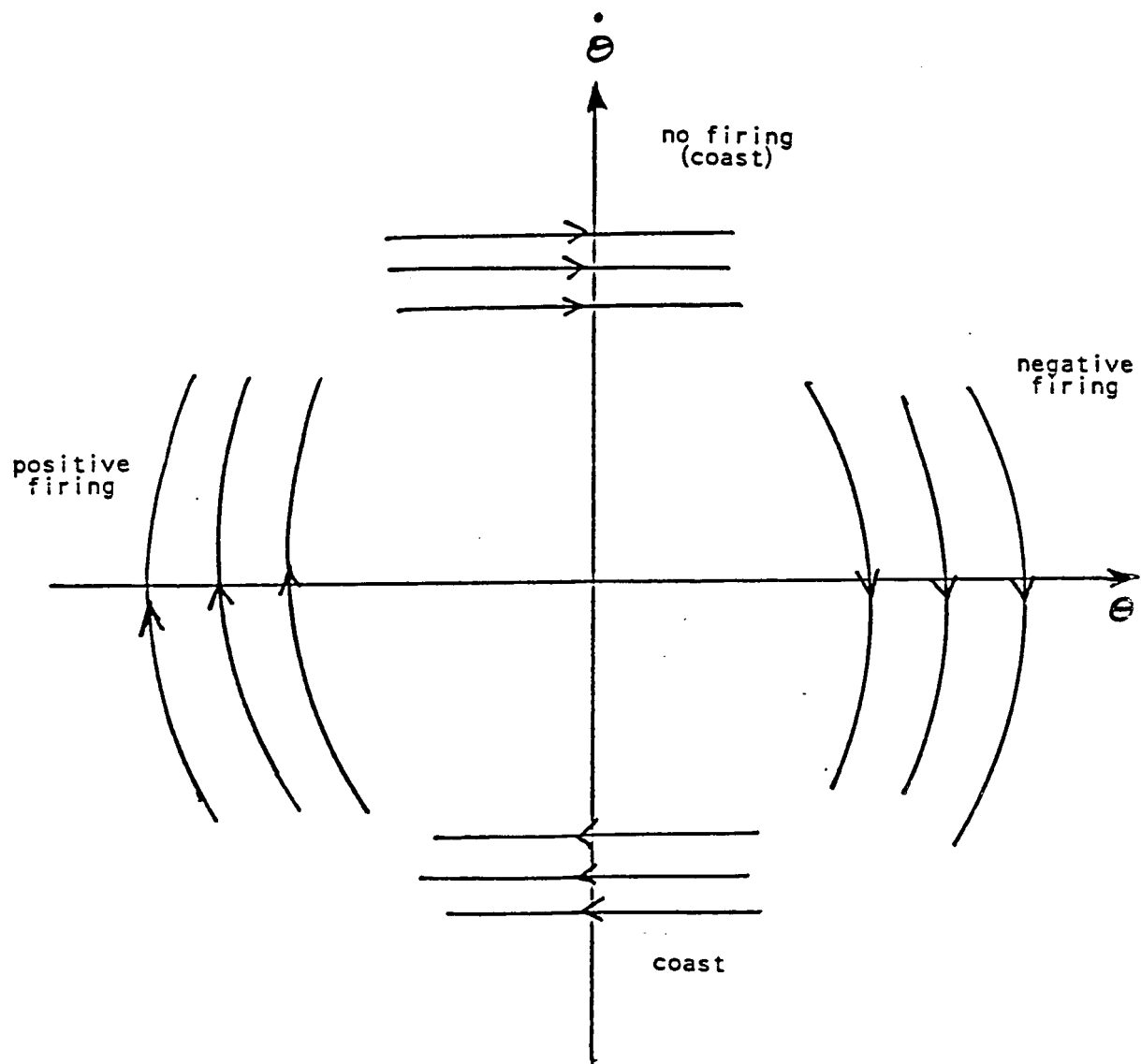
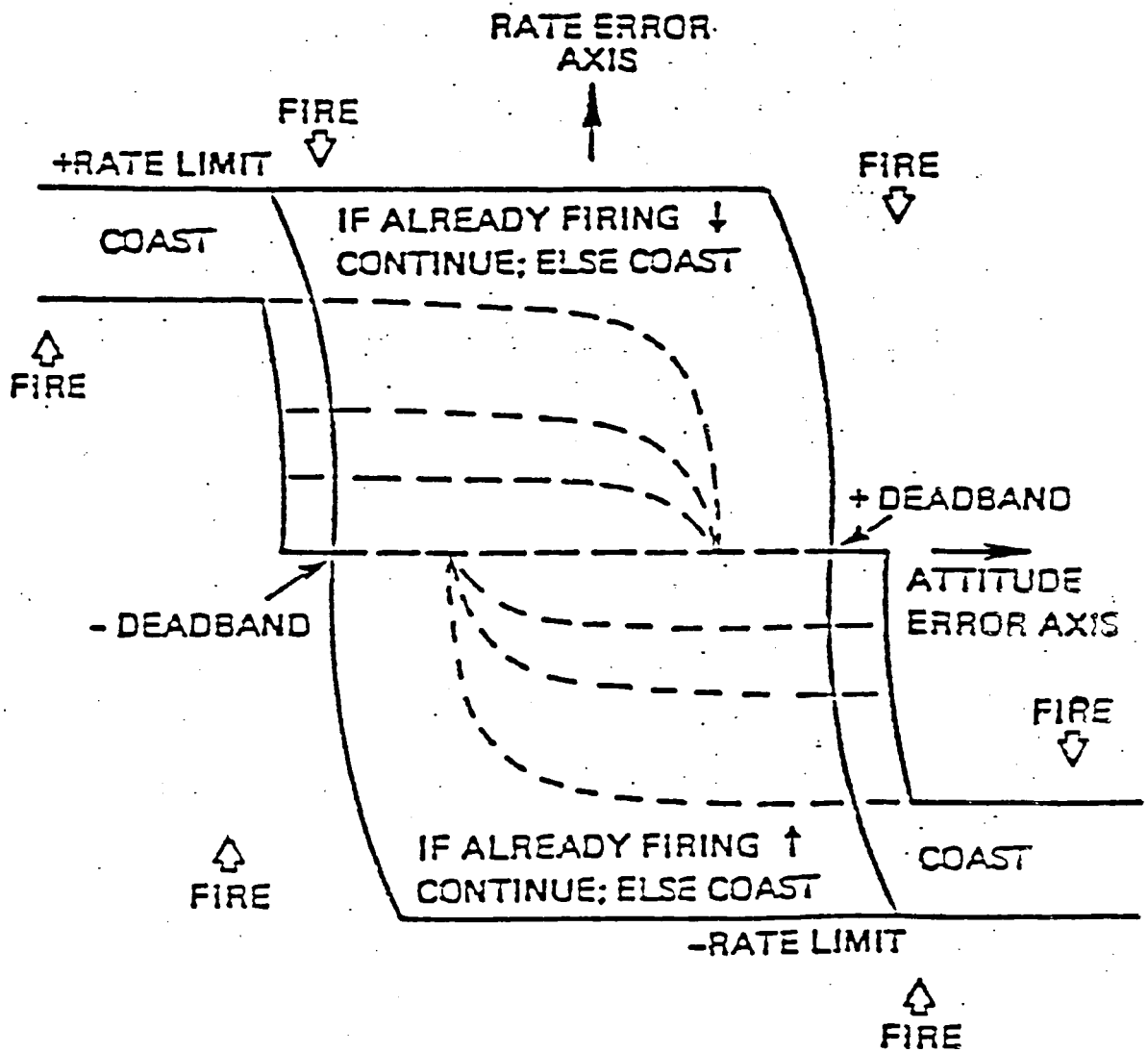


Figure 5.6 Typical Phase Plane Trajectories



----- TYPICAL LOCATIONS FOR MOVABLE CUTOFF LINE

Figure 5.7 Phase Plane Controller

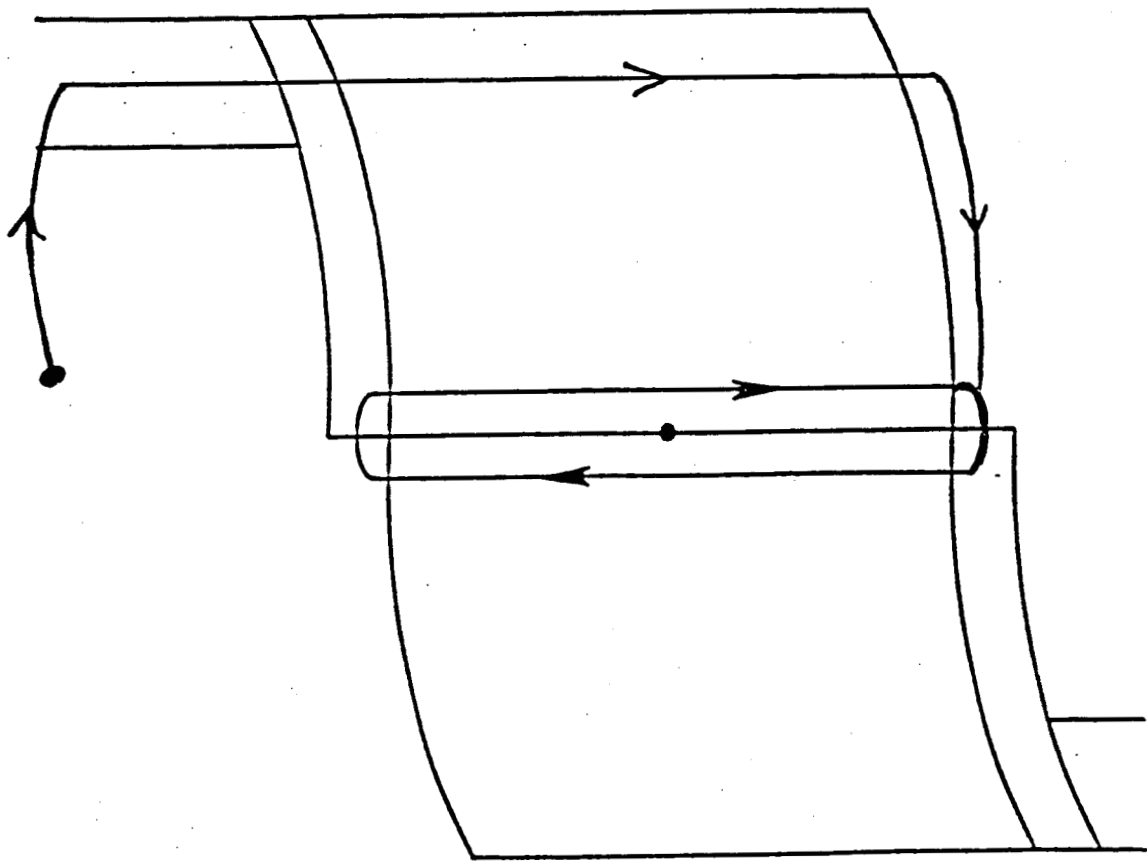


Figure 5.8 Typical Trajectory for Stable Limit Cycle

Payloads attached to the Shuttle's Remote Manipulator System (RMS) are another source of low frequency bending motion. This type of payload-orbiter connection can be particularly troublesome because it may involve many bending modes which may be hard to predict and that will tend to vary with time as the RMS changes in configuration. Figure 5.11 shows roughly how the fundamental bending frequency tends to vary with height above orbiter for different payload masses.

5.8 Problems Caused By Flexibility

The bending modes that can cause problems are those that are sensed by the IMU but are not filtered out by the state estimator. These modes are only partially attenuated by the rate estimator and will be shifted in phase by the delay in the IMU and from the phase lag introduced by the estimator. With tight rate limits, the bending motion that gets through may be large enough to cause jet firings. The added phase lag may cause the jets to fire at the wrong time, further exciting rather than controlling the flexible motion.

This destabilizing jet firing will lead to forced limit cycling, which is undesirable for many reasons including excessive motion of the orbiter, wasted fuel, and large excitation of the payload. To avoid this unstable jet firing, various payload positions and orientations are carefully analyzed with computer simulations with different deadbands and rate limits before each flight. These simulations take a lot of time and money. The range of stable RMS configurations is often found to be very limited for large payloads.

By adding notch filters, it is hoped that the potentially destabilizing bending modes can be removed from the feedback signal. In some cases the forced limit cycling may be prevented from starting, or once started, the frequency estimator can lock onto the unstable mode and stop the jets from firing.

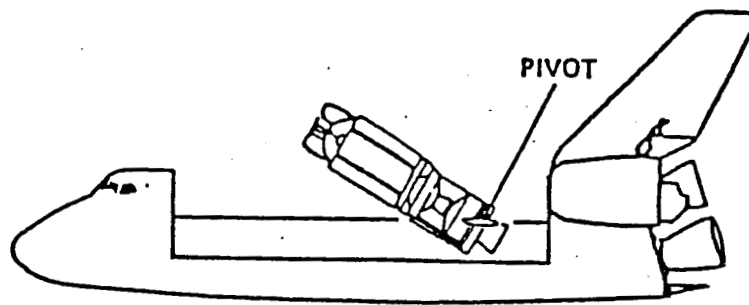


Figure 5.9 Payload Pivoted out of Shuttle Bay

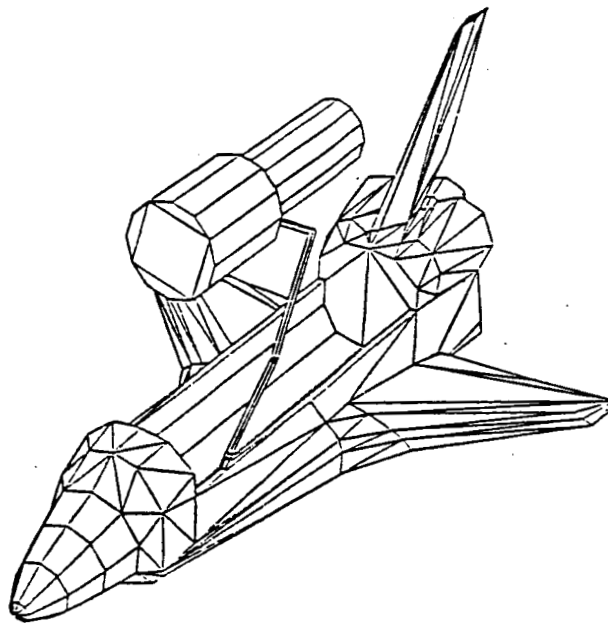
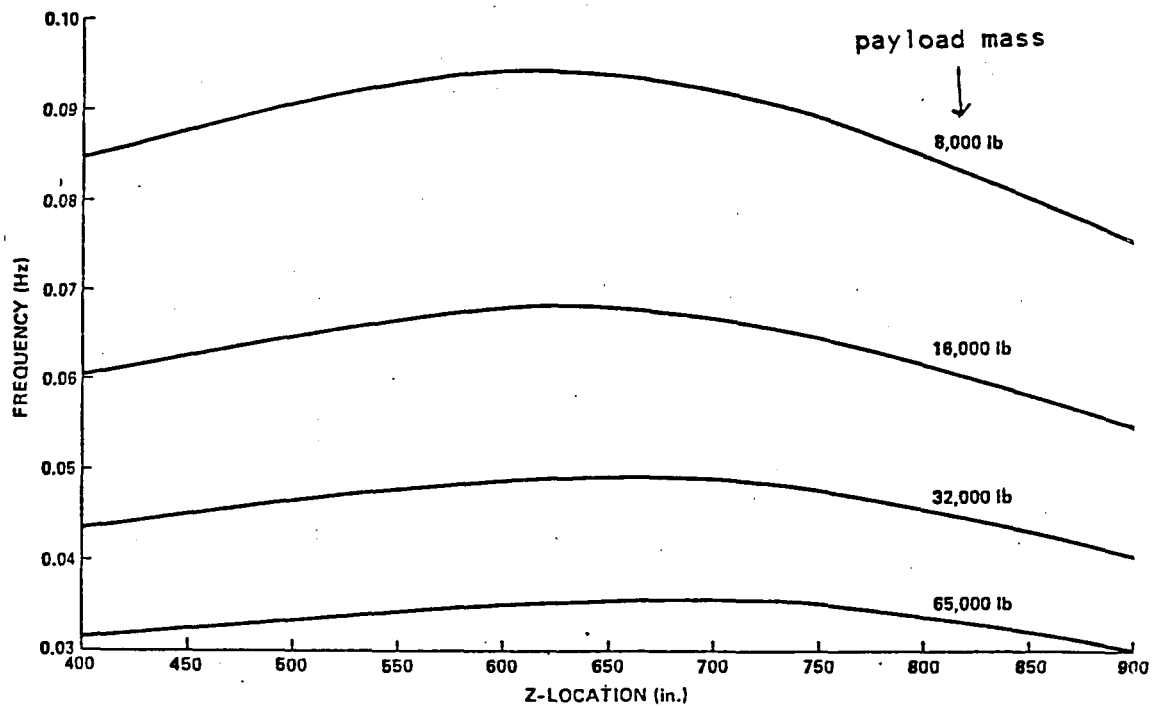


Figure 5.10 Payload Attached to RMS



z = height of payload center of mass above orbiter plus 400 inches

Figure 5.11 Typical Fundamental Frequencies for Payloads Attached to RMS

CHAPTER 6

ANALYTIC ANALYSIS OF CLOSED-LOOP SYSTEM

6.1 Introduction

In this chapter a simplified s-plane model of the Shuttle's dynamics and control system along with a describing function approximation of the nonlinear phase plane controller are used to analyze the effect different notch filters will have on the closed-loop system. Replacing the nonlinear phase plane with a describing function allows for closed-loop limit cycle prediction. The ability of the different notch filters to prevent limit cycles is studied to select a filter design.

In addition to choosing the order of the filters, the describing function analysis is also used to determine the best location for placing the notch filters. How errors in the bending frequency estimate will affect the closed-loop system is also investigated. The results of this analysis will help in deciding when the notch filter coefficients should be changed.

6.2 Sinusoidal Input Describing Function¹⁰

Describing functions are used to approximate the output of nonlinearities for a given input form. The sinusoidal input describing function is calculated based on the assumption that the input to the nonlinearity is a single sinusoid. The describing function is a quasilinear approximation; it is not strictly linear since it is generally a function of the input amplitude and sometimes of the input frequency.

The describing function, $N(A, \omega)$, is chosen to minimize the integral of the squared error between the actual output of the nonlinearity and the describing function output over one period, Figure 6.1.

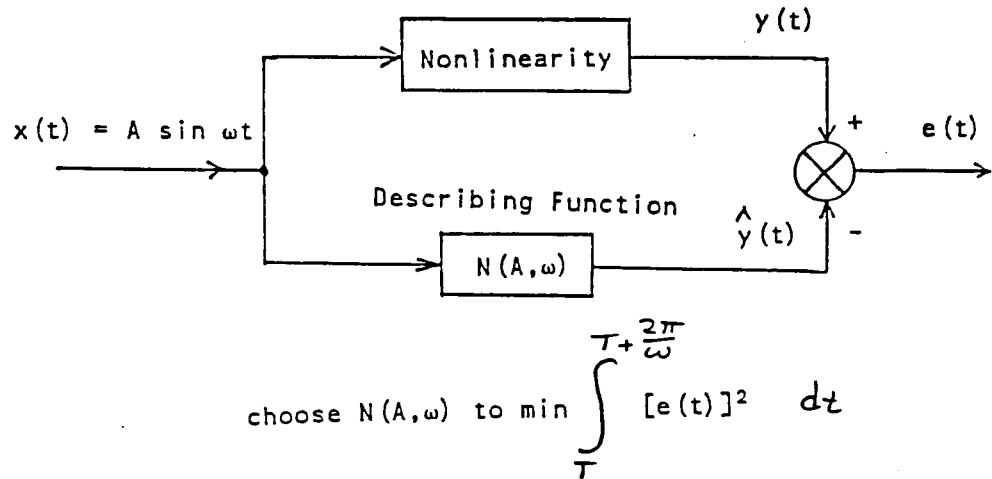


Figure 6.1 Describing Function Approximation

The output of a symmetric nonlinearity can be expanded in a Fourier series as

$$y(t) = \sum_{n=1}^{\infty} (A_n \sin n\psi + B_n \cos n\psi) \quad (6.1)$$

where $\psi = \omega t$. The approximate output component at the input frequency that minimizes the integral squared error will simply be the first terms of the series,

$$y(t) = A_1 \sin \psi + B_1 \cos \psi \quad (6.2)$$

where

$$A_1 = \frac{1}{\pi} \int_0^{2\pi} y(t) \sin \psi \, d\psi \quad (6.3)$$

$$B_1 = \frac{1}{\pi} \int_0^{2\pi} y(t) \cos \psi \, d\psi \quad (6.4)$$

The input signal has the form

$$x(t) = A \sin \psi \quad (6.5)$$

$$\dot{x}(t) = A\omega \cos \psi \quad (6.6)$$

Equation 6.2 can be rewritten as

$$y(t) = \frac{A_1}{A} x(t) + \frac{B_1}{A\omega} \dot{x}(t) \quad (6.7)$$

Replacing the time derivative by the Laplace transform variable s ,

$$y(t) = \left(\frac{A_1}{A} + \frac{B_1 s}{A\omega} \right) x(t) \quad (6.8)$$

But since the input is sinusoidal, $s \rightarrow j\omega$ and Eq. 6.7 becomes

$$y(t) = \left(\frac{A_1}{A} + \frac{B_1}{A} j \right) x(t) = N(A, \omega) x(t) \quad (6.8)$$

The describing function is often broken up into two components, the in-phase and quadrature gains,

$$\begin{aligned} n_p(A, \omega) &= \frac{A_1}{A} = \frac{1}{\pi A} \int_0^{2\pi} y(t) \sin \psi \, d\psi \\ n_q(A, \omega) &= \frac{B_1}{A} = \frac{1}{\pi A} \int_0^{2\pi} y(t) \cos \psi \, d\psi \end{aligned} \quad (6.10)$$

6.2.1 Using Describing Functions to Predict Limit Cycles

For a closed-loop system with a nonlinearity as shown in Figure 6.2, describing functions can be used to predict limit cycles.

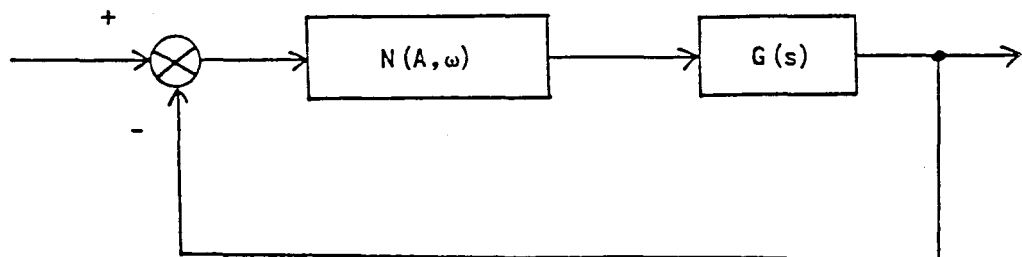
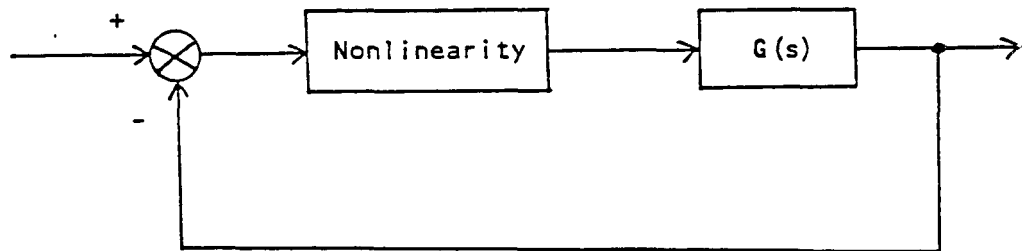


Figure 6.2 Describing Function in Closed-Loop System

The closed-loop system shown in Figure 6.2 is similar to the linear system in Figure 6.3.

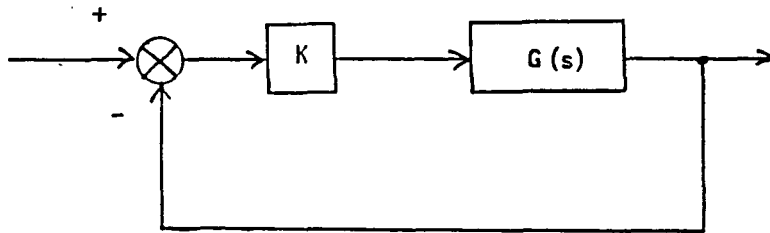


Figure 6.3 Linear Closed-Loop System

The linear system will have a closed-loop transfer function of

$$G_{cl}(s) = \frac{KG(s)}{1 + KG(s)} \quad (6.11)$$

Poles of the closed-loop system will lie on the imaginary axis if

$$1 + KG(j\omega) = 0 \quad (6.12)$$

or

$$G(j\omega) = -1/K \quad (6.13)$$

Equation 6.11 can be solved numerically to find the appropriate gain K , or K can be found graphically by plotting $G(j\omega)$ for various frequencies ω , and plotting $-1/K$ for various gains K . If these plots intersect, then there will be a gain that will place closed-loop poles on the imaginary axis. The particular gain that will do this is the value of K at

the intersection. Figure 6.4 shows an example of this graphical technique with polar and gain-phase plots.

With the describing function, a limit cycle will be predicted if a solution can be found to

$$1 + N(A, \omega) G(j\omega) = 0 \quad (6.14)$$

or

$$G(j\omega) = -1/N(A, \omega) \quad (6.15)$$

And as in the linear system, the above condition can be tested graphically. An intersection of the $G(j\omega)$ and $-1/N(A, \omega)$ plots will indicate a limit cycle. For most common nonlinearities, the describing function will not depend upon the input frequency, but just upon the input amplitude. This is true for the nonlinearity studied in this chapter, so $N(A, \omega) = N(A)$. Figure 6.5 shows this graphical technique on polar and gain-phase plots.

In addition to predicting the presence of a limit cycle, the plots can also be used to predict the limit cycle amplitude, frequency, and stability. Figure 6.6 shows how this is accomplished by marking various amplitudes on the $-1/N(A)$ curve, and marking various frequencies on the $G(j\omega)$ curve.

To determine the stability of the limit cycle, the amplitude is perturbed slightly higher and lower than the limit cycle amplitude. If the higher amplitude tends to increase further, then the limit cycle will be unstable; if it tends to decrease, then the limit cycle will be stable. Figure 6.7 show this stability determination on a polar plot.

It should be noted that since the describing function is only an approximation to the nonlinearity, the presence or absence of a limit cycle can only be predicted by this graphical method. To check whether

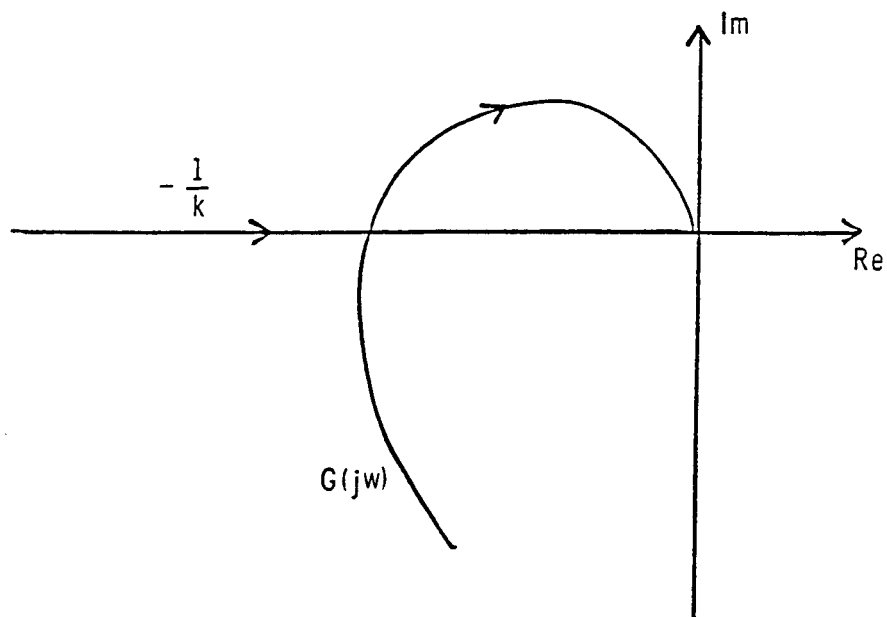
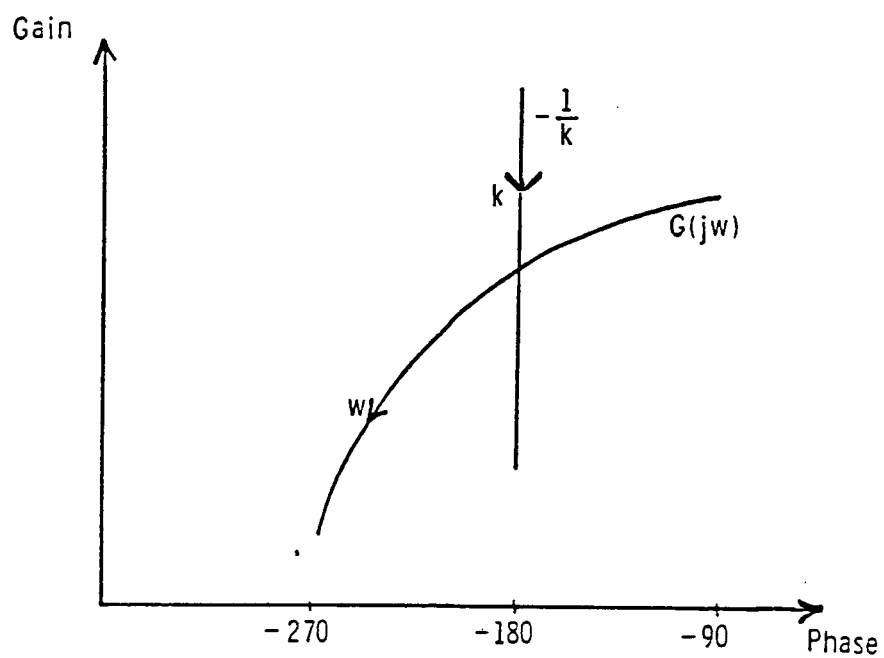


Figure 6.4 Finding Gain That Places Poles on Imaginary Axis

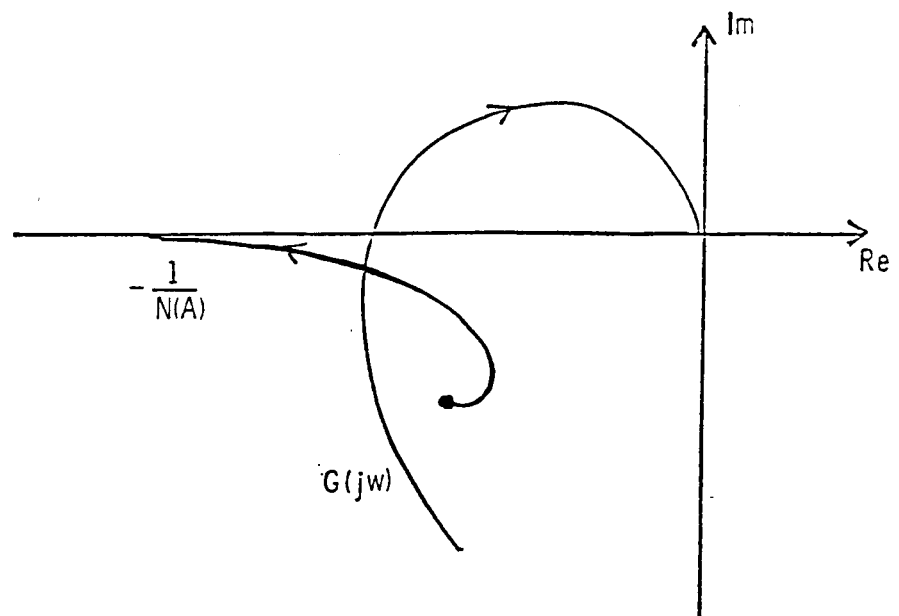
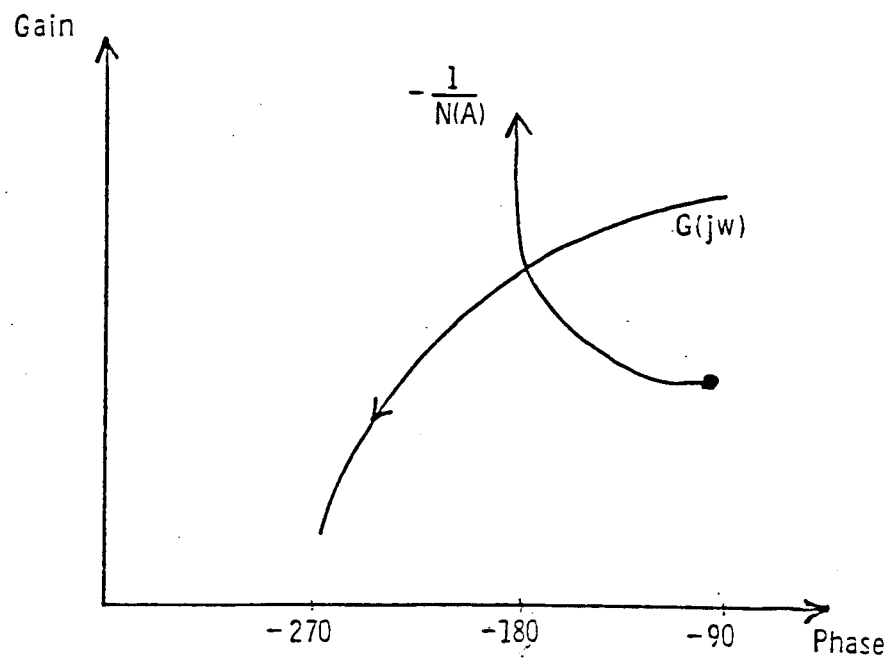


Figure 6.5 Limit Cycle Prediction

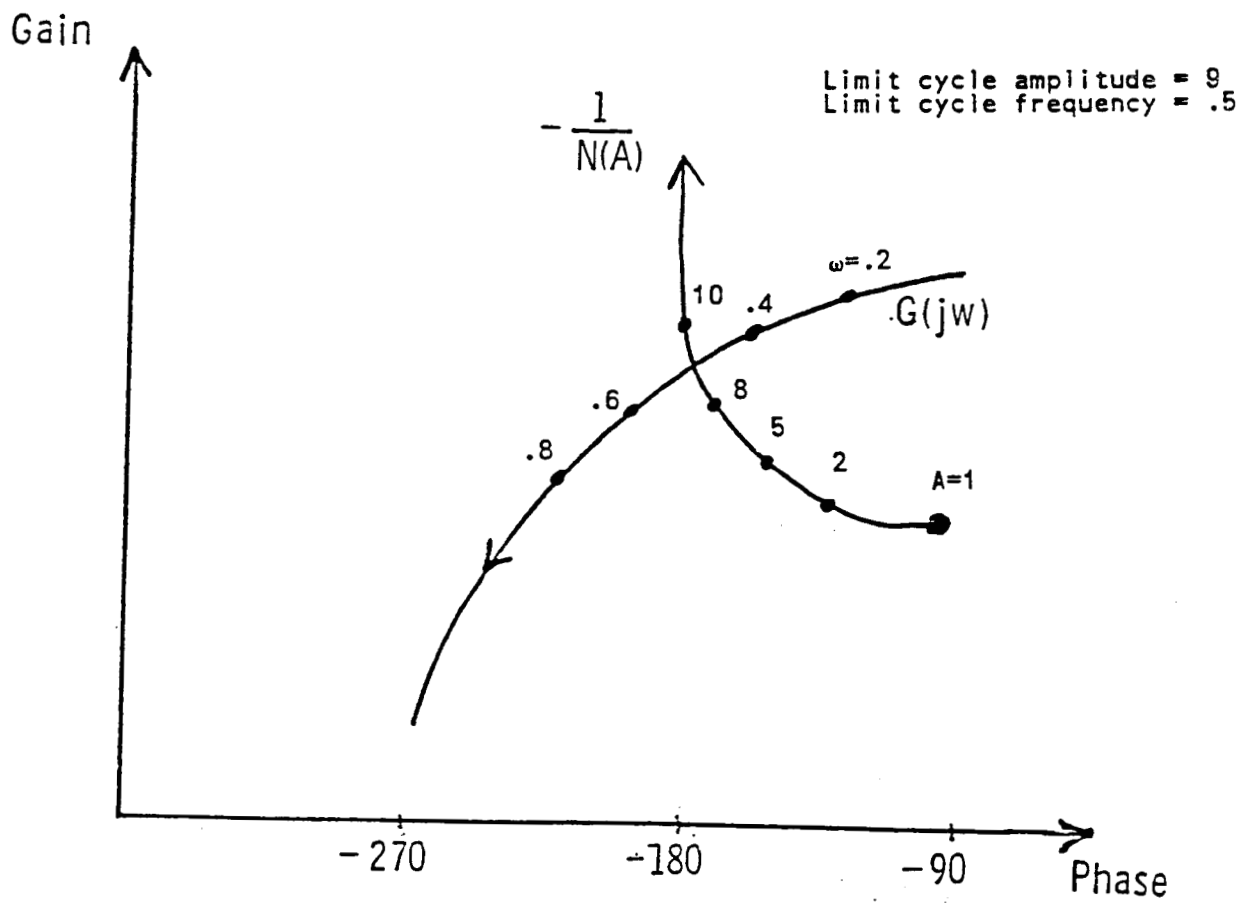


Figure 6.6 Limit Cycle Amplitude and Frequency Determination

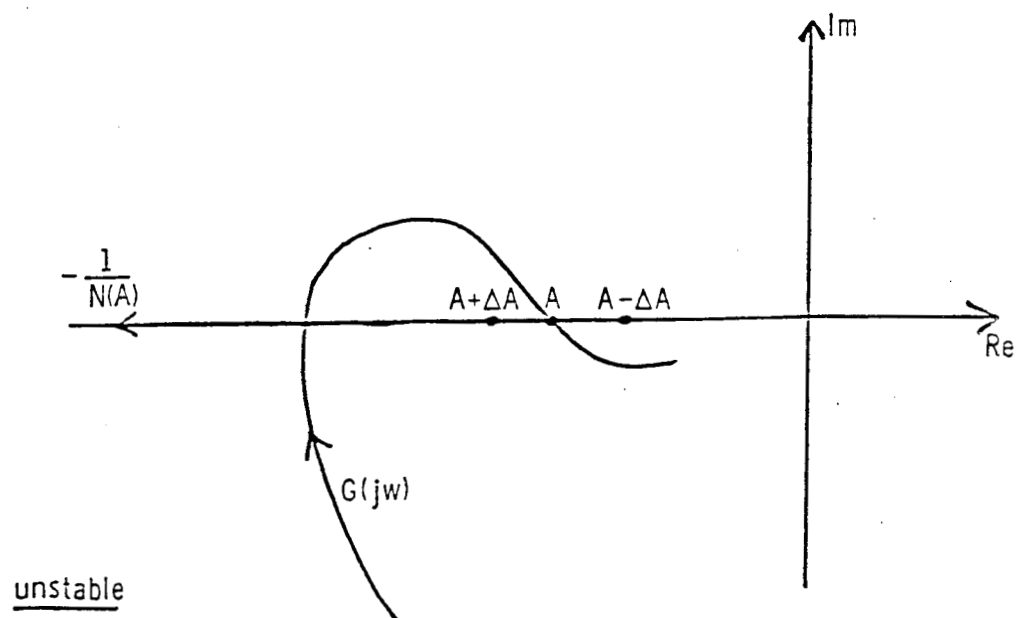
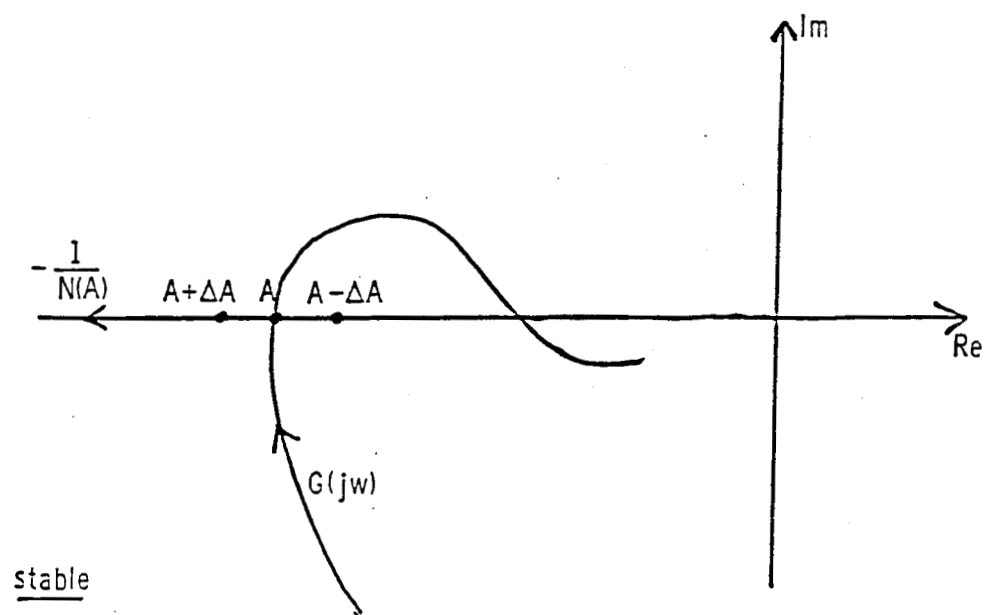


Figure 6.7 Limit Cycle Stability Determination

a limit cycle really exists, the actual nonlinearity must be used in a simulation.

6.2.2 Accuracy of Describing Function Approximation

The accuracy of the describing function in modelling a nonlinearity can be evaluated by looking at what is ignored. From Equations 6.1 and 6.2 it can be seen that the error in the approximation will simply be the higher order terms of the Fourier series.

$$e(t) = \sum_{n=2}^{\infty} (A_n \sin n\psi + B_n \cos n\psi) \quad (6.16)$$

For the closed-loop system, the single sinusoidal input assumption will be good if the higher order terms are filtered out by the linear system, $G(s)$. For the Space Shuttle, the sharp cutoff of the rate estimator will filter higher harmonics making the use of the describing function approximation a good way of checking for limit cycles.

6.3 Describing Function Representation of Phase Plane

For most payload-orbiter interaction cases, flexural motion will cause the rate limits to be exceeded before the deadbands. The forced limit cycling that can occur will therefore generally involve rate limit firings. The describing function representation of the phase plane will be for rate limit firings only. The bias switch line is also ignored for this analysis.

With these simplifications, the phase plane will act like a positive hysteresis loop, Figure 6.8.

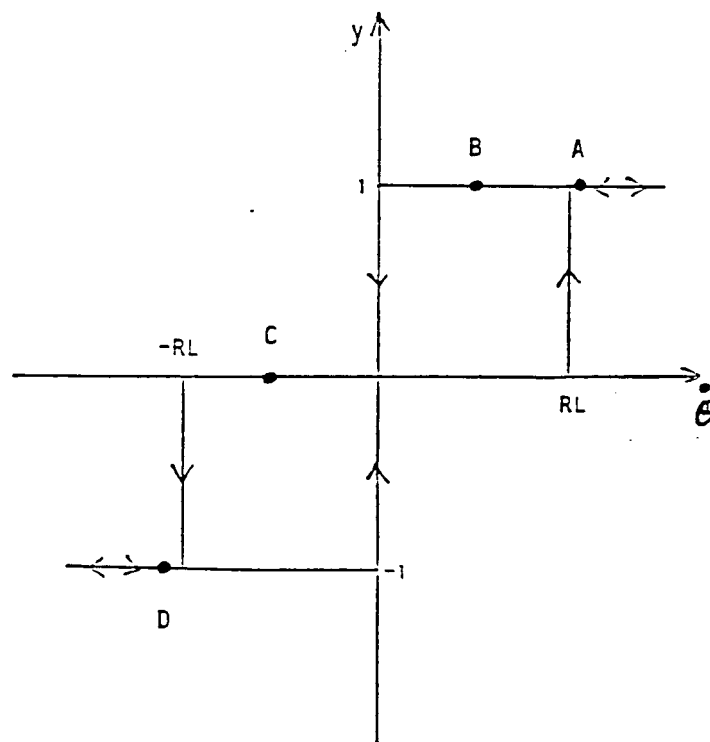
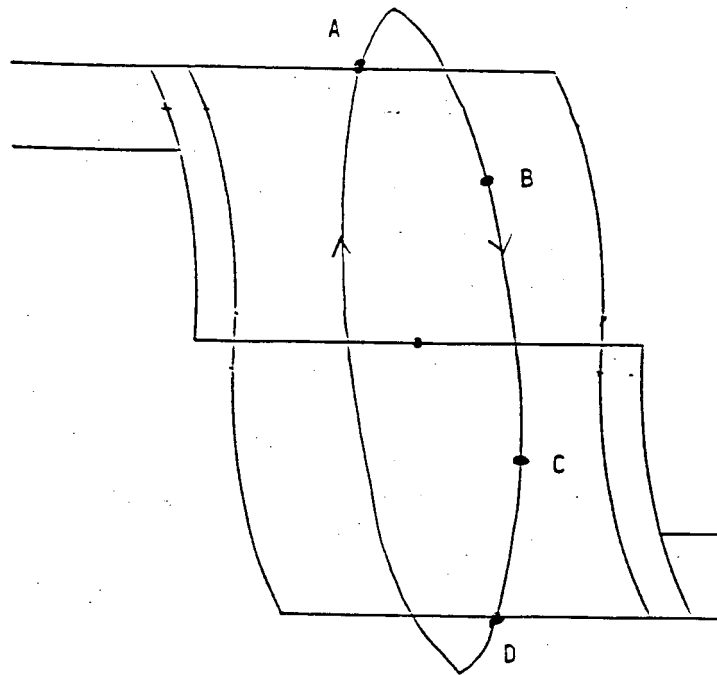


Figure 6.8 Nonlinearity for Rate Limit Firing

The sinusoidal input describing function for this will be

$$N(A) = \begin{cases} \frac{2}{\pi A^2} [(A + \sqrt{A^2 - 1}) - j] & \text{for } A > 1 \\ 0 & \text{for } A < 1 \end{cases} \quad (6.17)$$

A plot of $-1/N(A)$ is shown on a gain-phase plot in Figure 6.9.

6.4 Simplified Representation of Shuttle

A simplified s-plane representation of the Shuttle's dynamics and control system has been developed⁸ to be used for limit cycle prediction. The effect of adding various notch filters in different locations in the control system can be studied with this simplified system. This analysis of the closed-loop system will help in designing the notch filters that will best prevent forced limit cycling from occurring.

6.4.1 Shuttle Dynamics

The Shuttle-payload dynamics are modelled as a rigid body plus one bending mode. This representation will be particularly good for the pivoted payloads, but will also give some intuitive insights for more complicated structures. Figure 6.10 shows this simplified model. The variable, β , can be thought of as a weighting of the control spillover.

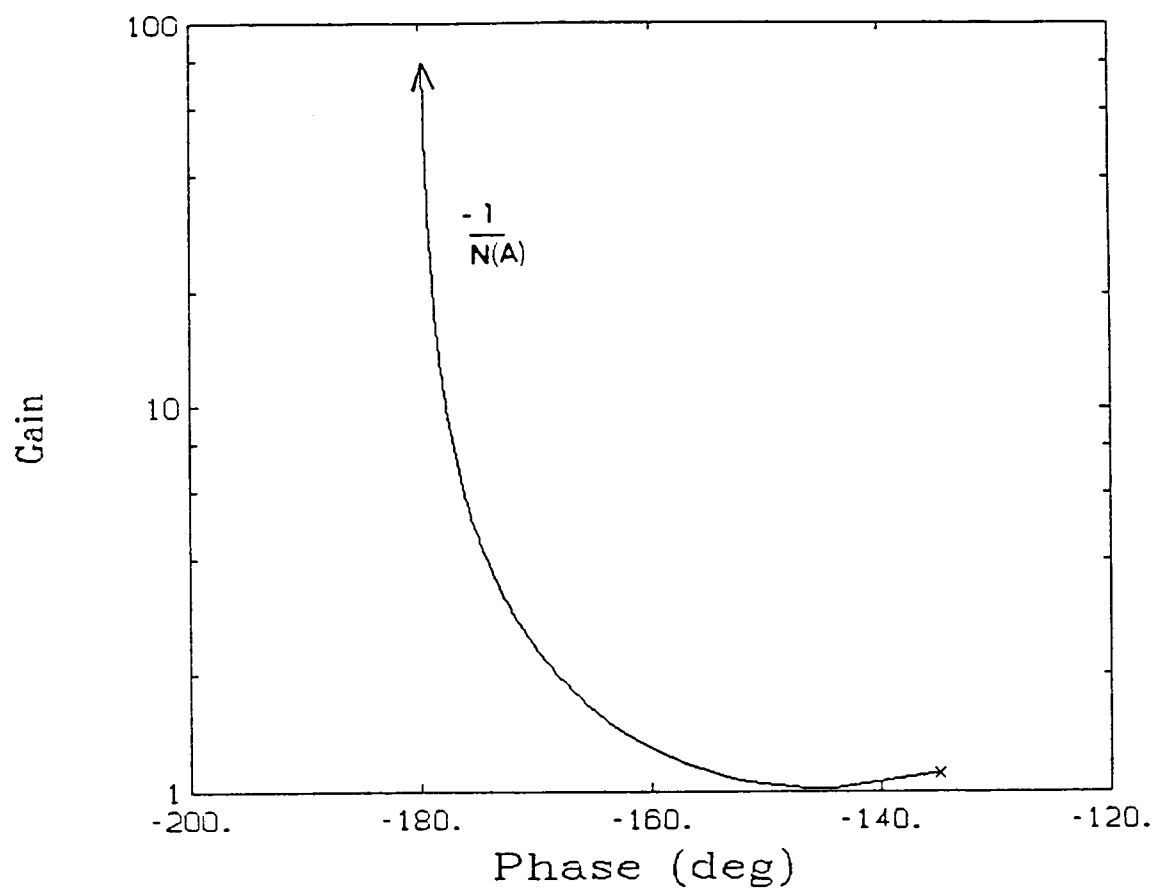


Figure 6.9 Describing Function for Rate Limit Firing

$$\zeta_B = 0.005$$

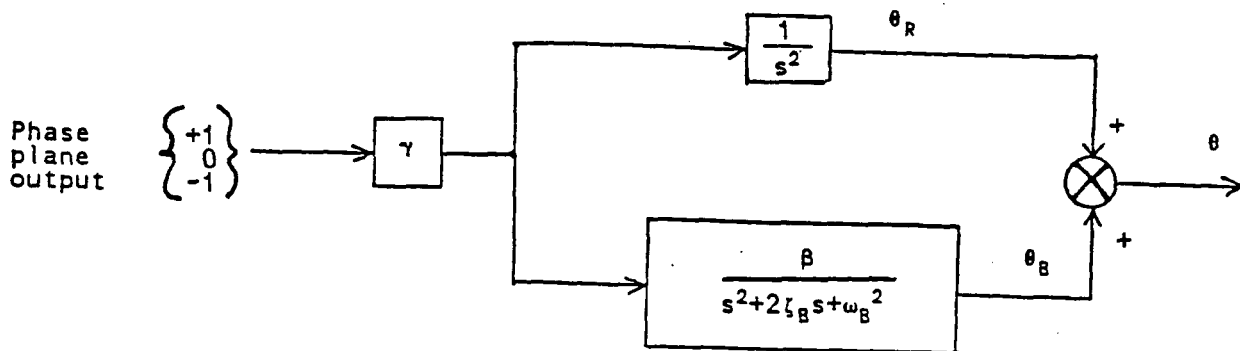


Figure 6.10 Simplified Model of Shuttle Dynamics

6.4.2 Inertial Measurement Unit

The IMU is modelled as giving delayed, noise-free measurements. The s-plane model will therefore be

$$e^{-sT} \approx \frac{1-sT/2}{1+sT/2} \quad (6.18)$$

where T is the time delay. This first order Pade approximation of the delay was used to keep the model analytic. Both the delay and the approximation have unity magnitude response and will introduce a phase lag. Figure 6.11 shows that for the range of frequencies of interest, the approximation is very good.

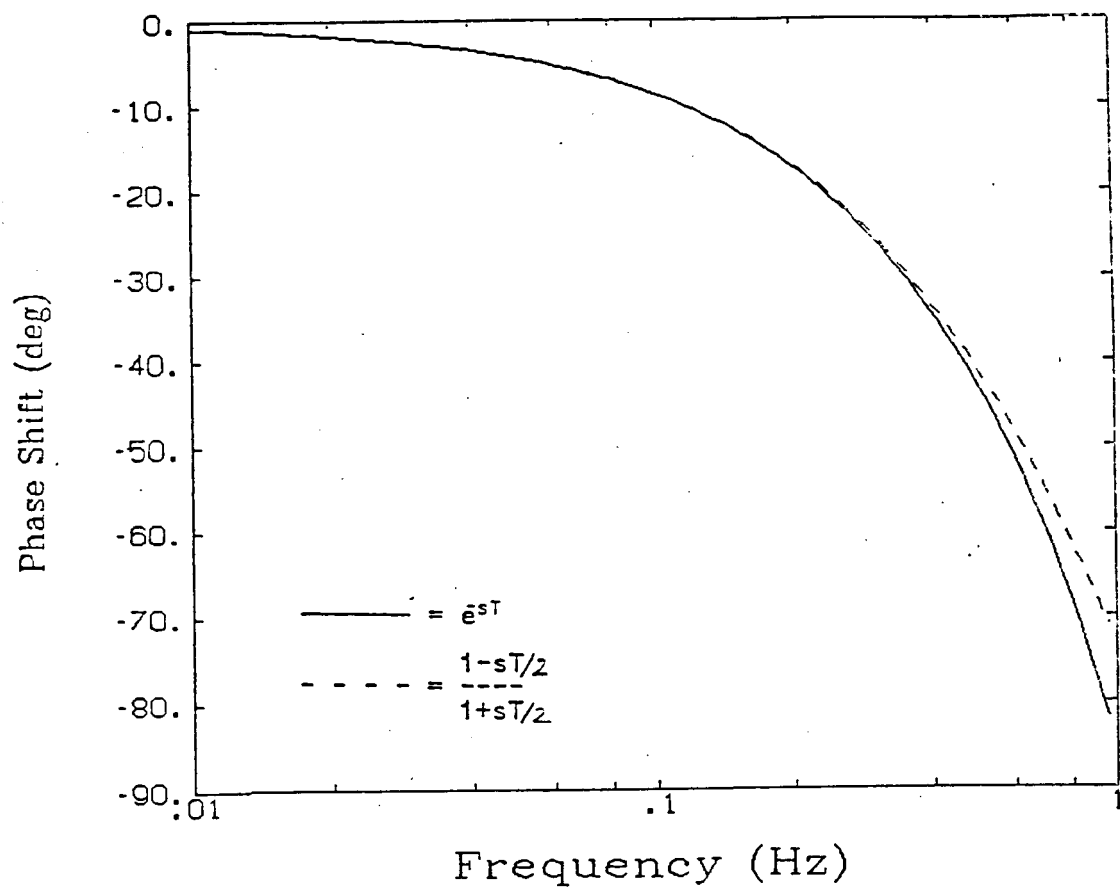


Figure 6.11 Delay Approximation

6.4.3 State Estimator

A second-order transfer function is used to represent the rate filter. The jet feedforward information is assumed to be accurate with respect to rigid body motion, so the input to the estimator will be the measured attitude minus the rigid body attitude, Figure 6.12.

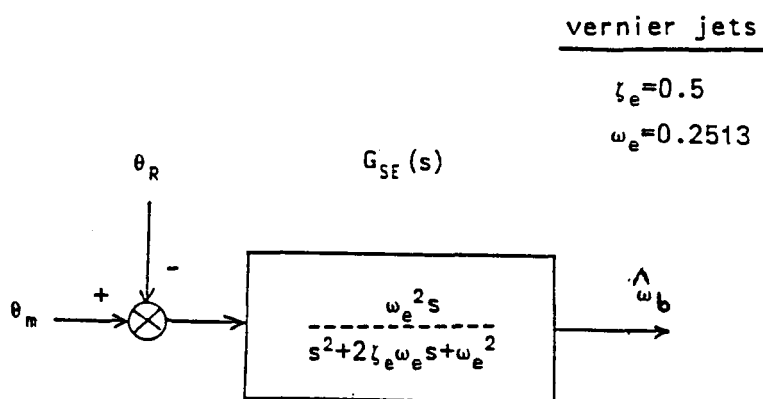


Figure 6.12 Simplified State Estimator

The frequency response of this simplified model of the estimator is shown in Figure 6.13. Comparing this to Figure 5.5 shows that the simplified model is a good approximation to the vernier rate filter.

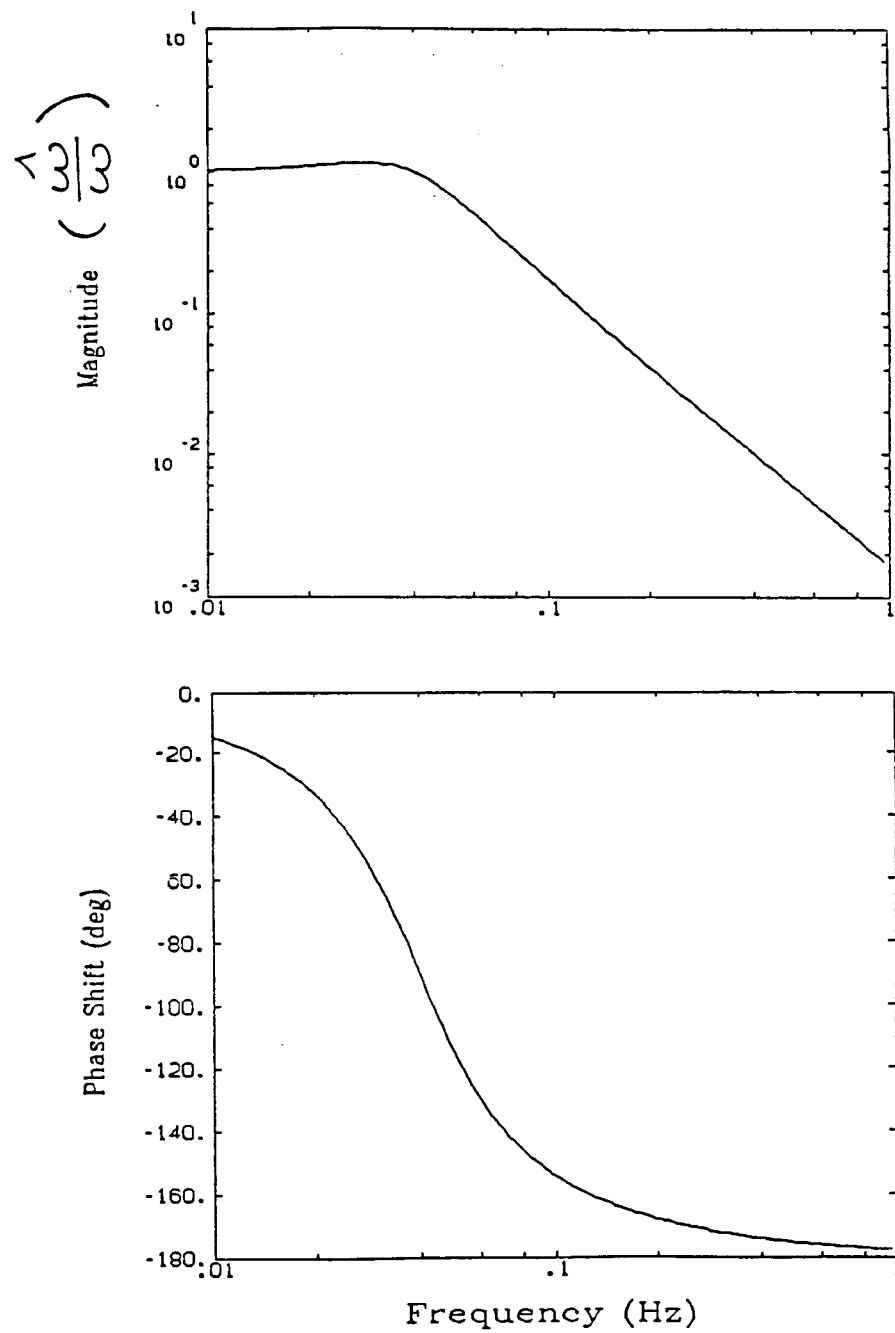
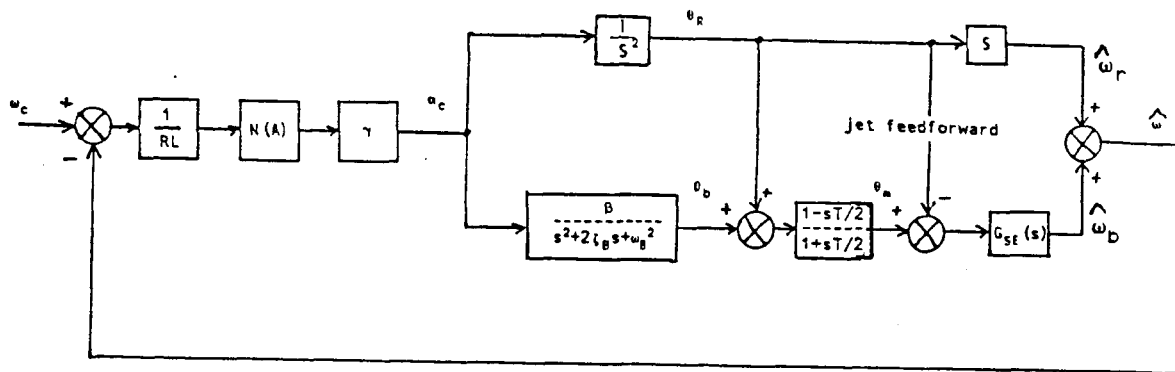


Figure 6.13 Simplified Estimator Frequency Response

6.4.4 Combined System

Figure 6.14 shows the combined system model. Two possible locations for the notch filters would be after the measurement and after the rate estimator. These two locations will give a different response because of the jet feedforward information.



RL = rate limit

$N(A)$ = describing function representation of phase plane

Figure 6.14 Combined Simplified System

6.5 Stability Analysis

Figure 6.15 shows stability plots for different amounts of control spillover. Larger β leads to intersections of the $G(j\omega)$ and $-1/N(A)$ curves which will indicate a limit cycle. For the Shuttle, a limit cycle will mean jet sustained oscillations.

Figure 6.16 shows how a notch filter added to the linear system can affect the stability. Figure 6.17 shows a case where the 2nd order filter prevents a limit cycle but the 4th order does not. When the notch filter center frequency is in error, this phase lag can be destabilizing, therefore only 2nd order filters are considered.

This graphical technique for finding limit cycles can be used to form a stability boundary. At a given bending frequency, β is varied until the $G(j\omega)$ and $-1/N(A)$ curves intersect. A higher β will give limit cycles, lower β will be stable. This analysis is carried out for a number of bending frequencies to create a stability boundary as shown in Figure 6.18. Figure 6.19 shows the stability boundary with a notch filter added after the measurement and after the state estimator. Both notch filters should dramatically reduce limit cycling, but the notch filter placed after the measurement is seen to give the best performance.

Errors in the notch filter center frequency will reduce the effectiveness of the filters. Figure 6.20 shows how the stability boundary changes when the frequency estimate is in error by 5% low and high. A high center frequency is seen to lead to greatly reduced stability. This occurs because a phase lag is introduced at the bending frequency with only partial attenuation.

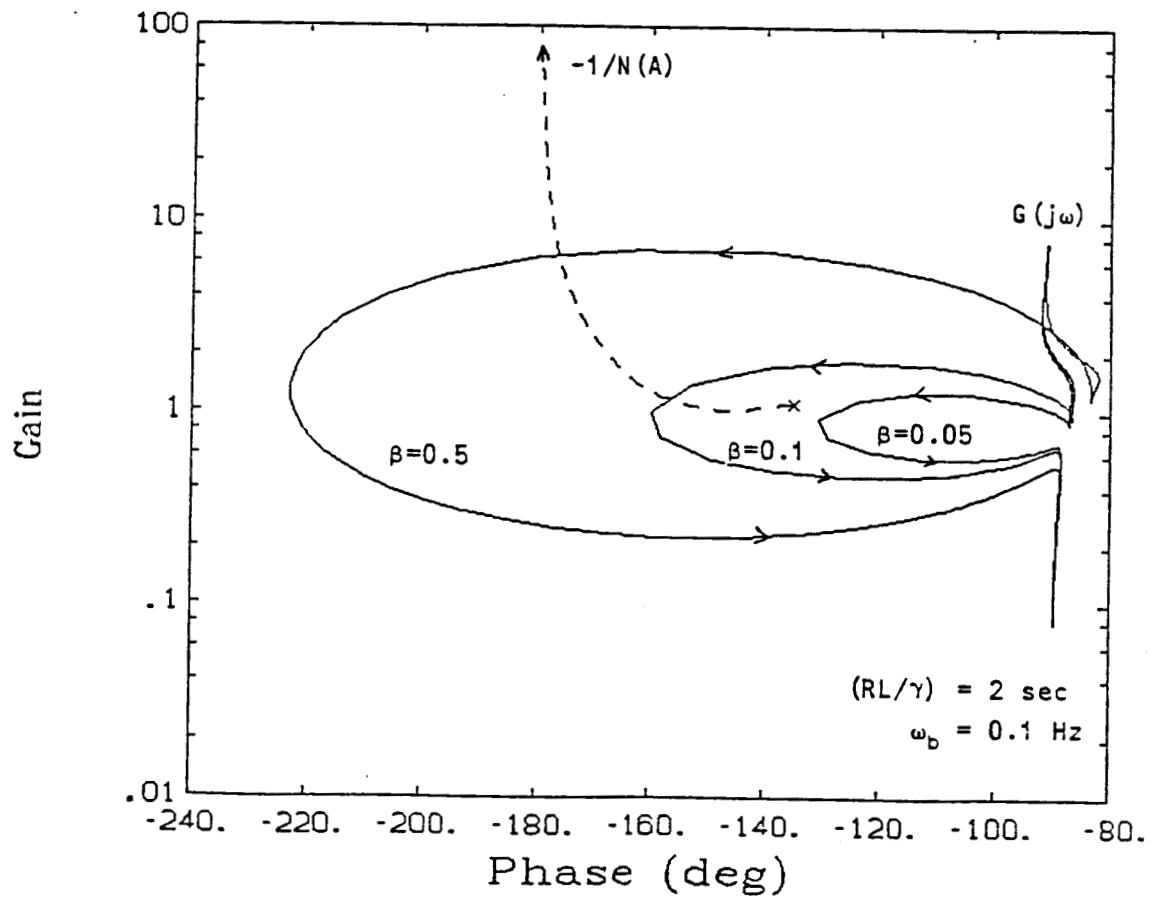


Figure 6.15 Effect of Control Spillover

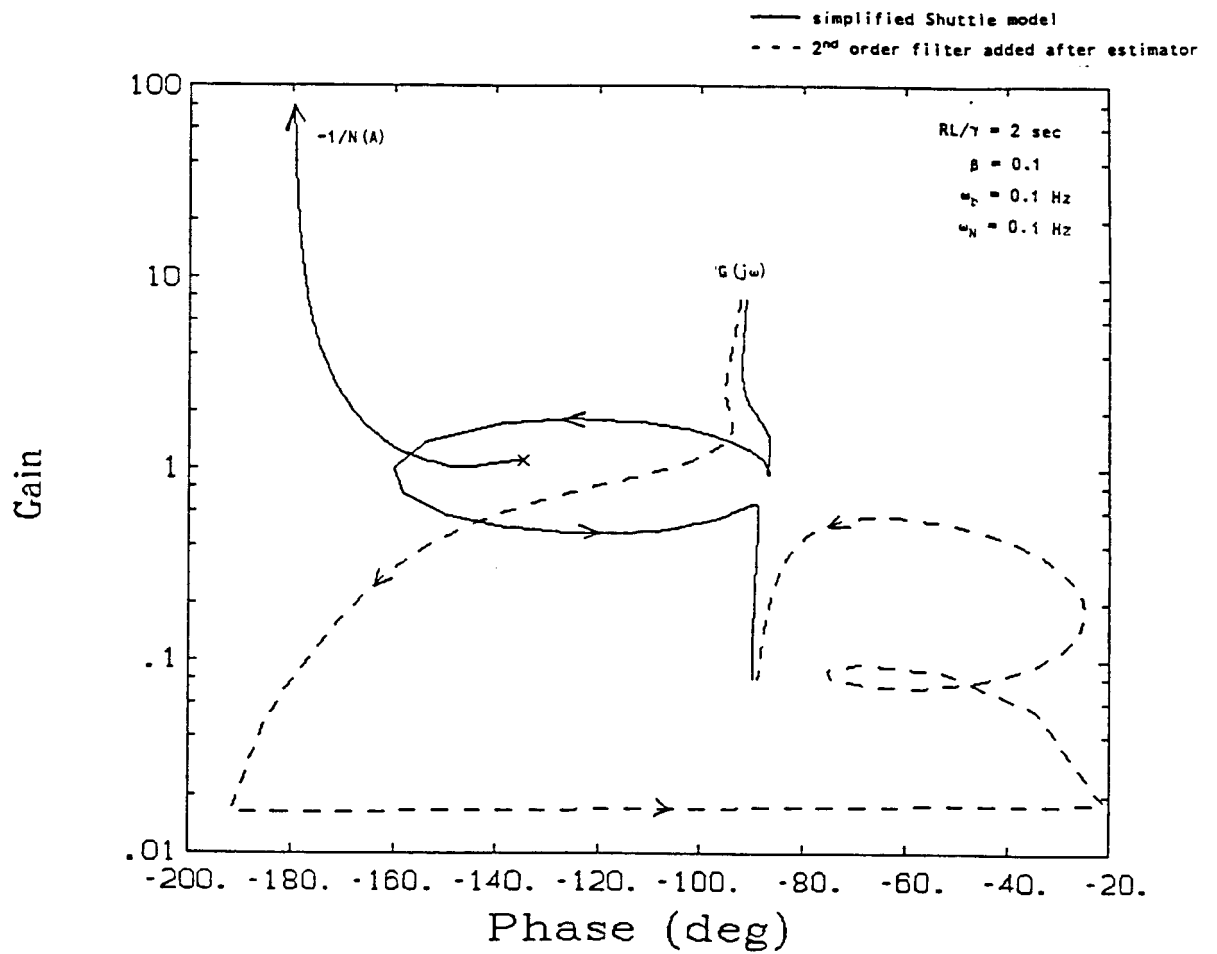


Figure 6.16 Effect of Adding Notch Filter

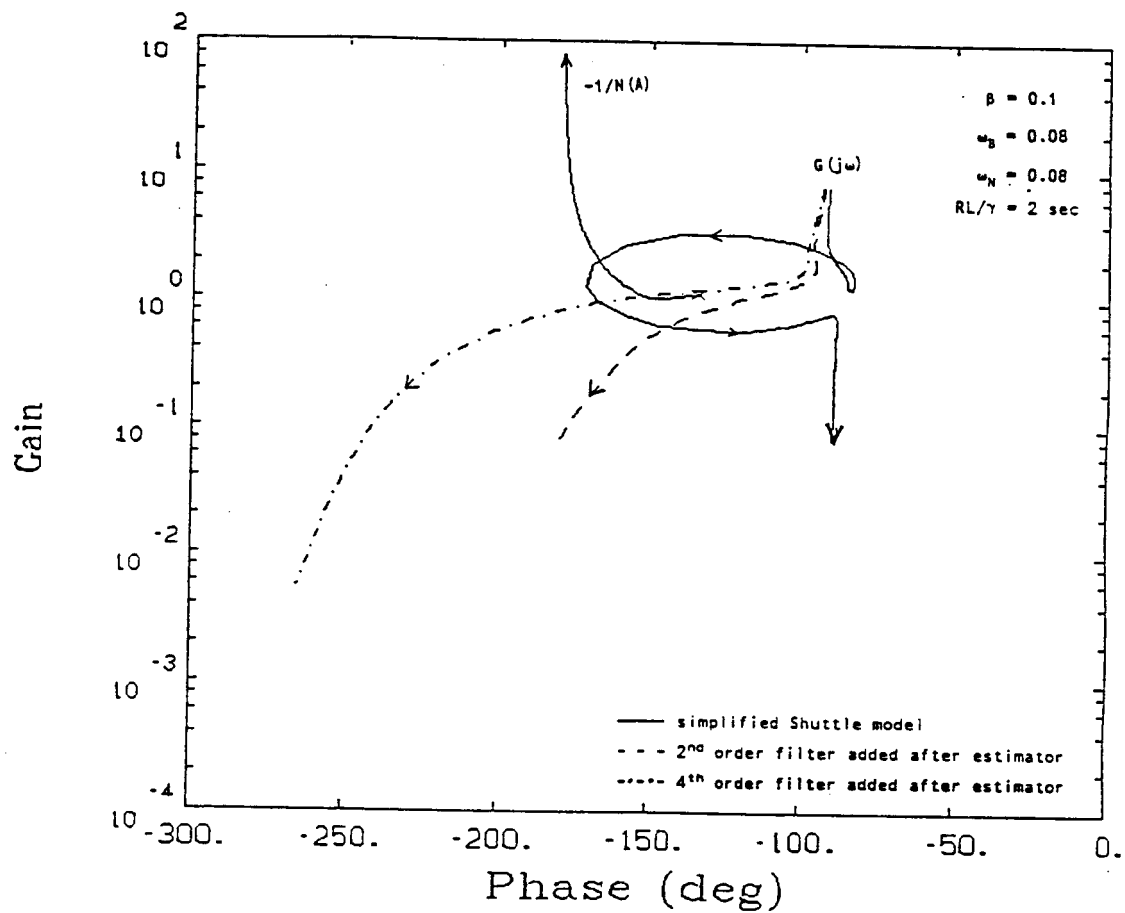


Figure 6.17 How 2nd Order Filter Can Be Better at Preventing Limit Cycles

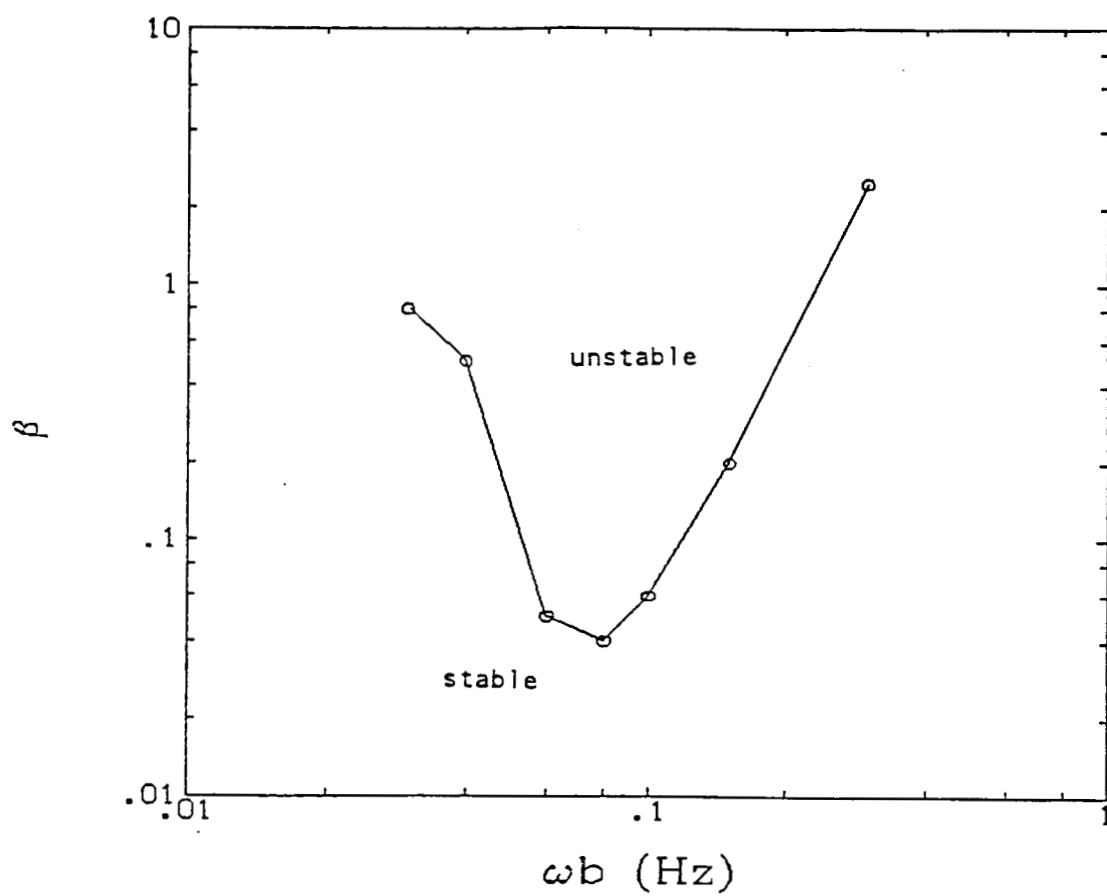


Figure 6.18 Stability Boundary without Notch Filters

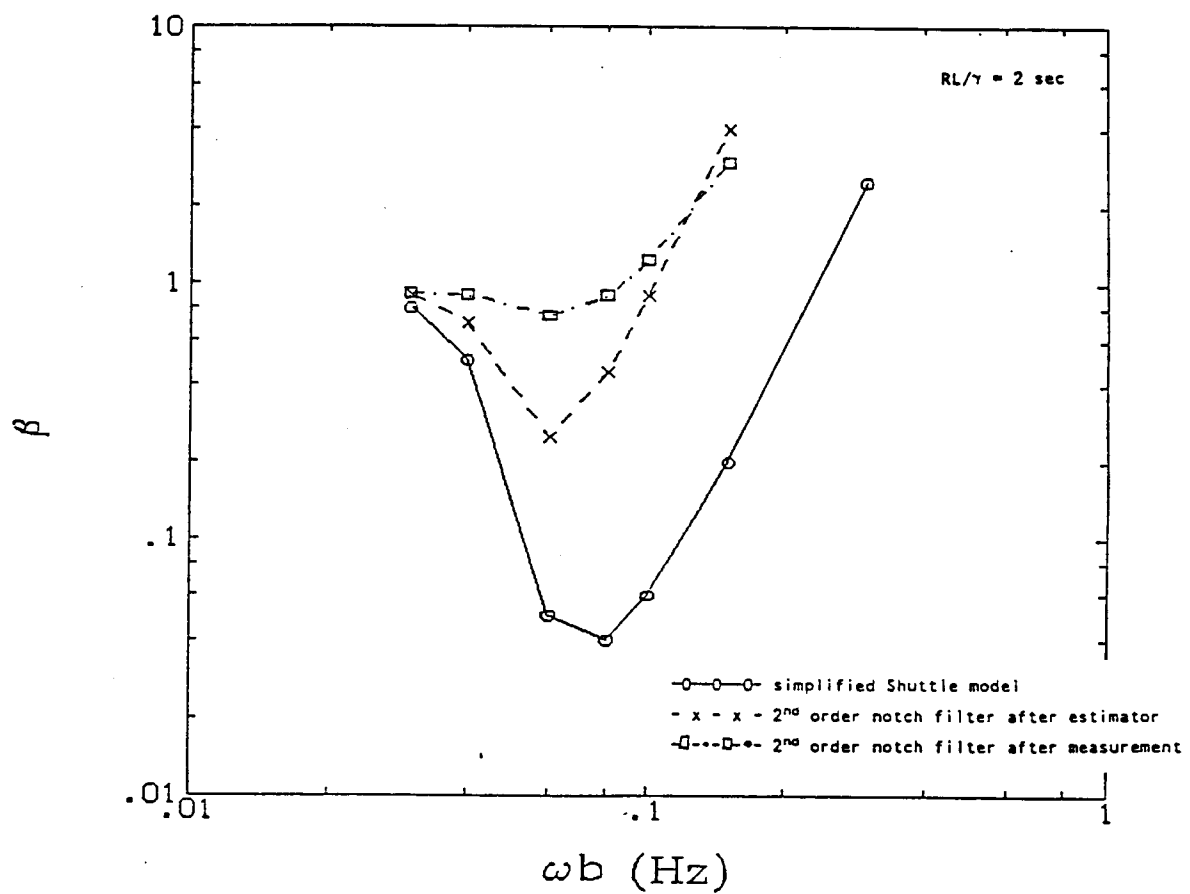


Figure 6.19 Stability Boundary with Notch Filters

C-2

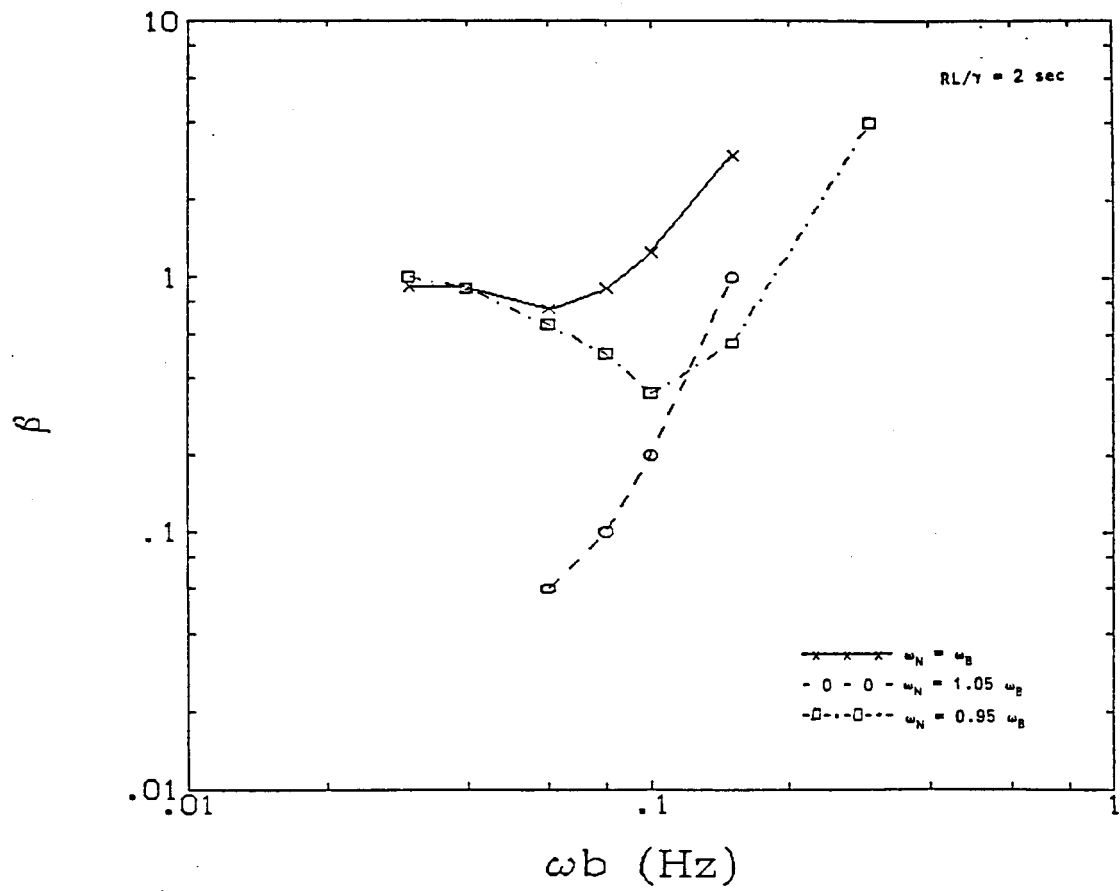


Figure 6.20 Effect of Errors in Notch Center Frequency

6.6 Design Considerations

The stability analysis in the last section indicates that second-order notch filters placed after the measurements will give the best performance. This will also give a choice between the measured attitude and the notch filtered attitude for the feedback signal. Deadband firings may occur with large amplitude bending motion usually involving low-frequency payload-orbiter interactions. In such cases, feeding the filtered attitude back may prevent instabilities.

Deciding when to change the notch filter coefficients has not yet been addressed. Changing the coefficients on every cycle is unnecessary and is probably undesirable. The frequency response of the notch filters is for steady-state. Constantly changing the coefficients will give a complicated filter response. The coefficients should only be changed when the frequency estimate differs from the center frequency by a significant amount. The analysis in the last section showed that having a notch center frequency above the bending frequency should be avoided. The filter coefficients should therefore be changed sooner when the frequency estimate goes below the notch center frequency than when it goes above. For this thesis, the notch filters have bandstop frequencies 10% above and below the center frequency. The filter coefficients are changed when the estimate goes 2% lower than the center frequency and 5% higher.

CHAPTER 7

SIMULATION RESULTS

7.1 Introduction

A computer simulation of the Space Shuttle with payloads attached to its robot arm is used to evaluate the effectiveness of the notch filters in reducing instability. The payload-orbiter dynamics are highly dependent upon the arm configuration. A particular payload will have stable and unstable regions in which it can operate. The objective of adding notch filters is to expand the stable operating range of payloads attached to the Shuttle's flexible arm. The notch filtering scheme is therefore evaluated by how well it expands the safe operating volume for different size payloads.

7.2 Computer Simulation

The computer simulation used is called LSAD (Less Singing And Dancing). LSAD was developed at Draper¹¹ for engineering analysis involving the Shuttle with payloads attached to its RMS. LSAD has a simplified, linearized model of the arm dynamics along with a model of the Shuttle and its control system.

LSAD was used for testing the notch filtering scheme because it has been demonstrated to provide representative payload-orbiter dynamics and is much cheaper to run than the high fidelity simulations that incorporate many second order effects.

7.2.1 Stability Testing

To test the stability of a particular payload-orbiter configuration, LSAD calculates the dominant bending mode and fires a jet couple to excite this mode. If the resulting oscillation decays toward zero while in a closed-loop attitude control mode, then the system is stable.

An array of different payload locations can be tested to determine the stable and unstable operating regions. Figure 7.1 shows the simulation results for stable and unstable cases using the Space Telescope as a typical payload. The plots are of body rates and rate estimates along with the vernier jet firings.

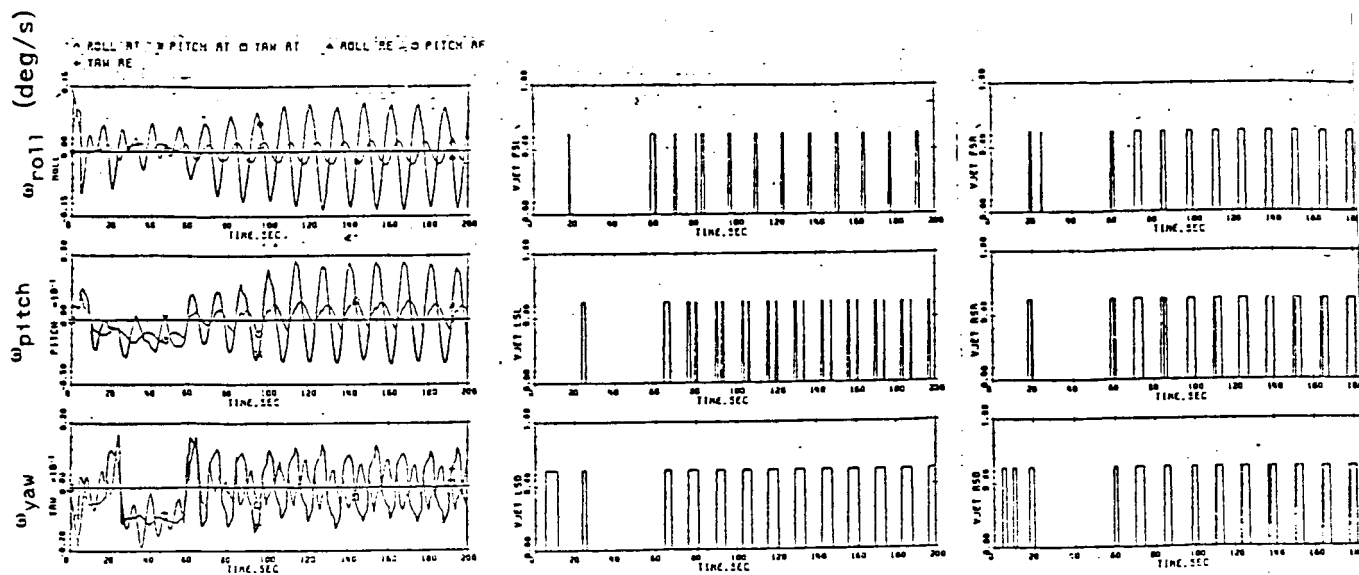
7.3 Simulation Results

Two large payloads, the Space Telescope and the generic 65,000 lb. payload, were used for the simulation analysis. The Space Telescope weighs around 25,000 lbs. and is a typical example of the larger payloads that the Shuttle deploys. The 65,000 lb. payload is the largest possible payload the Shuttle will deploy and therefore will present a worst case example in terms of low frequency payload-orbiter dynamic interaction.

An array of points in the plane above the Shuttle were tested for stability with and without notch filters. These points are plotted in the vehicle's structural frame of reference which is shown in Figure 7.2. Figures 7.3 and 7.4 show the simulation results for the two payloads. The addition of the notch filters is seen to dramatically increase the stable operating region.

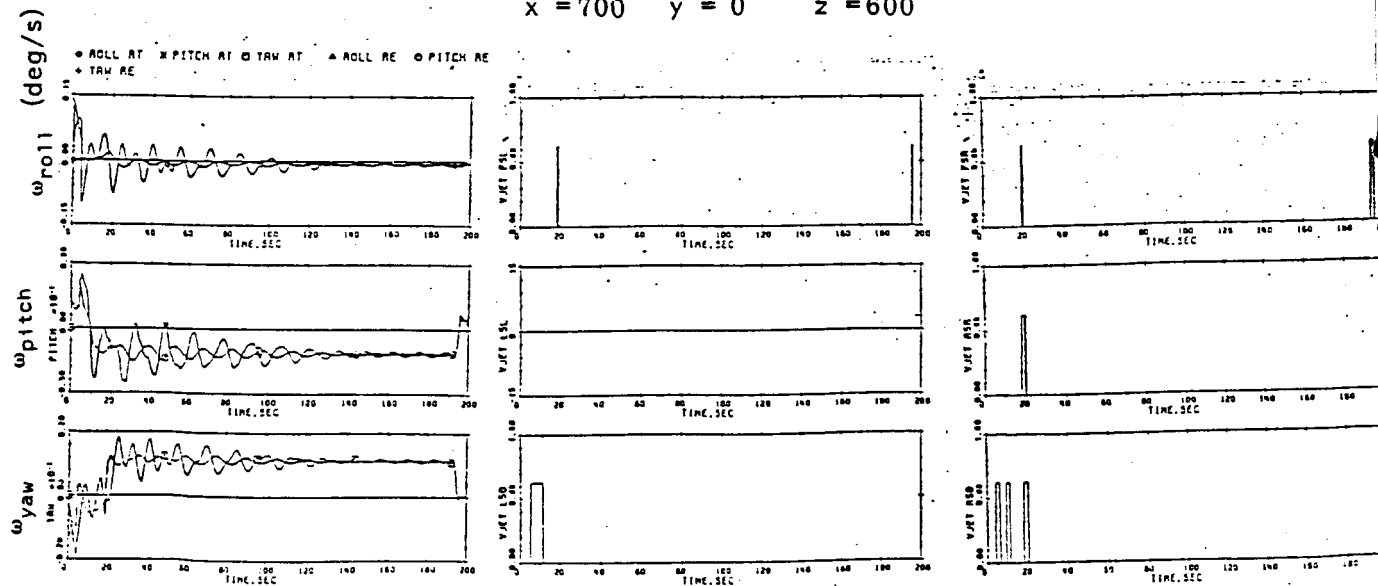
Figures 7.5 and 7.6 show what the stable limits of operation look like at $x=700$ and $x=900$ inches for the Space Telescope. These figures

ORIGINAL PAGE IS
OF POOR QUALITY



UNSTABLE (without notch filters)

x = 700 y = 0 z = 600



STABLE (with notch filters)

Figure 7.1 LSAD Stability Simulation for Space Telescope

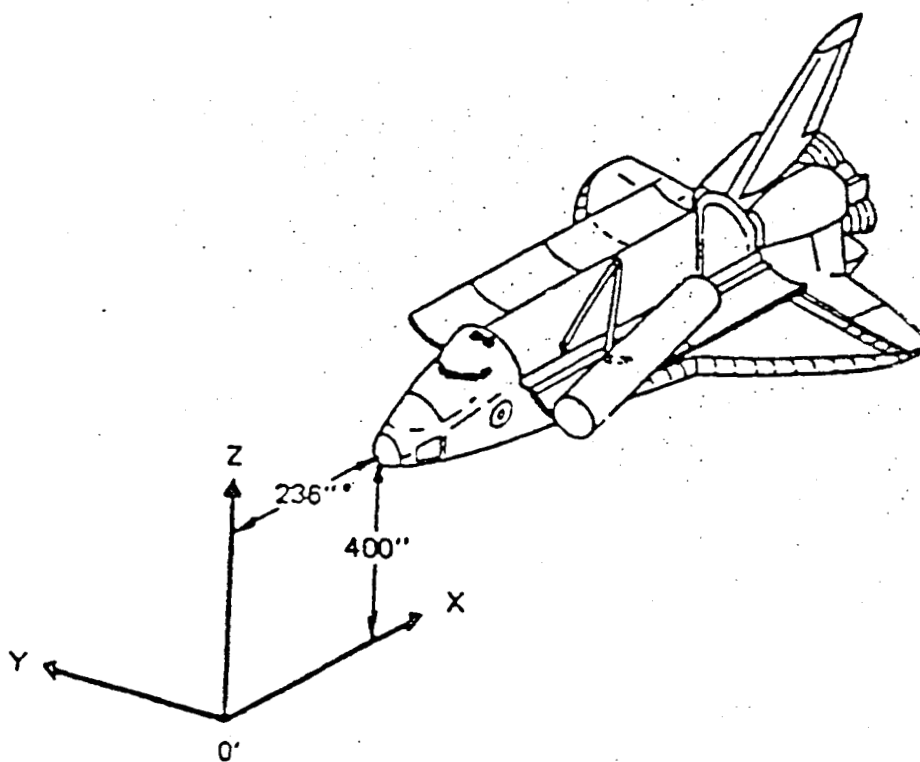


Figure 7.2 Structural Frame of Reference

ORIGINAL PAGE IS
OF POOR QUALITY

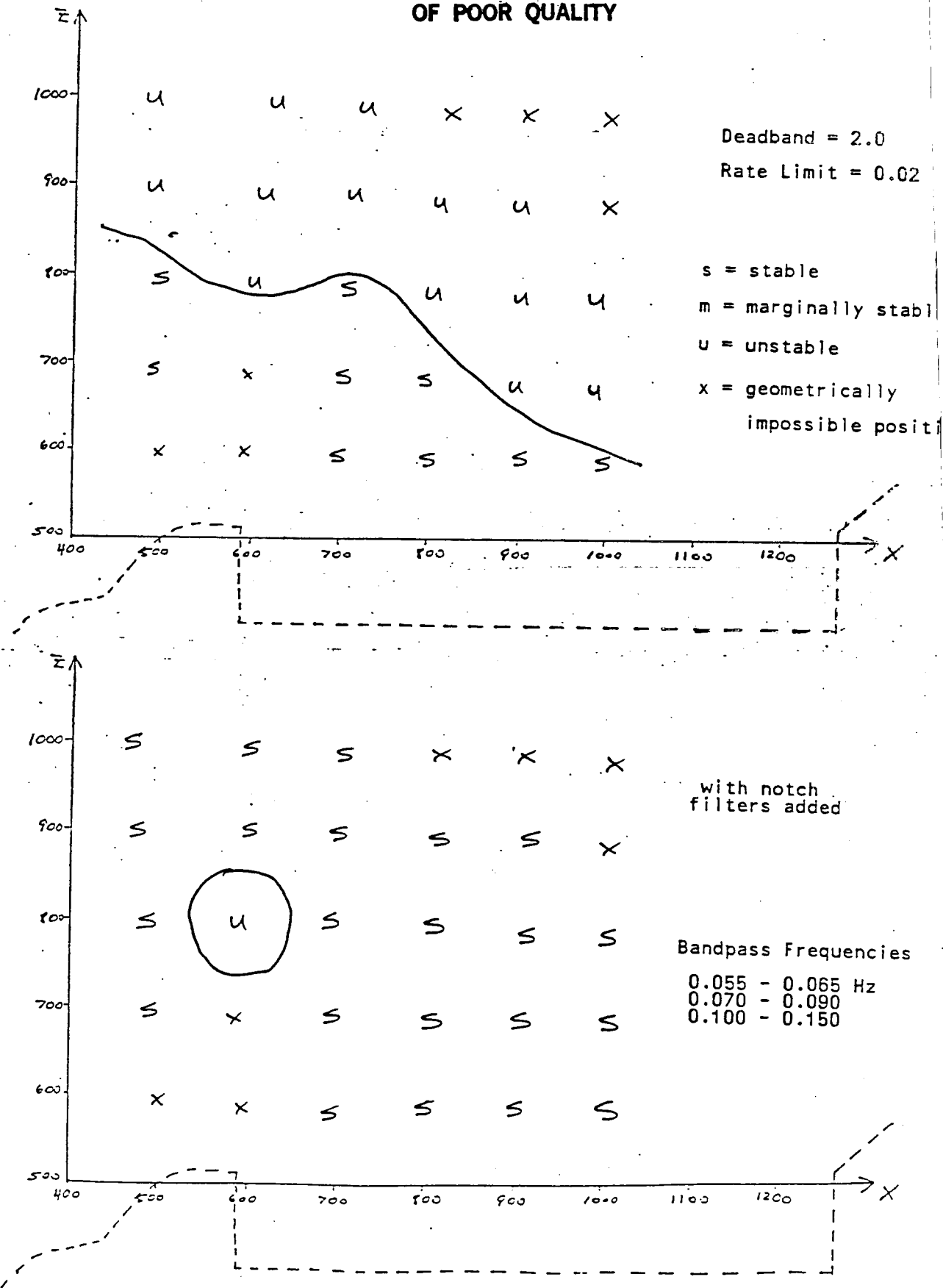


Figure 7.3 Stability Range for the Space Telescope

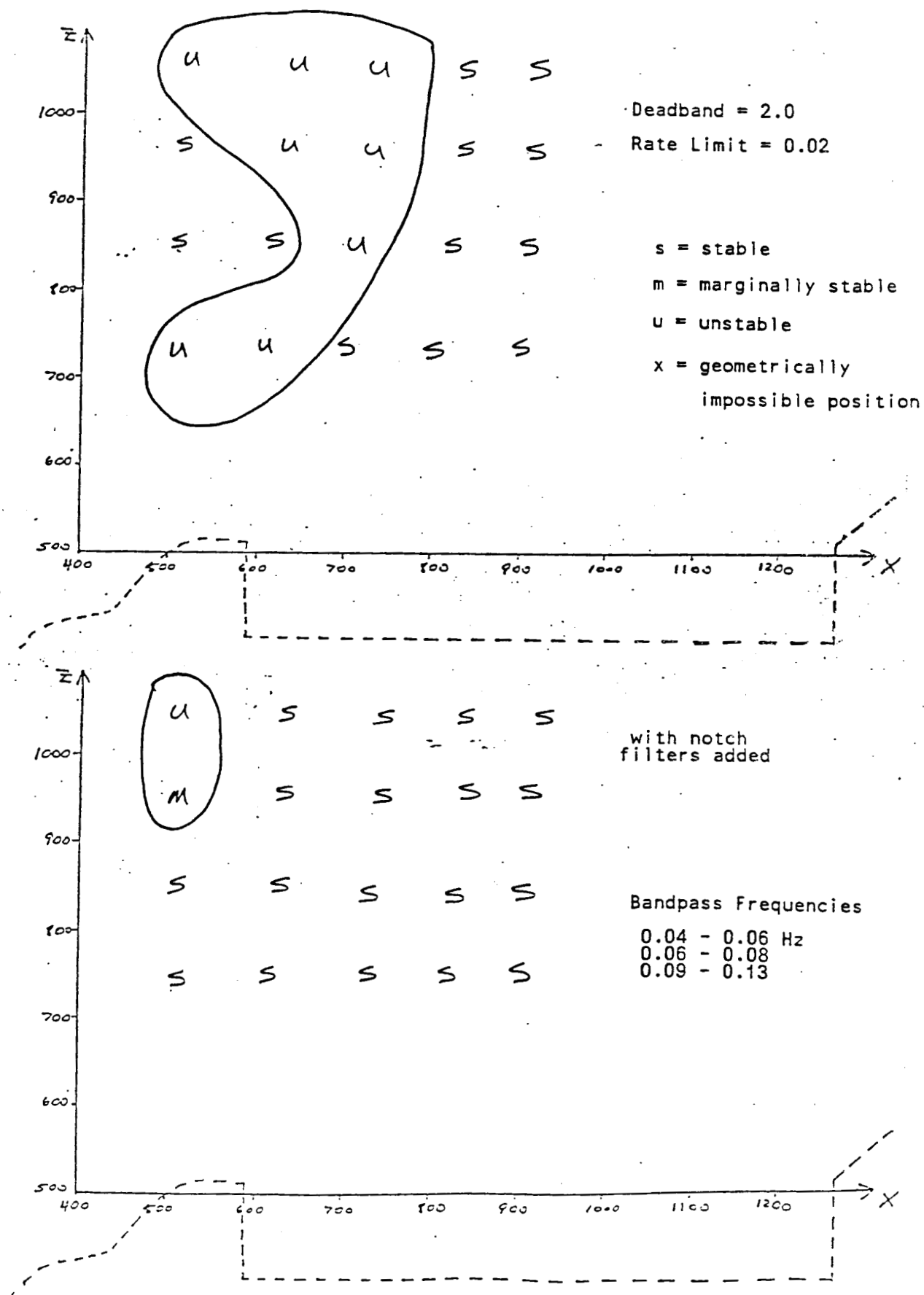


Figure 7.4 Stability Range for the 65k Payload

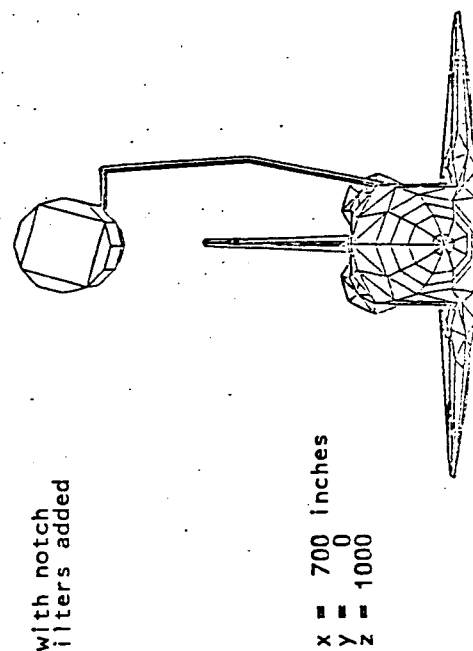
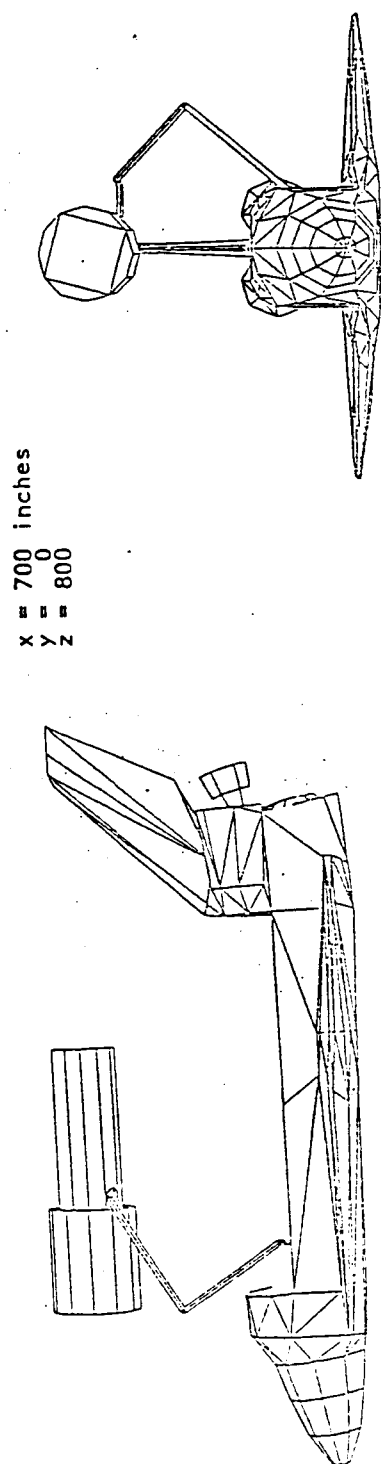


Figure 7.5 Limits of Stable Operation for Space Telescope (x=700)

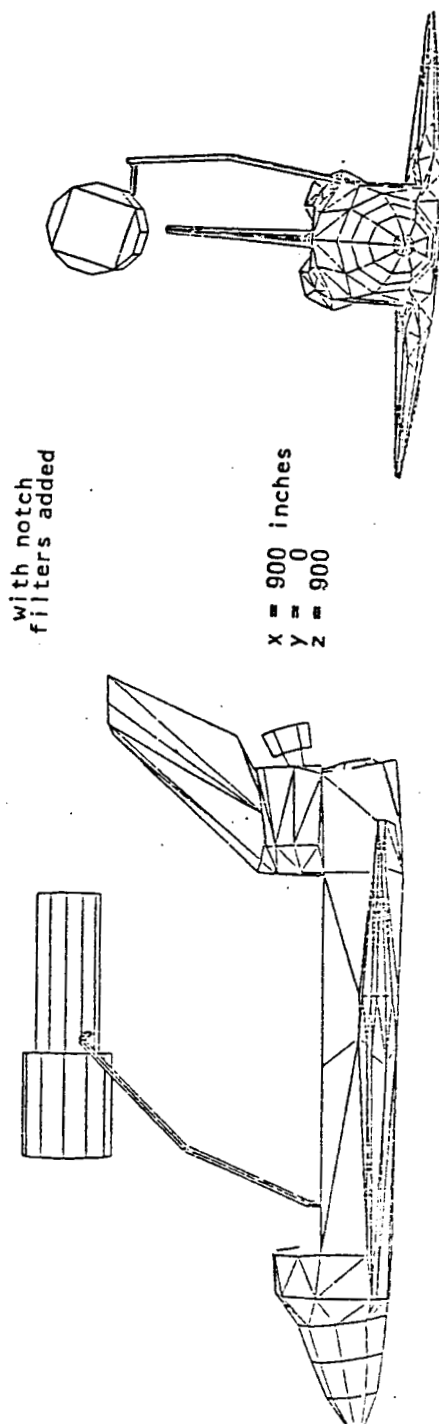
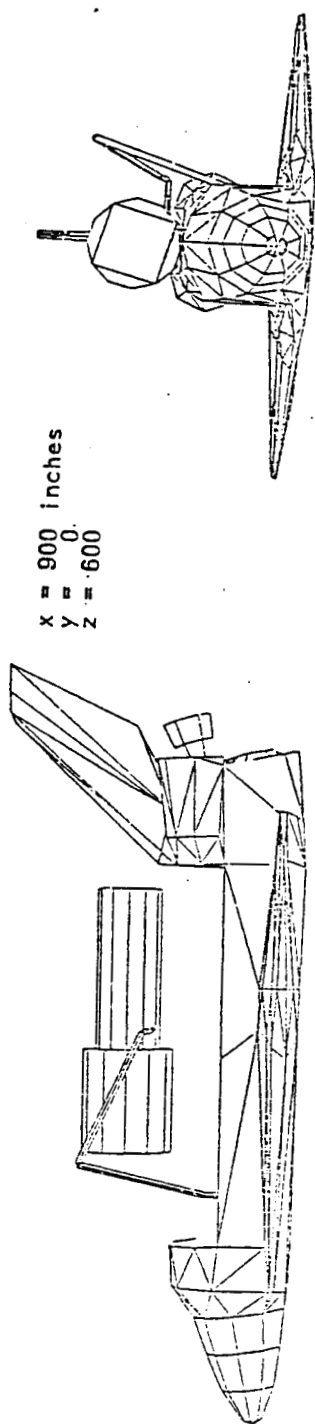
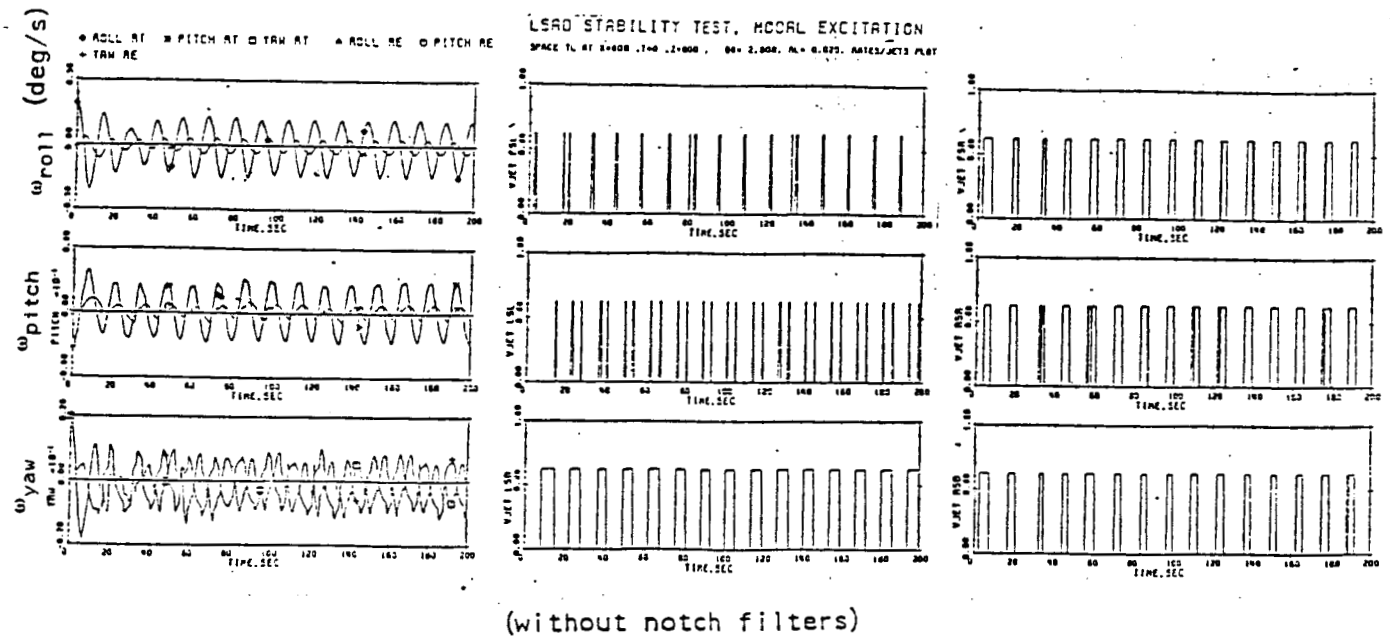


Figure 7.6 Limits of Stable Operation for Space Telescope ($x=900$)

show the difference adding notch filters can make in the stable handling of large payloads.

Figure 7.1 shows one typical case where adding notch filters prevents unstable jet firings from occurring. Figure 7.7 shows another typical case where the system with notch filters initially experiences unstable jet firings until the frequency estimator locks on to the bending modes and the notch filters center frequencies become close enough to the bending frequencies to stop further unstable firings. For this example, stability was regained after about seven low-frequency bending cycles.

ORIGINAL PAGE IS
OF POOR QUALITY



x = 700 y = 0 z = 900

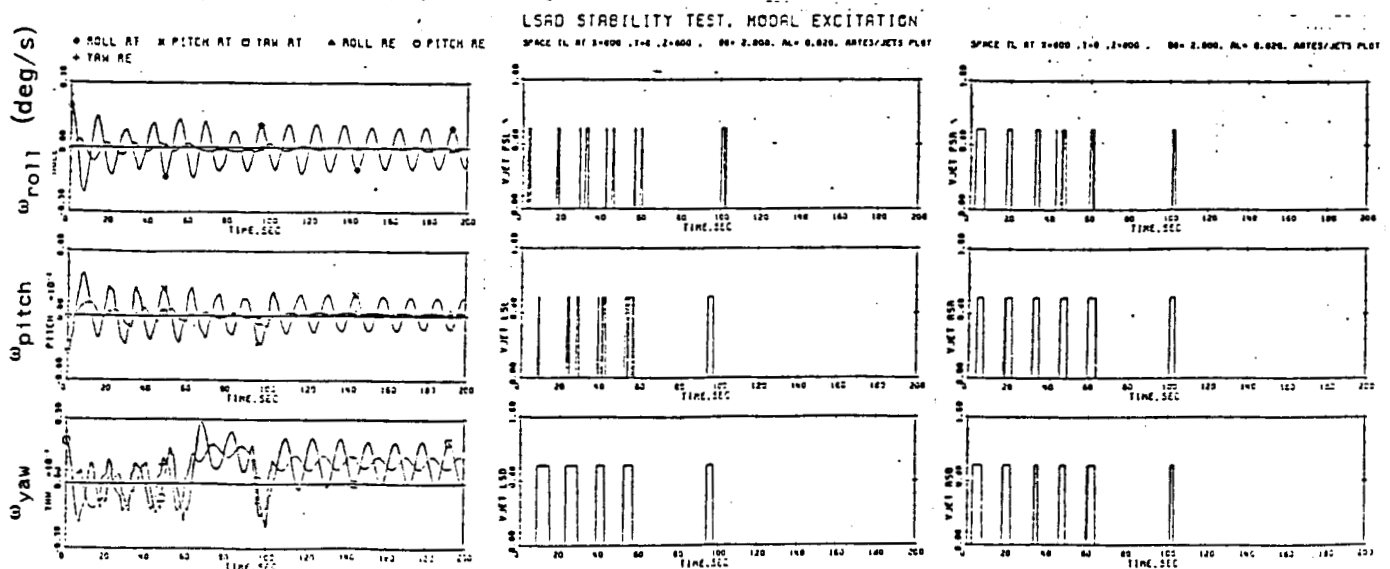


Figure 7.7 Typical Simulation Run for Space Telescope

CHAPTER 8

CONCLUSIONS AND RECOMMENDATIONS

The combination of frequency identification and notch filters can help reduce instabilities caused by flexible body dynamics spilling over into the rigid body control system. The algorithm used is relatively simple and easy to implement on a digital computer. Simulation results for two large payloads attached to the Shuttle's robot arm show a large increase in the range of stable operation when notch filters are added.

The frequency identification uses bandpass filters to isolate each bending mode. Engineering judgment must be used in determining the number of filters and their passband frequencies for a given payload. The identification method will work well when reasonable a priori knowledge of the bending frequencies is available or when use of many, narrow bandpass filters is acceptable.

The system might be made more adaptable by using the estimated frequencies to vary the bandpass cutoffs. Allowing the passbands to vary would place less importance on the initial cutoff frequencies, and thus would make the system more autonomous. Perhaps one set of initial conditions could be used for any payload which would remove the necessity for preflight, payload specific analysis.

The ability of the system to identify and notch filter bending frequencies requires that the low-frequency flexibility consists of a few distinct, dominant modes. The Shuttle-payload dynamic interaction can generally be characterized by a few distinct modes. For many flexible spacecraft, this may not be the case. The bending modes may be very closely spaced together. The notch filtering scheme method for stabilizing flexible systems will not work well for spacecraft with tightly-packed modes, requiring investigation of alternate filtering methods for these applications.

The frequency identification - notch filtering method reduces instability by filtering out the bending dynamics component of the measurement signal. The bending modes are left to damp themselves out. A more sophisticated technique might use the identified bending mode frequencies in conjunction with an active flexible body control system.

The use of notch filters to reduce observation spillover has been shown to be effective in simulations of the Space Shuttle with large payloads attached to its robot arm. Further work could be done, particularly on the frequency identification, to improve performance and to make the system more autonomous. The notch filtering scheme shows a potential for greatly expanding the range of stable payload operation. It might also be useful for other flexible spacecraft.

BIBLIOGRAPHY

1. Strunce, R.R., Lin, Y.H., "State-of-the-Art in Vibration Control Techniques for Large Space Structures", Draper Report P-885.
2. Balas, M.J., "Feedback Control of Flexible Systems", IEEE Trans. Auto. Cont., vol.AC-23, pp. 673-679, 1978.
3. Greene, C.S., Cunningham, T.B., "Integrated Controls/Structures Study of Advanced Space Systems", 1981 Large Space System Technology, Third Annual Technical Review, N82-18275.
4. Longman, R.W., "Annihilation or Suppression of Control and Observation Spillover in the Optimal Shape Control of Flexible Spacecraft", The Journal of Astronautical Sciences, vol.27, No.4, Oct-Dec. 1979, pp. 381-399.
5. Macala, G.A., "Tuned Feedback Damping with Application to the Galileo Spacecraft", Paper 81-200, AAS/AIAA Astrodynamics Specialist Conference, Lake Tahoe, Nevada, Aug. 3-5, 1981.
6. Stearns, S., Digital Signal Analysis, Hayden Book Co., Rochelle Park, NJ, 1975.
7. "Simplified Model of the Space Shuttle On-Orbit Flight Control System", July 1982, Draper Report CSDL-R-1562.
8. Penchuk, A., Hattis, P., Kubiak, E., "A Frequency Domain Stability Analysis of a Phase Plane Control System", Journal of Guidance, Control, and Dynamics, Vol. 8, No. 1, Jan.-Feb. 1985, pp. 50-55.

9. Kirchwey,C., Sackett,L., "Stability of the Shuttle On-Orbit Flight Control System for a Class of Flexible Payloads", Proc. of the AIAA Guidance and Control Conf., Aug. 1983, pp. 128-141.
10. Gelb,A., Vander Velde,W., Multiple-Input Describing Functions and Nonlinear System Design, McGraw-Hill Book Company, New York, 1968.
11. Barrows,T., "A Simplified Simulation for the Analysis of RMS Motion with Heavy Payloads", July 29, 1984, Draper Memo TMB-84-2.

APPENDIX: HAL CODE

ORIGINAL PAGE IS
OF POOR QUALITY

HAL/S STD 360-24.20

INTERMETRICS, INC.

MARCH 4, 1986

11:28:41.60

PAGE 94

SRN	STMT	SOURCE	CURRENT SCOPE
000100	1058 M	FILTER:	FILTER
000100	1058 M	PROCEDURE:	FILTER
000700	1059 M	DECLARE ARRAY(3, 3, 2) SCALAR INITIAL(0),	FILTER
000700	1059 M	U_BP, U_BP_1, U_BP_2, U_BP_3, U_BP_4, Y_BP, Y_BP_1, Y_BP_2, Y_BP_3, Y_BP_4, F_BP_1,	FILTER
000700	1059 M	F_BP_2, F_BP_3, F_BP_4, G_BP;	FILTER
001000	1060 M	DECLARE MATRIX(3, 3) INITIAL(0),	FILTER
001000	1060 M	Y_OLD, T_MEAS, OMEGA_MEAS, OMEGA_EST, U_EST_1, U_EST_2, Y_EST_1, Y_EST_2, F_EST_1,	FILTER
001000	1060 M	F_EST_2, G_EST, OMEGA_N, OMEGA_BP_1, OMEGA_BP_2, OMEGA_NAT_EST, ZETA_EST, NOTCH_WIDTH	FILTER
001000	1060 M	, OMEGA_INIT, Y_A, Y_A_1, Y_A_2, Y_A_3, U_A, U_A_1, U_A_2, U_A_3;	FILTER
001500	1061 M	DECLARE MATRIX(3, 3) INITIAL(0),	FILTER
001500	1061 M	U_N, U_N_1, U_N_2, Y_N, Y_N_1, Y_N_2, F_N_1, F_N_2, G_N_0, G_N_1, G_N_2;	FILTER
001800	1062 M	DECLARE INTEGER INITIAL(0),	FILTER
001800	1062 M	AXIS, FREQ, BP, COUNTER, XAXIS, NAXIS;	FILTER
001900	1063 M	DECLARE SCALAR,	FILTER
001900	1063 M	GAMMA_BP, FRAC, ANGLE_BP, TIME_STEP, OMEGA_A, F_A_1, F_A_2, F_A_3, G_A, Y_RATE;	FILTER
002000	1064 M	DECLARE ARRAY(3, 3) BOOLEAN,	FILTER
002000	1064 M	SWITCH_N INITIAL(ON);	FILTER
002100	1065 M	DECLARE BOOLEAN INITIAL(ON), FIRST;	FILTER
002800	1069 M	IF FIRST = ON THEN	FILTER
002800	1070 M	DO;	FILTER
003000	1071 M	1 READ(4) NAXIS, [NFREQ];	FILTER
003800	1077 M	1 READ(4) OMEGA_BP_1;	FILTER
003900	1078 M	1 READ(4) OMEGA_BP_2;	FILTER
004100	1079 M	1 GAMMA_BP = 0.8;	FILTER
004200	1080 M	1 OMEGA_BP_1 = OMEGA_BP_1 2 3.1416;	FILTER
004300	1081 M	1 OMEGA_BP_2 = OMEGA_BP_2 2 3.1416;	FILTER
004500	1082 M	1 READ(4) NOTCH_WIDTH;	FILTER
004600	1083 M	1 OMEGA_INIT = (OMEGA_BP_1 + OMEGA_BP_2) / 2;	FILTER
004700	1084 M	1 OMEGA_N = OMEGA_INIT;	FILTER
004800	1085 M	1 OMEGA_MEAS = OMEGA_INIT;	FILTER
004900	1086 M	1 OMEGA_EST = OMEGA_INIT;	FILTER
005000	1087 M	1 U_EST_1 = OMEGA_INIT;	FILTER
005100	1088 M	1 U_EST_2 = OMEGA_INIT;	FILTER

ORIGINAL PAGE IS
OF POOR QUALITY

005200	1089	E	1	Y_EST_1 = OMEGA_INIT;	FILTER
005300	1090	E	1	Y_EST_2 = OMEGA_INIT;	FILTER
005500	1091	E	1	READ(4) OMEGA_NAT_EST;	FILTER
005600	1092	E	1	OMEGA_NAT_EST = OMEGA_NAT_EST 2 3.1416;	FILTER
005700	1093	E	1	READ(4) ZETA_EST;	FILTER
005710	1094	M	1	READ(4) OMEGA_A;	FILTER
005900	1095	M	1	XAXIS = 1;	FILTER
005920	1096	M	1	DO FOR AXIS = 1 TO NAXIS;	FILTER
006100	1097	M	2	DO FOR FREQ = 1 TO NFREQ ;	FILTER
		S		AXIS	
006300	1098	M	3	TIME_STEP = 0.16 NAXIS;	FILTER
007000	1100	M	3	DO FOR BP = 1 TO 2;	FILTER
007200	1101	M	4	IF BP = 1 THEN	FILTER
007200	1102	M	4	ANGLE_BP = 22.5;	FILTER
007300	1103	M	4	ELSE	FILTER
007300	1103	M	4	ANGLE_BP = 67.5;	FILTER
007500	1104	M	4	CALL BANDPASS;	FILTER
007600	1105	M	3	END;	FILTER
007800	1106	M	3	CALL NOTCH;	FILTER
007900	1107	M	3	CALL FREQ_EST;	FILTER
008100	1108	M	2	END;	FILTER
008200	1109	M	1	END;	FILTER
008210	1110	M	1	CALL LOWPASS;	FILTER
008400	1111	E	1	FIRST = OFF;	FILTER
008600	1112	M		END;	FILTER
008700		C		*****	FILTER
008800		C		START OF RECURSIVE FILTER	FILTER
008900		C		*****	FILTER
009110	1113	M		AXIS = XAXIS;	FILTER
009310	1114	M		IF XAXIS = NAXIS THEN	FILTER
009310	1115	M		XAXIS = 1;	FILTER
009320	1116	M		ELSE	FILTER
009320	1116	M		XAXIS = XAXIS + 1;	FILTER
009400	1117	M		DO FOR FREQ = 1 TO NFREQ ;	FILTER
		S		AXIS	
009600	1118	M	1	U_BP = MEASURED_ATTITUDE ;	FILTER
		S		AXIS,FREQ,1 AXIS	
010000		C		BANDPASS FILTERS;	FILTER
010200	1119	M	1	DO FOR BP = 1 TO 2;	FILTER
010400	1120	M	2	Y_BP = F_BP_1 Y_BP_1 + F_BP_2 Y_BP_2	FILTER
		S		AXIS,FREQ,BP AXIS,FREQ,BP AXIS,FREQ,BP AXIS,	
010400	1120	M	2	FREQ,BP + F_BP_3 Y_BP_3 + F_BP_4 Y_BP_4	FILTER
		S		AXIS,FREQ,BP AXIS,FREQ,BP AXIS,FREQ,BP AXIS,FREQ,BP +	
010400	1120	M	2	G_BP (U_BP - 2 U_BP_2 + U_BP_4);	FILTER
		S		AXIS,FREQ,BP AXIS,FREQ,BP AXIS,FREQ,BP AXIS,FREQ,BP	
011000	1121	M	2	U_BP_4 = U_BP_3	FILTER
		S		AXIS,FREQ,BP AXIS,FREQ,BP	
011100	1122	M	2	U_BP_3 = U_BP_2	FILTER
		S		AXIS,FREQ,BP AXIS,FREQ,BP	
011200	1123	M	2	U_BP_2 = U_BP_1	FILTER
		S		AXIS,FREQ,BP AXIS,FREQ,BP	
011300	1124	M	2	U_BP_1 = U_BP	FILTER
		S		AXIS,FREQ,BP AXIS,FREQ,BP	
011400	1125	M	2	Y_BP_4 = Y_BP_3	FILTER
		S		AXIS,FREQ,BP AXIS,FREQ,BP	

```

011500 1126 M| 2      Y_BP_3      = Y_BP_2      ;
                      AXIS,FREQ,BP      AXIS,FREQ,BP
011600 1127 M| 2      Y_BP_2      = Y_BP_1      ;
                      AXIS,FREQ,BP      AXIS,FREQ,BP
011700 1128 M| 2      Y_BP_1      = Y_BP      ;
                      AXIS,FREQ,BP      AXIS,FREQ,BP
011900 1129 M| 2      U_BP      = Y_BP      ;
                      AXIS,FREQ,2      AXIS,FREQ,1
012100 1130 M| 1      END;
012108      C| CHECK AMPLITUDE OF BANDPASS OUTPUT
012116 1131 E| 1      U_A      = 2 (Y_BP2);
                      S|      AXIS,FREQ      AXIS,FREQ,2
012124 1132 M| 1      Y_A      = F_A_1 Y_A_1      + F_A_2 Y_A_2      + F_A_3 Y_A_3      + G_A (U_A
                      S|      AXIS,FREQ      AXIS,FREQ      AXIS,FREQ      AXIS,FREQ
012124 1132 M| 1      + 3 U_A_1      + 3 U_A_2      + U_A_3      );
                      S|      AXIS,FREQ      AXIS,FREQ      AXIS,FREQ      AXIS,FREQ
012136 1133 M| 1      Y_A_3      = Y_A_2      ;
                      S|      AXIS,FREQ      AXIS,FREQ
012140 1134 M| 1      Y_A_2      = Y_A_1      ;
                      S|      AXIS,FREQ      AXIS,FREQ
012144 1135 M| 1      Y_A_1      = Y_A      ;
                      S|      AXIS,FREQ      AXIS,FREQ
012148 1136 M| 1      U_A_3      = U_A_2      ;
                      S|      AXIS,FREQ      AXIS,FREQ
012152 1137 M| 1      U_A_2      = U_A_1      ;
                      S|      AXIS,FREQ      AXIS,FREQ
012156 1138 M| 1      U_A_1      = U_A      ;
                      S|      AXIS,FREQ      AXIS,FREQ
012160 1139 M| 1      Y_RATE = SORT(ABS(Y_A      + .000001)) OMEGA_N
                      S|      AXIS,FREQ      AXIS,FREQ
012168 1140 M| 1      IF Y_RATE < (RL_REQUEST / 3) THEN
012168 1141 E| 1      SWITCH_N      = OFF;
                      S|      AXIS,FREQ:
012172 1142 M| 1      ELSE
012172 1142 M| 1      DO;
012176 1143 E| 2      IF Y_RATE < (RL_REQUEST / 2) AND SWITCH_N      = OFF THEN
                      S|      AXIS,FREQ:
012180 1144 E| 2      SWITCH_N      = OFF;
                      S|      AXIS,FREQ:
012200 1145 M| 2      ELSE
012200 1145 E| 2      SWITCH_N      = ON;
                      S|      AXIS,FREQ:
012210 1146 M| 1      END;
012300      C| MEASURE FREQUENCY FROM CROSSING TIMES;
012500 1147 M| 1      IF SIGN(Y_BP      ) NOT = SIGN(Y_OLD      ) THEN
                      S|      AXIS,FREQ,2      AXIS,FREQ
012500 1148 M| 1      DO;
012600 1149 M| 2      FRAC = TIME_STEP Y_OLD      / (Y_OLD      - Y_BP      );
                      S|      AXIS,FREQ      AXIS,FREQ      AXIS,FREQ,2
012800 1150 M| 2      T_MEAS      = T_MEAS      + FRAC;
                      S|      AXIS,FREQ      AXIS,FREQ
012900 1151 M| 2      OMEGA_MEAS      = 3.1416 / T_MEAS      ;
                      S|      AXIS,FREQ      AXIS,FREQ
013000 1152 M| 2      IF COUNTER < 300 THEN
013000 1153 M| 2      OMEGA_MEAS      = OMEGA_INIT      ;
                      S|      AXIS,FREQ      AXIS,FREQ
013400 1156 M| 2      T_MEAS      = TIME_STEP - FRAC;
                      S|      AXIS,FREQ

```

```

013700 1158 M| 2      OMEGA_MEAS      = OMEGA_EST      (1.0 + 0.1 SIGN(OMEGA_MEAS      -
S|                AXIS,FREQ      AXIS,FREQ      AXIS,FREQ      )
013700 1158 M| 2      OMEGA_EST      ));
S|                AXIS,FREQ
014000 1159 M| 1      END;
014100 1160 M| 1      ELSE
014100 1160 M| 1      T_MEAS      = T_MEAS      + TIME_STEP;
S|                AXIS,FREQ      AXIS,FREQ
014300 1161 M| 1      Y_OLD      = Y_BP
S|                AXIS,FREQ      AXIS,FREQ,2
014500 C| ESTIMATE FREQUENCY FROM NOISY MEASUREMENTS;
014700 1162 M| 1      OMEGA_EST      = F_EST_1      Y_EST_1      + F_EST_2      Y_EST_2
S|                AXIS,FREQ      AXIS,FREQ      AXIS,FREQ      AXIS,FREQ      AXIS,FREQ
014700 1162 M| 1      G_EST      (OMEGA_MEAS      * 2 U_EST_1      + U_EST_2
S|                AXIS,FREQ      AXIS,FREQ      AXIS,FREQ
015000 1163 M| 1      Y_EST_2      = Y_EST_1
S|                AXIS,FREQ      AXIS,FREQ
015100 1164 M| 1      Y_EST_1      = OMEGA_EST
S|                AXIS,FREQ      AXIS,FREQ
015200 1165 M| 1      U_EST_2      = U_EST_1
S|                AXIS,FREQ      AXIS,FREQ
015300 1166 M| 1      U_EST_1      = OMEGA_MEAS
S|                AXIS,FREQ      AXIS,FREQ
015700 C| TEST REASONABLENESS OF ESTIMATE
015900 1167 M| 1      IF (OMEGA_EST      < OMEGA_BP_1      0.8) OR (OMEGA_EST      > OMEGA_BP_2
S|                AXIS,FREQ      AXIS,FREQ      AXIS,FREQ      AXIS,FREQ
015900 1167 M| 1      FREQ 1.2) THEN
S|
016100 1168 M| 1      SWITCH_N      = OFF;
S|                AXIS,FREQ
016300 C| DECIDE WHETHER OR NOT TO CHANGE NOTCH CENTER FREQUENCY
016500 1169 M| 1      IF (OMEGA_EST      - OMEGA_N      ) / OMEGA_N      > NOTCH_WIDTH
S|                AXIS,FREQ      AXIS,FREQ      AXIS,FREQ      AXIS,FREQ
016500 1169 M| 1      OMEGA_N      - OMEGA_EST      ) / OMEGA_N      > NOTCH_WIDTH
S|                AXIS,FREQ      AXIS,FREQ      AXIS,FREQ      AXIS,FREQ
016800 1170 M| 1      DO;
016900 1171 M| 2      OMEGA_N      = OMEGA_EST
S|                AXIS,FREQ      AXIS,FREQ
017000 1172 M| 2      CALL NOTCH;
017200 1173 M| 1      END;
017400 1174 M| 1      END;
017700 1175 M| 1      COUNTER = COUNTER + 1;
019915 C| NOTCH FILTERS

```

```

019920 1191 M| DO FOR AXIS = 1 TO NAXIS: | FILTER
020100 1192 M| 1 DO FOR FREQ = 1 TO NFREQ | FILTER
S| AXIS
020300 1193 M| 2 U_N = MEASURED_ATTITUDE | FILTER
S| AXIS,1 AXIS
020500 1194 M| 2 IF SWITCH_N = ON THEN | FILTER
S| AXIS,FREQ:
020500 1195 M| 2 DO: | FILTER
020600 1196 M| 3 Y_N = F_N_1 Y_N_1 + F_N_2 Y_N_2 + G_N_0 | FILTER
S| AXIS,FREQ AXIS,FREQ AXIS,FREQ AXIS,FREQ
020600 1196 M| 3 U_N = G_N_1 U_N_1 + G_N_2 U_N_2 | FILTER
S| AXIS,FREQ AXIS,FREQ AXIS,FREQ AXIS,FREQ
020600 1196 M| 3 FREQ: | FILTER
021100 1197 M| 3 Y_N_2 = Y_N_1 | FILTER
S| AXIS,FREQ AXIS,FREQ
021200 1198 M| 3 Y_N_1 = Y_N | FILTER
S| AXIS,FREQ AXIS,FREQ
021300 1199 M| 3 U_N_2 = U_N_1 | FILTER
S| AXIS,FREQ AXIS,FREQ
021400 1200 M| 3 U_N_1 = U_N | FILTER
S| AXIS,FREQ AXIS,FREQ
021600 1201 M| 2 END: | FILTER
021800 1202 M| 2 ELSE | FILTER
021800 1202 M| 2 DO: | FILTER
022000 1203 M| 3 Y_N_2 = U_N | FILTER
S| AXIS,FREQ AXIS,FREQ
022100 1204 M| 3 Y_N_1 = U_N | FILTER
S| AXIS,FREQ AXIS,FREQ
022200 1205 M| 3 Y_N = U_N | FILTER
S| AXIS,FREQ AXIS,FREQ
022300 1206 M| 3 U_N_2 = U_N | FILTER
S| AXIS,FREQ AXIS,FREQ
022400 1207 M| 3 U_N_1 = U_N | FILTER
S| AXIS,FREQ AXIS,FREQ

022600 1208 M| 2 END: | FILTER
022800 1209 M| 2 IF FREQ < NFREQ THEN | FILTER
S| AXIS
022800 1210 M| 2 U_N = Y_N | FILTER
S| AXIS,FREQ+1 AXIS,FREQ
023100 1211 M| 1 END: | FILTER
1212 M| 1 IF NFREQ = 0 THEN | FILTER
S| AXIS
1213 M| 1 ATTITUDE = MEASURED_ATTITUDE | FILTER
S| AXIS AXIS
1214 M| 1 ELSE | FILTER
1214 M| 1 ATTITUDE = Y_N | FILTER
S| AXIS AXIS,NFREQ
S| AXIS
023400 1215 M| END: | FILTER

```


023515	1216	M	LOWPASS:		LOWPASS
023515	1216	M	PROCEDURE;		LOWPASS
023525	1217	M	DECLARE SCALAR,		LOWPASS
023525	1217	M	DEN, R;		LOWPASS
023530	1218	M	R = TAN(OMEGA_A 3.1416 TIME_STEP);		LOWPASS
		E			
023535	1219	M	DEN = 1 + 2 R + 2 R ² + R ³ ;		LOWPASS
		E			
023540	1220	M	F_A_1 = (3 + 2 R - 2 R ² - 3 R ³) / DEN;		LOWPASS
		E			
023545	1221	M	F_A_2 = (-3 + 2 R + 2 R ² - 3 R ³) / DEN;		LOWPASS
		E			
023550	1222	M	F_A_3 = (1 - 2 R + 2 R ² - R ³) / DEN;		LOWPASS
		E			
023555	1223	M	G_A = (R ³) / DEN;		LOWPASS
023560	1224	M	CLOSE LOWPASS;		LOWPASS

**** B L O C K S U M M A R Y ****

OUTER VARIABLES USED
OMEGA_A, TIME_STEP, F_A_1*, F_A_2*, F_A_3*, G_A*

023600	1225	M	FREQ_EST:		FREQ_EST	
023600	1225	M	PROCEDURE;		FREQ_EST	
023800	1226	M	DECLARE SCALAR,		FREQ_EST	
023800	1226	M	DUMMY, W_EST:		FREQ_EST	
024000	1227	M	W_EST = TAN(OMEGA_NAT_EST	TIME_STEP / 2);	FREQ_EST	
		S	AXIS,FREQ			
		E				
024100	1228	M	DUMMY = 1 + 2 ZETA_EST	W_EST + W_EST ² ;	FREQ_EST	
		S	AXIS,FREQ			
		E				
024300	1229	M	F_EST_1	= (2 - 2 W_EST ²) / DUMMY;	FREQ_EST	
		S	AXIS,FREQ			
		E				
024400	1230	M	F_EST_2	= (-1 + 2 ZETA_EST	W_EST - W_EST ²) / DUMMY;	FREQ_EST
		S	AXIS,FREQ	AXIS,FREQ		
		E				
024500	1231	M	G_EST	= (W_EST ²) / DUMMY;	FREQ_EST	
		S	AXIS,FREQ			
024600	1232	M	CLOSE FREQ_EST;		FREQ_EST	

**** B L O C K S U M M A R Y ****

OUTER VARIABLES USED
AXIS, FREQ, OMEGA_NAT_EST, TIME_STEP, ZETA_EST, F_EST_1*, F_EST_2*, G_EST*

024800	1233	M	BANDPASS:		BANDPASS
024800	1233	M	PROCEDURE:		BANDPASS
025000	1234	M	DECLARE SCALAR DOUBLE,		BANDPASS
025000	1234	M	OMEGA_1, OMEGA_2, D3, D2, D1, D0, N2, DUMMY, OMEGA_C, ZETA_BP, ANGLE;		BANDPASS
025300	1235	M	OMEGA_1 = TAN(OMEGA_BP_1	TIME_STEP / 2);	BANDPASS
		S	AXIS,FREQ		
025400	1236	M	OMEGA_2 = TAN(OMEGA_BP_2	TIME_STEP / 2);	BANDPASS
		S	AXIS,FREQ		
025500	1237	M	OMEGA_C = OMEGA_2 - OMEGA_1;		BANDPASS
026000	1238	M	ANGLE = ANGLE_BP 3.1416 / 180;		BANDPASS
026200	1239	M	ZETA_BP = COS(ANGLE);		BANDPASS
		E			
026400	1240	M	N2 = OMEGA_C ² ;		BANDPASS
026500	1241	M	D3 = 2 ZETA_BP OMEGA_C;		BANDPASS
026600	1242	M	D2 = 2 OMEGA_1 OMEGA_2 + N2;		BANDPASS
026700	1243	M	D1 = D3 OMEGA_1 OMEGA_2;		BANDPASS
		E			
026800	1244	M	D0 = OMEGA_1 ² OMEGA_2 ² ;		BANDPASS
026900	1245	M	DUMMY = 1 + D0 + D1 + D2 + D3;		BANDPASS
027100	1246	M	F_BP_1	(4 + 2 D3 - 2 D1 - 4 D0) / DUMMY;	BANDPASS
		S	AXIS,FREQ,BP		
027200	1247	M	F_BP_2	(-6 + 2 D2 - 6 D0) / DUMMY;	BANDPASS
		S	AXIS,FREQ,BP		
027300	1248	M	F_BP_3	(4 - 2 D3 + 2 D1 - 4 D0) / DUMMY;	BANDPASS
		S	AXIS,FREQ,BP		
027400	1249	M	F_BP_4	(-1 + D3 - D2 + D1 - D0) / DUMMY;	BANDPASS
		S	AXIS,FREQ,BP		
027500	1250	M	G_BP	N2 / DUMMY;	BANDPASS
		S	AXIS,FREQ,BP		
027600	1251	M	CLOSE BANDPASS;		BANDPASS
028100	1252	M	NOTCH:		NOTCH
028100	1252	M	PROCEDURE:		NOTCH
028300	1253	M	DECLARE SCALAR,		NOTCH
028300	1253	M	OMEGA_1, OMEGA_2, OMEGA_C, N2, N1, N0, D2, D1, D0;		NOTCH
028600	1254	M	OMEGA_1 = (1 - NOTCH_WIDTH	OMEGA_N	NOTCH
		S	AXIS,FREQ	AXIS,FREQ	
028700	1255	M	OMEGA_2 = (1 + NOTCH_WIDTH	OMEGA_N	NOTCH
		S	AXIS,FREQ	AXIS,FREQ	
028900	1256	M	OMEGA_1 = TAN(OMEGA_1 0.16 / 2);		NOTCH
029000	1257	M	OMEGA_2 = TAN(OMEGA_2 0.16 / 2);		NOTCH
029100	1258	M	OMEGA_C = OMEGA_2 - OMEGA_1;		NOTCH
029300	1259	M	N2 = 1 + OMEGA_1 OMEGA_2;		NOTCH
029400	1260	M	N1 = -2 + 2 OMEGA_1 OMEGA_2;		NOTCH
029500	1261	M	N0 = N2;		NOTCH
029600	1262	M	D2 = 1 + OMEGA_C + OMEGA_1 OMEGA_2;		NOTCH
029700	1263	M	D1 = N1;		NOTCH
029800	1264	M	D0 = 1 - OMEGA_C + OMEGA_1 OMEGA_2;		NOTCH
030000	1265	M	F_N_1	-D1 / D2;	NOTCH
		S	AXIS,FREQ		
030100	1266	M	F_N_2	-D0 / D2;	NOTCH
		S	AXIS,FREQ		
030200	1267	M	G_N_O	N2 / D2;	NOTCH
		S	AXIS,FREQ		
030300	1268	M	G_N_1	N1 / D2;	NOTCH
		S	AXIS,FREQ		
030400	1269	M	G_N_2	N0 / D2;	NOTCH
		S	AXIS,FREQ		
030500	1270	M	CLOSE NOTCH;		NOTCH